International Review of
Automatic Control
(IREACO)

Theory and Applications

Contents

Praise Worthy Prize

International Review of Automatic Control (I.RE.A.CO.), Vol. 8, N. 2
ISSN 1974-6059 March 2015

Direct and Inverse Neural Modelization of Mobile Robots

Ines Mahmoud, Ayachi Errachdi, Mohamed Benrejeb

Abstract – *In this paper, direct and inverse models determination of a mobile robot using artificial neural networks are proposed.*
The effectiveness of the proposed algorithm applied to the modeling of behavior of CHAR and KHEPERA robots is verified by simulation experiments. The results of simulation show that the use of the neural networks in the determination of direct model and inverse model is very interesting since it enables to guarantee the time competition and the quality of the modeling.

Keywords: *Direct Model, Inverse Model, Artificial Neural Network, Robotic Model, Learning Rate*

Nomenclature

$y(k)$ Process output
$u(k)$ Process input
E Error vector
f Unknown function of model robot
I ANN the input vector
ncc Number of nodes of hidden layer
W Synaptic weights of the layer towards the hidden layer
Z Synaptic weights of the layer towards the output layer
s Activation function
η Learning rate
λ Regularization coefficient
TDL Tapped delay line block
N Number of measures
v_r Speed of the right wheel
v_l Speed of the left wheel
ω Angular velocity
Yr $\left[yr_1(k) \quad yr_2(k) \quad ... \quad yr_{ns}(k) \right]^T, (ns \times 1)$ output vector of the ANN
E $\left[e_1(k) \quad e_2(k) \quad ... \quad e_{ns}(k) \right]^T, (ns \times 1)$ error vector
$e_i(k)$ $y_i(k) - yr_i(k)$ error between the i^{th} measured output and the $i^{ème}$ ANN output at time k
W $\{w_{ij}\} \in R^{ncc \times (nu+us)}; l = 1,...,ncc \text{ and } j = 1,...,nu+us$
Z $\{z_{ij}\} \in R^{ns \times ncc}; i = 1,...,ns$ and $l=1,\ldots,ncc$
Ur $\left[ur_1(k) \quad ur_2(k) \quad ... \quad ur_{nu}(n) \right]^T, (nu \times 1)$ beeing n the output vector of the ANN
E $\left[e_1(k) \quad e_2(k) \quad ... \quad e_{nu}(k) \right]^T, (nu \times 1)$ being the error vector
$e_i(k)$ $u_i(k) - ur_i(k)$ error between the i^{th} measured input and the i^{th} ANN output
I ANN input vector, $(t \times 1), (t = nu + ns)$

I. Introduction

Nowadays, research community have increased its interest in robots performing social tasks, consequently the need of studying new abilities for human-robot interaction and task cooperation have become important issues [1].

Robotics technology is emerging rapidly, offering new possibilities for automating tasks in many challenging applications, in domestic services, medical procedures, military operations, underwater missions and space exploration. In this latter, robotic devices are formally known as planetary rovers or simply rovers and they are aimed at conducting physical analysis of planetary terrains and astronomical bodies and collecting data about climate, wind, air pressure, temperature and other atmospheric phenomena surrounding the landing sites [2]. A mobile robot is an electromechanical system able of autonomous motion. Mobile robots can be classified into several mobility configurations as wheels number and type, single or multi-body structure and so on [3].

In [4], the exact discrete-time model of a mobile robot is obtained by direct integration. In [5], the authors present the transformation of the original kinematic system in chained form through an appropriate feedback.

The obtained equations are closed-form integrable, thereby yielding a linear discrete-time model which provides exact odometric prediction and associated covariance [3].

In [6], mathematical model is used for the design of advanced robot control systems. Its calculation requires knowledge of exact values of a robot's physical parameters. It is rather difficult to obtain the data without disassembling a robot. One of the methods which enable the determination of a robot mathematical model without a priori knowledge of these parameters is using the neural networks [7]-[9].

The Artificial Neural Networks (ANN) is nonconventional methods not requiring a mathematical model but based on the training for the example ([10]-[21], [37]-[39]). These ANN are well used for robot modeling. Indeed, the ANN are proposed for robust control of space robots [10], for controlling robot manipulators [11], for space robots based on fuzzy logic [12], for solving the wheel slip problem in space rover exploration devices [13], for moving robots with translational and rotational motion deployed in partially structured environment [14], for the Rover Mars robot [15], for robotic systems based on the Jordan architecture [16], for intelligent control of an autonomous robot [17], for control of a Car-Like mobile robot [18], for Control of a Robotic Arm [19], for Reinforcement Learning on a Humanoid Robot [20] and for control robot manipulator [21].

This paper presents determination method of a robot model using neural networks. The model strategy will be based on the exact discrete time model of the robot.

The proposed ANN is a multilayer network made out of three layers: an input, a hidden and an output layer.

The network is trained in off-line mode using back-propagation supervised learning algorithm. The paper is organized as follows. The second Section contains the neural networks approach for robotic model.

The third Section treats the simulation of two examples of robotic model by the ANN. The simulation of the inverse robotic model is seen on the forth section. Conclusions are presented in the last Section.

II. Neural Networks Approach for Robotic Model

In this section, firstly, we present a robotic model defined in Fig. 1, secondly, we present the principle of the neural network for robotic model presented in Fig. 2.

The robotic model is defined by the number nu of input signals $\{u_1,\ldots,u_{nu}\}$ and the number ns of output variables $\{y_1,\ldots,y_{ns}\}$. A robot model can be given on the following form:

$$y(k+1)=f\begin{bmatrix} y(k),...,y(k-ns+1),...,u(k), \\ ...,u(k-nu+1) \end{bmatrix} \quad (1)$$

with:

$$u(k)=\begin{bmatrix} u_1(k) & u_2(k) & ... & u_{nu}(k) \end{bmatrix},(nu\times 1)$$

being the value of the input vector of the robot at time k:

$$y(k)=\begin{bmatrix} y_1(k) & y_2(k) & ... & y_{ns}(k) \end{bmatrix}^T,(ns\times 1)$$

being the value of the output vector of the robot at time *k*.

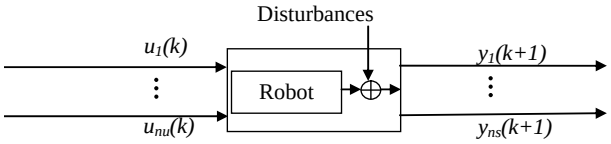

Fig. 1. Inputs and outputs of studied robot model

In order to find a neural direct model or a neural inverse one for a robot, we consider using its input-output signals. The algorithm of training of such a ANN is based on the updating of the synaptic weights and on a fixed learning rate.

The stages of the ANN modelling of a robot are: firstly to standardize and to center all the input variables, secondly to choose the suitable structure of a model, thirdly to estimate the synaptic weights, finally to validate the obtained model [22]-[24], [34]-[36].

The principle of the neural modelling of a robot is presented in Fig. 2.

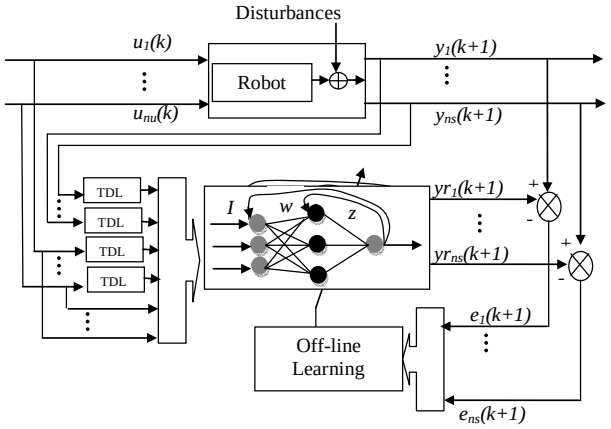

Fig. 2. The general training architecture

The i^{th} ANN output $(i=1,...,ns)$ is given by the following relation:

$$yr_i(k+1)=\lambda s\left(\sum_{l=1}^{ncc} s\left(\sum_{j=1}^{nu+us} w_{ij}I_i\right)z_{il}\right) \quad (2)$$

Finally, the compact form can be defined as:

$$Yr(k+1)=\lambda s\left[Z^T S(WI)\right] \quad (3)$$

with:

$$I=\{I_j\}\in R^{(nu+us)\times 1};\ j=1,...,nu+us$$

$$S(WI)=\left\{s\left(\sum_{j=1}^{nu+us} w_{lj}I_j\right)\right\}\in R^{ncc\times 1};l=1,...,ncc$$

The Gradient Descent (GD) method is able of speeding up the learning process, guarantees the convergence of ANN weights and can simultaneously provide stability of the learning process [22]-[24].

The principle is to minimize the i^{th} criterion such as:

$$J_i(k)=\frac{1}{2}\sum_{k=0}^{N}\left(e_i(k)\right)^2=\frac{1}{2}\sum_{k=0}^{N}\left[y_i(k)-yr_i(k)\right]^2 \quad (4)$$

By application of the GD method, we find then the variation of the synaptic weights of the hidden layer towards the output layer with $(i=1,...,ns)$:

$$z_{il}(k)=z_{il}(k-1)+\lambda\eta_i s'\left(\sum_{j=1}^{(nu+us)} w_{lj}I_j\right)S(WI)e_i(k) \quad (5)$$

where s is an activation function and s' is its derivative $s'(v)=\frac{ds(v)}{dv}$, is a sigmoid function. The variation of the synaptic weights of the input layer towards the hidden layer with $(i=1,...,ns)$ and $(j=1,...,t)$ is such that:

$$w_{lj}(k)=w_{lj}(k-1)+ +\lambda\eta_i s'\left(\sum_{j=1}^{t} w_{lj}I_j\right)S'(WI)z_{il}(k)e_i(k) \quad (6)$$

In these expressions, $\eta_i(i=1,...,ns)$ is a positive constant value which represents the learning rate $(0\le\eta_i\le 1)$ and $S'(WI)$ represents Jacobean matrix of $S(WI)$ [33]:

$$S'(WI)=diag\left[s'\left(\sum_{j=1}^{t} w_{lj}I_j\right)\right]$$

with:

$$s'\left(\sum_{j=1}^{t} w_{lj}I_j\right)=\frac{\partial s\left(\sum_{j=1}^{t} w_{lj}I_j\right)}{\partial\left(\sum_{j=1}^{t} w_{lj}I_j\right)};l=1,...,ncc$$

Next, simulations and comparison of the robot neural network models are presented. The performance of ANN models are evaluated by Normalized root Mean Square Error between the system output and the model output, denoted *NMSE* [32]:

$$NMSE(e)=\frac{\sum_{k=1}^{N}\left(y(k)-yr(k)\right)^2}{\sum_{k=1}^{N}\left(y(k)\right)^2}$$

III. Simulation Results of Direct Robots Models

In this section, two types of robot model are presented. The robot model (R1) [25] and (R2) [26]-[29] are described respectively by Eqs. (7), (8) and (12) equations. Where u_1 and u_2 are the inputs of the robot whose evolution is defined by the Eqs. (9) and (10).

The first robot model, called in this paper CHAR is given by the Fig. 3.

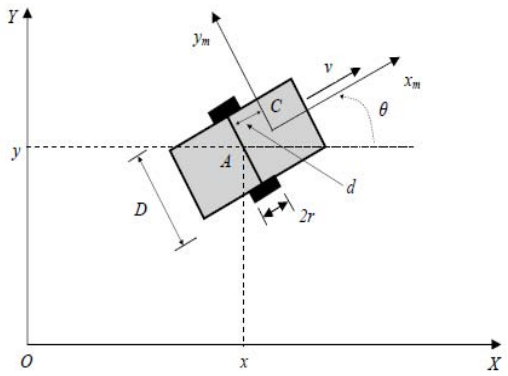

Fig. 3. CHAR Robot model

The model of the 2 dimensions $(ne=2,ns=3)$ robot CHAR is given by the following equations

$$\begin{cases}\dot{x}(t)=v(t)cos(\theta(t))\\ \dot{y}(t)=v(t)sin(\theta(t))\\ \dot{\theta}(t)=u_1(t)\\ \dot{v}(t)=u_2(t)\end{cases} \quad (7)$$

The time-discrete model of this robot can be described by the following equations:

$$(R1):\begin{cases}x(k+1)=x(k)+v(k)cos(\theta(k))\\ y(k+1)=y(k)+v(k)sin(\theta(k))\\ \theta(k+1)=\theta(k)+u_1(k)\\ v(k+1)=v(k)+u_2(k)\end{cases} \quad (8)$$

where $u_1(k)$ and $u_2(k)$ are the input signals and $x(k)$, $y(k)$ and $\theta(k)$ are the output signals.

The second robot model, called KHEPERA, is described Fig. 4.

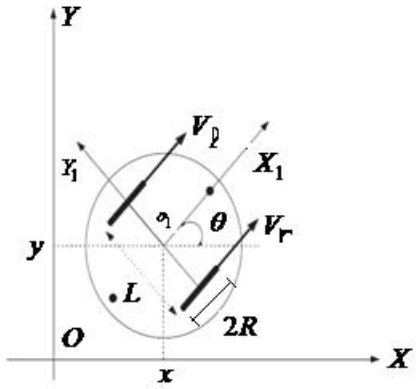

Fig. 4. KHEPERA robot model

The model of this robot with 2 dimensions $(ne = 2, ns = 3)$ is given by the following equations:

$$(R1): \begin{cases} \dot{x}(t) = \dfrac{v_r(t) + v_l(t)}{2} cos(\theta(t)) \\ \dot{y}(t) = \dfrac{v_r(t) + v_l(t)}{2} sin(\theta(t)) \\ \dot{\theta}(t) = \omega = \dfrac{(v_r(t) - v_l(t))R}{2L} \end{cases} \quad (9)$$

The v_r, v_l and ω parameters are the speeds respectively speed the right wheel, and the left wheel and the angular velocity of the mobile robot.

The time-discrete model of this robot is given by the following equation:

$$(R2): \begin{cases} x(k+1) = x(k) + T \cdot \dfrac{v_r(k) + v_l(k)}{2} cos(\theta(k)) \\ y(k+1) = y(k) + T \cdot \dfrac{v_r(k) + v_l(k)}{2} sin(\theta(k)) \\ \theta(k+1) = \theta(k) + T \cdot \dfrac{v_r(k) - v_l(k)}{2} \left(\dfrac{R}{L}\right) \\ v_r = u_1 \\ v_l = u_2 \end{cases} \quad (10)$$

where $u_1(k) = v_r(k)$ and $u_2(k) = v_l(k)$ are the input signals and $x(k)$, $y(k)$ and $\theta(k)$ the output signals.

III.1. Simulation Results of Robot CHAR (R1)

An artificial neural network is used to simulate the robot CHAR (R1) which is defined by the Eq. (8).

Fig. 5 presents the evolution of the robot output and the ANN output.

Fig. 6 presents the learning error between the output of char robot and ANN output. For all the simulation, we choose:

$$u_1(k) = sin\left(\frac{k\pi}{25}\right) \quad (11)$$

$$u_2(k) = cos\left(\frac{k\pi}{25}\right) \quad (12)$$

Then, for a fixed learning rate $\eta_1 = 0.32$, the ANN output y_r follows the measured output y with a $NMSE_{e_1}$ is $6\times10^{-4}\%$, θ_r follows the measured output θ with a $NMSE_{e_2}$ is $4\times10^{-4}\%$, whose learning rate is $\eta_2 = 0.27$ and x_r follows the measured output x with a $NMSE_{e_3}$ is $6\times10^{-4}\%$, whose learning rate is $\eta_3 = 0.42$.

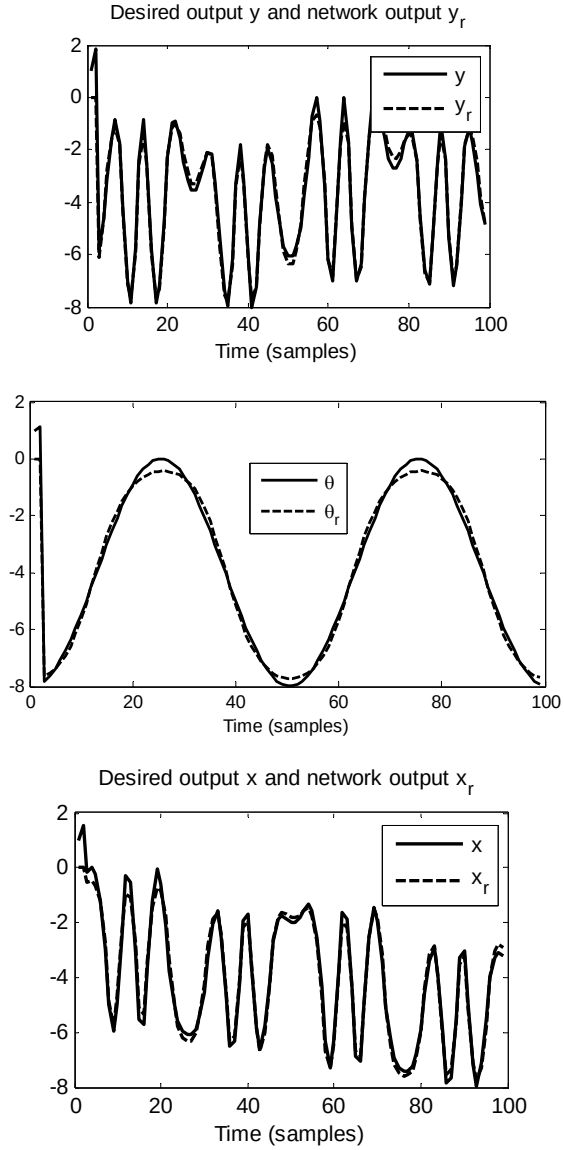

Fig. 5. Outputs of CHAR Robot $[y(k), \theta(k)$ and $x(k)]$ and ANN

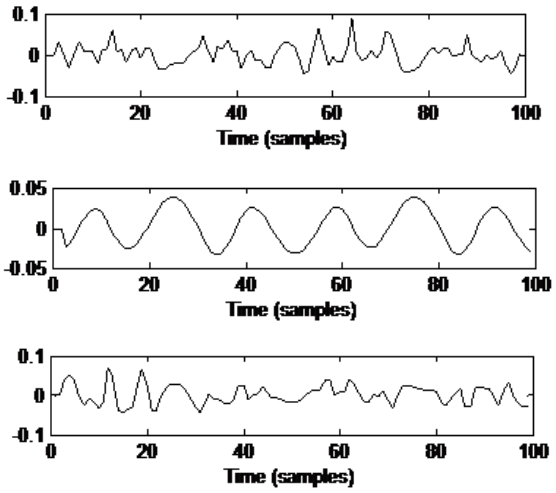

Fig. 6. Learning Errors between the Output of CHAR Robot and ANN

III.2. Simulation Results of Robot KHEPERA (R2)

Fig. 7 presents the evolution of the process output and the ANN output of the system (R2) defined by the Eq. (10). Fig. 8 presents the learning errors between the output robot and ANN. For a fixed learning rate $\eta_1 = 0.41$, the ANN output follows the measured output y with a $NMSE_{e_1}$ is $5\times10^{-4}\%$, θ_r follows the measured output θ with a $NMSE_{e_2}$ is $5\times10^{-4}\%$, whose learning rate is $\eta_2 = 0.39$ and x_r follows the measured output x with a $NMSE_{e_3}$ is $5\times10^{-4}\%$, whose learning rate is $\eta_3 = 0.47$.

IV. Simulation Results of Inverse Robots Models

In this section, we present the neural inverse model [22]-[24], [30]. Artificial neural networks with their inherent learning ability can approximate the inverse robot function and do not require any knowledge of the robot model. The Gradient Descent method is here also used to minimize the function criteria.

IV.1. The Inverse Model

An inverse robot model is given by the following form:

$$u(k) = f^{-1}\begin{bmatrix} y(k+1),...,y(k-ns+1),..., \\ u(k-1),...,u(k-nu+1) \end{bmatrix} \quad (13)$$

with f^{-1}: inverse of the unknown function of robot model. Fig. 9 presents the principle of the neural modelling of the inverse robot model.

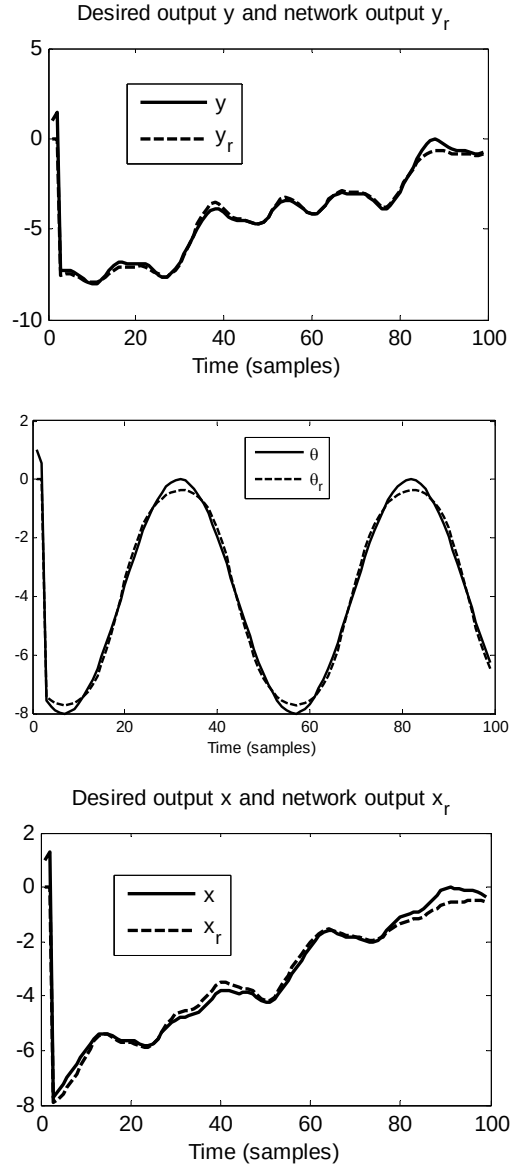

Fig. 7. Outputs of KHEPERA Robot $[y(k), th(k)$ and $x(k)]$ and ANN

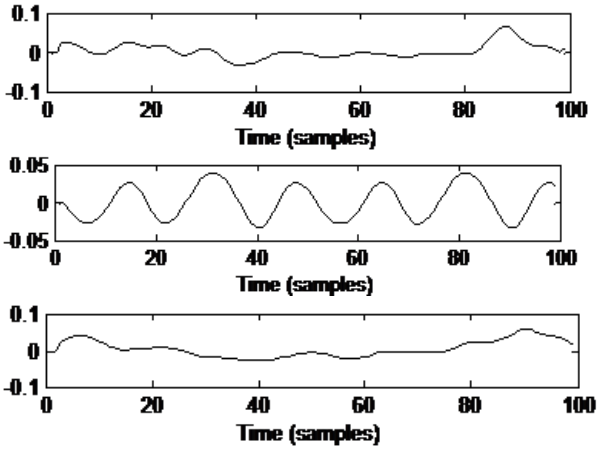

Fig. 8. Learning errors between the Outputs of KHEPERA Robot and ANN

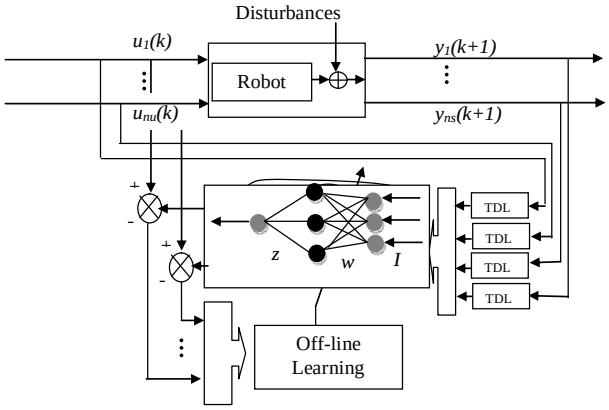

Fig. 9. The general training architecture

IV.2. Simulation Results of Robot CHAR (R1)

Fig. 10 presents the evolution of the process output and the ANN output of the robot (R1).

Fig. 11 presents the learning error between the output robot and ANN.

For a fixed learning rate $\eta_1 = 0.42$, the ANN output ur_1 follows the measured input u_1 with a $NMSE_e$ is $4\times10^{-4}\%$, and ur_2 follows the measured input u_2 with a $NMSE_e$ is $4\times10^{-4}\%$, whose learning rate is $\eta_2 = 0.36$.

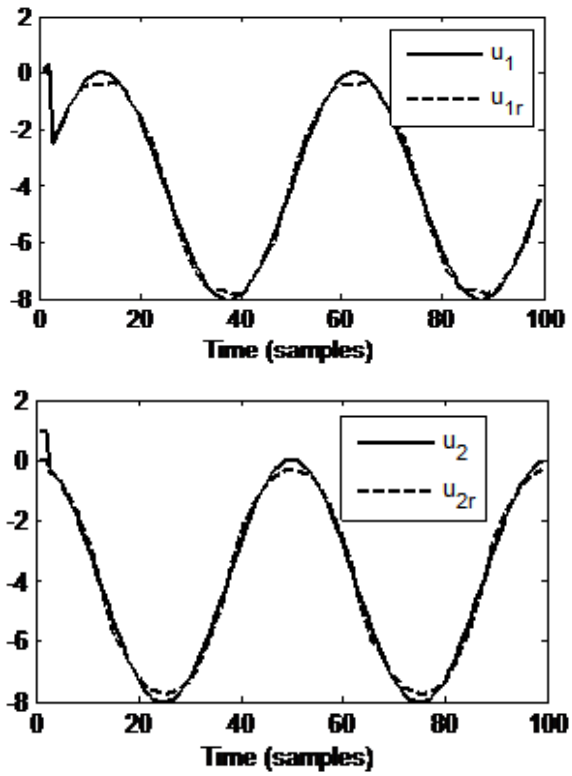

Fig. 10. Inputs of CHAR Robot $\left[u_1(k)\right.$ and $\left.u_2(k)\right]$ and ANN output

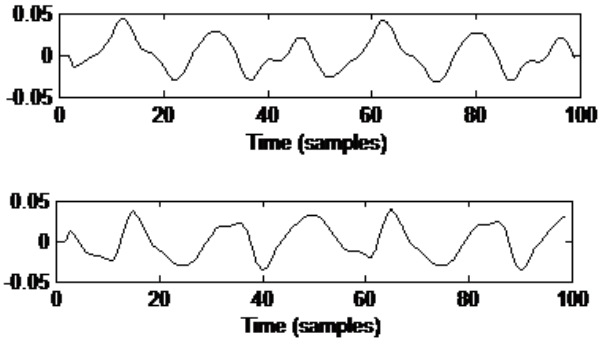

Fig. 11. Learning errors between the input CHAR robot and the output ANN

IV.3. Simulation Results of Robot KHEPERA (R2)

Fig. 12 presents the evolution of the process output and the ANN output of the robot (R2). Fig. 13 presents the learning errors between the output process and ANN.

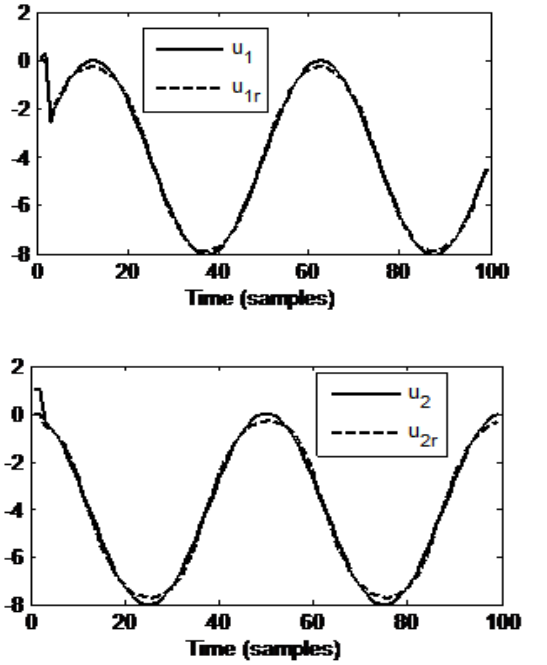

Fig. 12. Inputs of KHEPERA robot $\left[u_1(k)\right.$ and $\left.u_2(k)\right]$ and ANN output

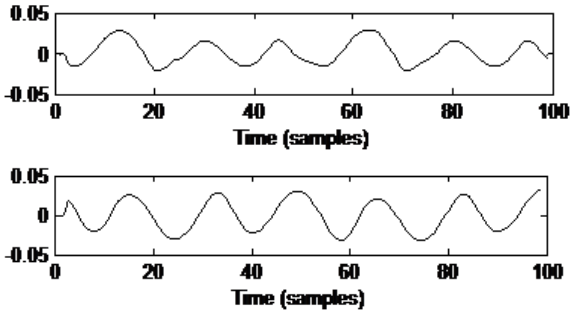

Fig. 13. Learning Error between the Input of KHEPERA Robot and ANN output

Then, for a fixed learning rate $\eta_1 = 0.45$, the ANN output ur_1 follows the measured input u_1 with a $NMSE_e$ is $4\times10^{-4}\%$ and ur_2 follows the measured input u_2 with a $NMSE_e$ is $5\times10^{-4}\%$, whose learning rate is $\eta_2 = 0.48$.

V. Conclusion

This work shows that is possible to use Artificial Neural Networks (ANN) in order to present a very good and reliable solution to the direct model and the inverse model of a mobile robot. This algorithm is tested for two mobile robots: CHAR robot and KHEPERA robot.

The results of used ANN show that it has good and acceptable training error both for the direct and the inverse robot model. At the same time, it is important to say that this technique is easy to implement and to compute. Furthermore, it shows a good performance in terms of the learning speed and the reduced training error.

References

[1] A. Garrell and A. Sanfeliu "Model Validation: Robot Behavior in People Guidance Mission using DTM model and Estimation of Human Motion Behavior problem" The *IEEE/RSJ International Conference on Intelligent Robots and Systems*,Taipei,October 18-22, 2010.

[2] Y. Bassil" Neural Network Model for Path-Planning Of Robotic Rover Systems" *International Journal of Science and Technology*, Vol. 2, No. 2, 2012.

[3] P. A. Nino-Suarez, E. Aranda-Bricaire and M. Velasco-Villa "Discrete-time sliding mode path-tracking control for a wheeled mobile robot" *Proceedings of the 45th IEEE Conference on Decision& Control*, San Diego, December 13-15, 2006.

[4] A. Errachdi and M. Benrejeb., "A new algorithm of neural internal model controller using variable learning rate", *International Journal of Neural and Advanced Applications*, Volume 1, 2014.

[5] E. Fabrizi, G. Oriolo, S. Panzieri and G. Ulivi, "A KF-based localization algorith for nonholonomic mobile robots", in 6th *IEEE Mediterranean Conference on Control and Automation*, pp 130-135.1998.

[6] J. Mo˙zaryn and J. E. Kurek, "Comparison of Neural Network Robot Models with Not Inverted and Inverted Inertia Matrix" W. Duch et al. (Eds.): ICANN, LNCS 3697, pp. 417–422, 2005.

[7] F.L. Lewis, K. Liu and A. Yesildirek, "Neural Net Robot Controller with Guaranteed Tracking Performance". *IEEE Transactions on Neural Networks* 6, pp. 703-715, 1995.

[8] J. Możaryn J. and E. Kurek, "Calculation of Industrial Robot Model Coefficients Using Neural Networks". *Artificial Intelligence and Soft Computing - ICAISC* 2004, pp. 792 - 797, 2004.

[9] J. Mo.zaryn and J.E. Kurek, "Neural Network Robot Model with Not Inverted Inertia Matrix". *Proc. 10th IEEE Int. Conf. on Methods and Models in Automation and Robotics* 2, pp. 1021-1026, 2004.

[10] B. Feng, G. Ma, W.Xie and C. Wang, "Robust tracking control of space robot via neural network", *1stInternational Symposium on Systems and Control in Aerospace and Astronautics*, 2006.

[11] S. Shuzhi, C.C. Ge Hang and L.C. Woon, "Adaptive neural network control of robot manipulators in task space", *IEEE Transactions on Industrial Electronics*, 1997.

[12] C. Wang, B. Feng, G. Ma and C. Ma, "Robust tracking control of space robots using fuzzy neural network", *IEEE International Symposium on Computational Intelligence in Robotics and Automation*, 2005.

[13] L. Mathew Joseph, "*Human-in-the-loop neural network control of a planetary rover on harsh terrain*", Thesis, Georgia Institute of Technology, 2008.

[14] D. Janglová, "Neural Networks in Mobile Robot Motion", *International Journal of Advanced Robotic Systems*, Vol. 1, No 1, pp. 15-22, 2004.

[15] M. Peniak, D. Marocco and A. Cangelosi, "Autonomous Robot Exploration Of Unknown Terrain: A Preliminary Model Of Mars Rover Robot", In *Proceedings of 10th ESA Workshop on Advanced Space Technologies for Robotics and Automation*, Noordwijk, The Netherlands, 2008.

[16] J. Tani, "Model-based Learning for Mobile Robot Navigation from the Dynamical Systems Perspective", *IEEE Trans. on Syst., Man and Cyb*., Vol. 26, No.3, pp. 421-436, 1996.

[17] D. Janglová,"Neural Networks in Mobile Robot Motion", *Inernational Journal of Advanced Robotic Systems*, Vol 1, No 1, pp. 15-22, 2004.

[18] A. Chatti, I. Ayari, P. Borne and M. Benrejeb, " On the use of neural techniques for path following control of a Car-Like mobile robot", *Studies in Informatics and Control*, Vol 14, No 4, pp. 221-234, 2005.

[19] M. Vaezi and M. Ali Nekouie, "Adaptive Control of a Robotic Arm Using Neural Networks Based Approach" *International Journal of Robotics and Automation*, Vo1, Issue: (5), pp. 87-99, 2007.

[20] T. Hester, M. Quinlan and P. Stone, "Generalized Model Learning for Reinforcement Learning on a Humanoid Robot", In *IEEE International Conference on Robotics and Automation*, 2010.

[21] S. Yildirim, "A proposed neural internal model control for robot manipulators", *Journal of Scientific and Industrial Research*, Vol 65, pp. 713-720, 2006.

[22] A. Errachdi and M. Benrejeb. "On-line direct inverse neural network control for nonlinear system". 13th *STA, International conference on Sciences and Techniques of Automatic control and computer engineering*, Monastir, 17-19 December 2012.

[23] A. Errachdi, I. Saad, M. Benrejeb, On-line Identification Method Based on Dynamic Neural Network, (2010) *International Review of Automatic Control (IREACO)*, 3 (5), pp. 474-479.

[24] A. Errachdi, "*Contribution to the adaptive neural control of nonlinear discrete systems with variable parameters*", Thesis, National Engineering School of Tunis El Manar, Tunisia 2012.

[25] Z.Ghania, "*Execution de trajectoire pour robot mobile d'interieur-Réseaux de neuronne*", Thesis, University of Batna Faculty of Engineering Sciences, Algeria 2009.

[26] J. Herrera,"*Trajectory tracking trough predictive control: application to the Khepera robot*", Diploma thesis, 1999.

[27] A.S.P. Niederberger, "*Predictive control Design for a Khepera robot: Principles, Simulations and Real-time Implementation*", Diploma thesis, February 2002.

[28] M. de K-Team : "*Khepera II user manuel*". Switzerland, 2002.

[29] L. Amouri-Jamail, "*Contribution on the Control and the Reactif Pilot of Wheeled Mobile Robots*" Thesis, National Engineering School of Sfax, Tunisia 2012.

[30] B. Hoang Dinh, "*Approximation of the inverse kinematics of a robotic manipulator using neural network*", Thesis, Heriot-Watt University, 2009.

[31] G. W. Irwin, K. Warwick and K. J. Hunt, "Neural Network Applications inControl". *IEE Control Engineering* Series 53, 1995.

[32] Karami-Mollaee, A. and Karami-Mollaee, M. R. (2006). A new approach for instantaneous pole placement with recurrent neural networks and its application in control of nonlinear time-varying systems. *Syst. Contr. Lett*., 55.

[33] A. Errachdi and M. Benrejeb., "A new algorithm for MRAC method using a neural variable learning rate", *International Journal of Neural and Advanced Applications*, Volume 1, 2014.

[34] Negadi, K., Mansouri, A., Marignetti, F., Touam, M., An MRAS based estimation method with artificial neural networks for high performance induction motor drives and its experimentation, (2014) *International Review of Automatic Control (IREACO)*, 7 (2), pp. 123-130.

[35] El Kebir, A., Chaker, A., Negadi, K., A neural network controller for a temperature control electrical furnace, (2013) *International Review of Automatic Control (IREACO)*, 6 (6), pp. 689-694.
[36] Mithra Noel, M., Sharma, A., Biologically inspired decentralized target location estimation using neural networks, (2013) *International Review of Automatic Control (IREACO)*, 6 (5), pp. 612-617.
[37] Filippetti, F., Franceschini, G., Ometto, A., Meo, S., Survey of neural network approach for induction machine on-line diagnosis, (1996) *Proceedings of the Universities Power Engineering Conference*, 1, pp. 17-20.
[38] Filippetti, F., Franceschini, G., Tassoni, C., Meo, S., Ometto, A., Neural network aided on-line diagnostics of induction machine stator faults, (1995) *Proceedings of the Universities Power Engineering Conference*, 1, pp. 148-151.
[39] Di Stefano, R., Meo, S., Scarano, M., Induction motor faults diagnostic via artificial neural network (ANN), (1994) *IEEE International Symposium on Industrial Electronics*, pp. 220-225.

Authors' information

Mahmoud Ines, was born in Ksar Hellal, Tunisia, in 1981.She received the Engineer Diploma degree in Technical of Armaments from the " Military Academy ", Tunisia, in 2006. She obtained the Master of automatic and treatment of signal in 2009 at the "National School of Engineer of Tunisia ". His research related to neural networks, adaptative control and robotic systems.
E-mail: ines.abdellatif.mahmoud@gmail.com

Errachdi Ayachi, was born in Kasserine, Tunisia, in 1982. He received the Engineer Diploma degree in Electrical from the "National School of Engineer of Monastir", Tunisia, in 2005. He obtained the Master of automatic and industrial maintenance in 2007 at the "National School of Engineer of Monastir" and he received the PHD in 2012. His research is related to neural networks, adaptive control and robotic systems
E-mail: errachdi_ayachi@yahoo.fr

Benrejeb Mohamed, was born in Tunisia in 1950. He obtained the Diploma of "Ingénieur IDN" (French "Big School") in 1973, The Master degree of Automatic Control in 1974, the PhD in Automatic Control of the University of Lille in 1976 and the DSc of the same University in 1980. Full Professor at "National School of Engineer of Tunisia" since 1985 and at "Central school of Lille" since 2003, his research interests are in the area of analysis and synthesis of complex systems based on classical and non conventional approaches.
E-mail: mohamed.benrejeb@enit.rnu.tn

Praise Worthy Prize

International Review of Automatic Control (I.RE.A.CO.), Vol. 8, N. 2
ISSN 1974-6059 *March 2015*

A Comparative Study for the Optimization of Active Power of an Electric Power Network

M. Khodja[1], B. Yssaad[2], A. Chaker[3], M. Khiat[4]

Abstract – *In our present article, we present a comparative study between the Hessians methods such as direct search methods (Nelder-Mead Simplex) and indirect research methods that are known as Quasi-Newtonian (BFGS, DFP, Steepest-Descent) and genetic algorithms for optimization of the active power by the minimization of cost and taking into account the constraints of equalities and inequalities. The methods were tested on an electrical network of 57 nodes and the result that we obtained shows the advantage of AG compared to Hessian methods.*

Keywords: *Optimization, Electrical Network, Genetic Algorithms, Hessians Methods, Cost Function*

Nomenclature

C_k	The cost function of the power plant *k* expressed in DA / hour
P_{gk}	Active power generated at the node *k*
P_{chm}	Active power consumed at the node *m*
P_L	Total active losses
N_G	Number of nodes producers
N_C	Number of nodes consumers
r_k	Adjustment constant of calculation (penalty coefficient)
α	Reflection coefficient
β	Coefficient of expansion and value greater than 1
γ	Coefficient of contraction, $0 < \gamma < 1$
K	Represents the reduction coefficient
λ	Linear search strategy
G	Sets of constraints type inequality
H	Sets of constraints type equality

I. Introduction

The primary role of any company responsible for the production of energy is to ensure at all times and in all places coverage active and reactive power required by all users and to ensure an acceptable quality of energy delivered with a cost as low as possible. The problem of economic distribution of energy has become increasingly important with the emergence of energy crisis that requiring more expensive fuel.

Until today, the demand for the consumption of fuel in power plants has become very important and therefore the cost of subsistence necessary for the production of electrical energy is becoming very higher [1]-[18].

The resolution of the cost function minimization task has become easy part especially with the advent of the computer allowing high speed of calculation from its application to the power systems and good control reliability of this distribution in real time. So we must find a way to distribute the production and spread under a minimum possible cost.

For this, we must take into account of everything that can define the cost function of each electrical plant and then assess the overall cost function that is non-linear and multivariate of all production units.

To minimize this function, we will address in this paper, the optimal distribution of active power by Hessian methods and Genetic Algorithms then we finish our work by comparing these methods. [6], [10].

II. Mathematical Model

We consider an electric network supplied by a set of power plant having each several of machines it is clear that at all times the sum of the active power produced by machines is equal to the sum of the active power consumed by the loads ([11]-[13]).

The cost of fuel needed to produce electric power is a monotonic function of the power [6], [10].

So the optimization problem of the active power for each unit of production is linked to the minimization of the total production cost. Mathematically, the problem can be posed as follows:

Minimize:

$$F(P_G) = \sum C_k(P_{Gk}) \tag{1}$$

under the constraints:

$$\sum_{k=1}^{N_G} P_{Gk} - \sum_{m=1}^{N_c} P_{chm} - P_L = 0 \qquad P_{Gk}^{min} \le P_{Gk} \le P_{Gk}^{max} \tag{2}$$

III. Hessian Methods

III.1. Methods of Penalties

The four optimization methods that we will discuss and to use, are methods of unconstrained minimization.

But, our problem is not devoid of these constraints. For this reason, we will use a method based on the transformation of the problem with constraints to an auxiliary problem without unconstrained where the minimum is the same as the original problem.

The basic principle of this method is to change the criteria by adding a penalty function $P(x)$, ie, it bring back the problem of constraint programming to a programming problem without constraints [6], [10].

The problem of nonlinear programming can be expressed by:

$$Min\{F(x), x \in D\} \tag{3}$$

where:

$$D = G \cap H \tag{4}$$

with:

$$G = \{x \ / \ G_i(x) \geq 0, i = 1,2, \dots, n\}$$

and: (5)

$$H = \{x \ / \ H_j(x) \geq 0, j = 1,2, \dots, m\}$$

There are several possibilities for the choice of the penalty function $P(x)$ [6], [10].

In our case, the penalty that is used is mixed. It includes terms of internal penalty represented by I (r_k, G_i) and terms of external penalty are represented by E (r_k, G_i, H_j).

The objective function is written as follows:

$$F_m = F(x) + r_k \sum_{i=1}^{n} \frac{A_i}{G_i(x)} + \\ + \frac{1}{r_k} \sum_{i=1}^{n} D_i G_i^2(x) + \frac{1}{r_k} \sum_{j=1}^{nm} B_j H_j^2(x) \tag{6}$$

along with:

$$\begin{cases} A_i > 0, \ if \ g_i(x) \geq 0 \\ A_i = 0, if \ g_i(x) < 0 \end{cases}$$

$$\begin{cases} D_i > 0, \ if \ g_i(x) < 0 \\ D_i = 0, if \ g_i(x) \geq 0 \end{cases} \tag{7}$$

$$\begin{cases} B_j > 0, \ if \ h_j(x) \neq 0 \\ B_j = 0, if \ h_j(x) = 0 \end{cases}$$

r_k is an adjustment constant of calculation (penalty coefficient). It is chosen such that:

$$r_k > 0 \text{ and } r_k \to 0 \text{ when } k \to \infty$$

with:

$$r_k = r_0(0.1)^k \text{ and } r_0 = 0.1 \tag{8}$$

III.2. Simplex Method of Nelder-Mead

Recall that in the plan En, the points can be represented by polygons. To search the minimum of the function $F(x)$, we select $(n + 1)$ vectors of n dimensions.

Thus the geometric figure formed by these values is called Simplex. In particular, the two-dimensional simplex is an equilateral triangle with three vertices. The objective function can be evaluated for each point representing one of the vertices of the polygon [6], [10].

A projection is made from the point giving the largest value of the objective function (point A) through the center of gravity ("centroid") of the polygon.

The point A is removed and a new polygon called "reflection" is formed. The latter is composed of the remaining items and new point being the symmetry of A.

The minimum values of $F(x)$ are found from a series of operations such as expansion, contraction. The two-dimensional case is illustrated by the following figure. [6], [10].

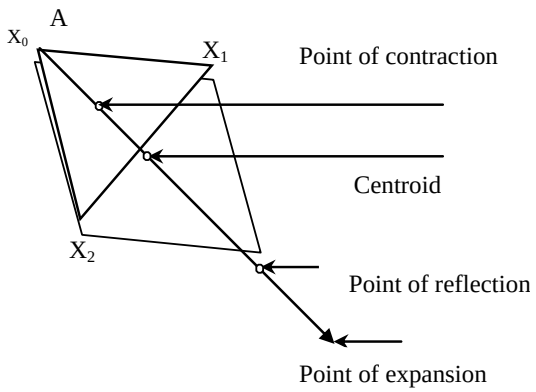

Fig. 1. Figure geometric called Simplex

Resolution algorithm

Step 1: Initialization of the vector x_i^0.
Step 2: Calculation of x_h, x_l such as:

$$F(x_h^k) = max[F(x_0^k), \dots, F(x_n^k)]$$

$$F(x_0^k) = min[F(x_0^k), \dots, F(x_n^k)] \tag{9}$$

Step 3: Calculation of xnh such as:

$$F(x_{nh}^k) \geq F(x_1^k) \text{ and } x_{nh} \neq x_h \tag{10}$$

Step 4: Calculation of xn + 2 is the center of gravity (centroid) of the $(n + 1)$ except items x_h^k:

$$x_{n+2}^k = \frac{1}{n} \sum_{i=1}^{n} x_i^k ; \quad i \neq h \tag{11}$$

Step 5: "Reflection".

Conduct reflection x_h through the centroid, calculating:

$$x_{n+3}^k = (1+\alpha)x_{n+2}^k - \alpha x_h^k \quad (12)$$

with $\alpha > 0$.

If $(x_i) \leq F(x_{n+3}^k) < F(x_n)$, replace x_h by x_{n+3}.

Hence, a new geometric shape is well formed and why, we will apply a second thought to this new simplex.

Step 6: "Expansion"

If the reflection is achieved with great success, we will have a new minimum:

$$F(x_{n+3}) < F(x_1) \quad (13)$$

We proceed with the expansion of the vector (x_{n+3} - x_{n+2}), we calculate:

$$x_{n+4}^k = \beta x_{n+3}^k + (1-\beta)x_{n+2}^k \quad (14)$$

If $F(x_{n+4}^k) \geq F(x_{n+3}^k)$, we replace x_l by x_{n+4} and we go back to the step (3) to calculate the new centroid.

Otherwise, we replace x_l by x_{n+3} and we go back to the step (3) to calculate the new.

Step 7: "Contraction"

If the reflection is not better (unsuccessfully) where:

$$(F(x_{n+3}^k) \geq F(x_h^k))$$

we proceed to the contraction of the vector (x_h - x_{n+2}) while calculating:

$$x_{n+5}^k = (1-\gamma)x_{n+2}^k + \gamma x_h \quad (15)$$

If the contraction is good ($F(x_{n+5}) < F(x_h)$).

This means that the result is the same as in the case where the reflection is reached

Step 8: «Reduction»

If $F(x_{n+5}) > F(x_h)$, we proceeded to the reduction of all vectors (x_i - x_l) i = 1,2,.., n, while calculating:

$$x_i^k = x_i^k + K(x_1^k - x_i^k) \quad (16)$$

and we return to the step (2).

III.3. Method of Davidon-Fletcher-Powel

This is a Quasi-Newton method based on a generalization of Newton's formula [1]-[4]. To apply to our case, we are forced to bring the problem with constraint to the problem without constraints, by applying a penalty method. The principle of the D.F.P method is based on a generalization of the iterative Newton formula:

$$x^{k+1} = x^k - \lambda_k H_k \nabla F(x^k) \quad (17)$$

To construct an approximation of the inverse of the Hessian, the algorithm uses the D.F.P following correction formula:

$$H_{k+1} = H_k + \frac{u_k u_k^t}{u_k^t y_k} - \frac{H_k y_k y_k^t H_k}{y_k^t H_k y_k} \quad (18)$$

where:

$$\begin{aligned} u_k &= x^{k+1} - x^k \\ y_k &= \nabla F(x^{k+1}) - \nabla F(x^k) \end{aligned} \quad (19)$$

Step 1: Initialization P_{G0}, and H_0 Hessian matrix is positive definite (we take $H_0 = I$ matrix unit), k=0.

Step 2: Determination of the direction of movement:

$$d_k = -H_k \nabla F_m(P_G^k) \quad (20)$$

Step 3: Calculate of:

$$P_G^{k+1} = P_G^k + \lambda d_k \quad (21)$$

λ is chosen to minimize $F_m(P_G^{k+1})$. We use it for a linear search strategy (line search).

Step 4: Calculate of:

$$\begin{aligned} u_k &= P_G^{k+1} - P_G^k \\ y_k &= \nabla F_m(P_G^{k+1}) - \nabla F_m(P_G^k) \end{aligned} \quad (22)$$

Step 5: Calculate of formula (18).

Step 6: Stop the test if not, we go back to step 2.

III.4. Method of Broiden-Fletcher-Goldfarb - Shanno (B.F.G.S)

The principle of this method is essentially a generalization of the iterative Newton formula (17) [3].

λ is selected so as to minimize $g(\lambda) = F(x^k + \lambda d_k)$ in the direction $d_k = -H_k \nabla F(x^k)$

The matrix H_k is modified at each iteration by the B.F.G.S correction formula (18) and (19).

Resolution algorithm

Step 1: Choice of P_{G0} and H_0, where H_0 Hessian matrix is positive definite (we take $H_0 = I$ matrix unit).

Step 2: Determination of the direction of movement formula 20.

Step 3: Calculate of formula (21).

Step 4: Calculate of formula (22).

Step 5: Calculate of formula (18).

Step 6: Stop the test if not, we go back to step 2.

III.5. Method of Stronger Slope (Steepest Descent)

The principle of this method is based on the steepest-descent direction $d_k = -\nabla F(x^k)$.

The basic equation of the iterative calculation is given as follows:

$$x^{k+1} = x^k - \lambda_k d_k \quad (23)$$

λ is selected so as to minimize: $F(x^k - \lambda \nabla F(x^k)$.

We used to do this, the quadratic interpolation.

Resolution algorithm

Step 1: Choose a starting point P_G, k=0

Step 2: calculation of the descent direction:

$$d_k = -\nabla F_m(P_G^k)$$

Step 3: Determination of λ to minimize the function $F_m(P_G^k + \lambda_k d_k$ with $\lambda \geq 0$ using the quadratic interpolation)

Step 4: Determination of the new value with formula (21).

Step 5: Stop the test if not, we go back to step 2.

IV. Genetic Algorithms

The Genetic Algorithms (GA) are part of a family of stochastic methods, there are called evolutionary methods based on an analogy with the theory of natural evolution, that individuals of a population best adapted to their environment are more likely to survive, recur from generation to generation, providing even better adapted descendants ([14]-[18]).

The characteristic of these algorithms is that they are assessing populations of individuals encoded by a binary string. They use operator's mutation and recombination of different types.

The purpose of a genetic algorithm is to optimize a particular function in a specific search space [6], [10].

Their research had two main objectives:

- To highlight and rigorously explain the process of adaptation in natural systems.
- Design artificial systems that have important properties of natural systems.

Genetic algorithms do not use the values of the function studied, not its derivative, or another auxiliary knowledge. It is the rules of probabilistic transitions, and non-deterministic.

The (GA) are evolving a population of solutions under the action of specific rules: elitist selection and genetic operators (crossing, mutation) in order to optimize a given behavior. In a very general level, the operation of a GA is then based on the following steps (Figure 2):

1. Initializing: an initial population of N chromosomes is randomly selected.
2 Evaluation: Each chromosome is decoded and evaluated.
3. Selection: Creating a new population of N chromosomes by using an appropriate method of selection.
4. Reproduction: Possibility of crossover and mutation (step (e)) within the new population.
5. Back to the assessment phase as the stop condition of the problem is not satisfied.

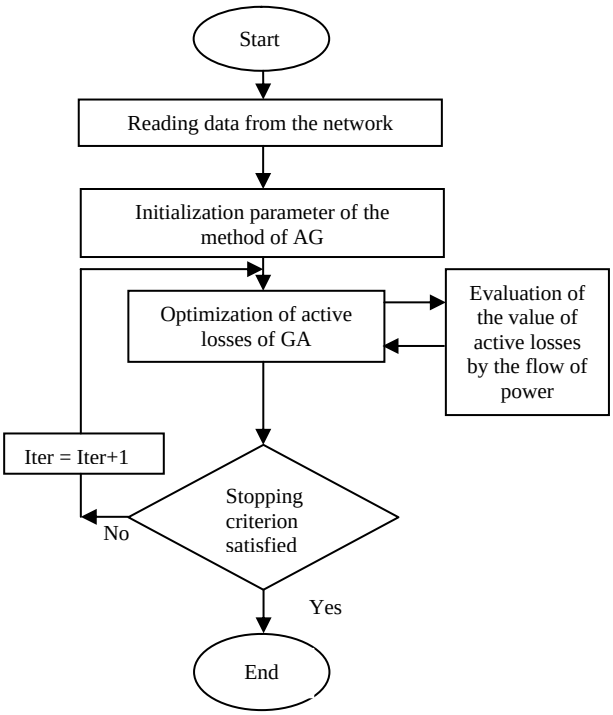

Fig. 2. Organization of optimization of active losses by AG

V. Numerical Results

The IEEE 57-bus power system [6], [10] consists of 7 generator buses, 42 load buses, and 78 branches. The fuel cost in ($/hr) equations for the generator are:

$$F_1(P_{G1}) = 0.0776\, P_{G1}^2 + 20\, P_{G1} + 0.0$$
$$F_2(P_{G2}) = 0.0100\, P_{G2}^2 + 40\, P_{G2} + 0.0$$
$$F_3(P_{G3}) = 0.2500\, P_{G3}^2 + 20\, P_{G3} + 0.0$$
$$F_6(P_{G6}) = 0.0100\, P_{G6}^2 + 40\, P_{G6} + 0.0$$
$$F_8(P_{G8}) = 0.0222\, P_{G8}^2 + 20\, P_{G8} + 0.0$$
$$F_9(P_{G9}) = 0.0100\, P_{G9}^2 + 40\, P_{G9} + 0.0$$
$$F_{12}(P_{G12}) = 0.0323\, P_{G12}^2 + 20\, P_{G12} + 0.0$$

and the constraints are: (the unit operating ranges in MW):

$$00 \leq P_{G1} \leq 575.88$$
$$00 \leq P_{G2} \leq 100$$
$$00 \leq P_{G3} \leq 140$$
$$00 \leq P_{G6} \leq 100$$
$$00 \leq P_{G8} \leq 550$$
$$00 \leq P_{G9} \leq 100$$
$$00 \leq P_{G12} \leq 410$$

The total load was 1250.8 MW. Transmission losses PL are computed using B coefficients.

➢ **Parameters values for GA**

The parameters values for GA have a number of population size, crossover and mutation probability, chromosomes length and number of generations:

- Population size: 30;
- Crossover probability: 0.75;

- Mutation probability :0.006
- Chromosomes length: 12;
- Number of generations: 300.

The minimum cost and active power are presented in Table I.

TABLE I
MINIMUM COST AND ACTIVE POWER

	B.F.G.S	Nelder Mead	Steep Descente	D.F.P	GA
P_{G1}^{opt} (MW)	146.2450	253.3937	148.2877	144.3520	140.3748
P_{G2}^{opt} (MW)	74.3554	97.4581	97.1819	82.4852	89.0269
P_{G3}^{opt} (MW)	50.7469	94.996	42.5168	45.7821	43.599
P_{G6}^{opt} (MW)	75.0718	40.5421	74.7290	78.2581	89.0269
P_{G8}^{opt} (MW)	508.5044	528.1941	509.5666	511.756	490.0603
P_{G9}^{opt} (MW)	75.3594	94.2465	75.9673	76.8546	89.0268
P_{G12}^{opt} (MW)	348.3431	170.6699	330.4405	339.197	337.5959
Cost ($/hr)	42201	44760	42190	42178	42170

The results of the genetic algorithm are shown in the Fig. 3 below. In this figure, we see clearly the importance of using genetic algorithms to optimize the active power of electric networks while comparing with other methods used in this work.

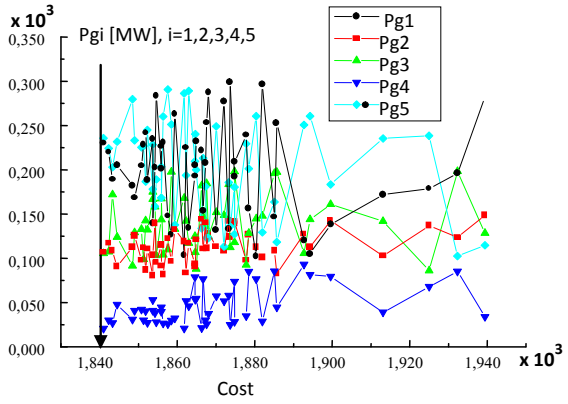

Fig. 3. Active power vs. cost by AG

VI. Conclusion

According to the results, we find that the Load flow method gives results with a very large cost. But, by optimizing the active power of an Electric Power Network with indirect methods of research (B.F.G.S, D.F.P, Steepest-Descent), we obtain more accurate results than the direct search method (Nelder-Mead simplex) .We can say that the Quasi-Newtonian BFGS method proves to be the best given the low value of the production cost and the time of calculation.

For both Quasi-Newtonian methods (B.F.G.S and D.F.P), we note that the gap in the optimal power generated and the cost of production is almost the same, we find that the BFGS method has a computation time much better than the D.F.P method.

We wish to emphasize that the illustration of the penalty method for the four methods require a choice of penalty coefficient (r (k)). Tests carried out for different values of (r (k)) clearly show the influence of the latter on the convergence of methods. This excludes the recommendation of a single value (r (k)) for different methods and different networks.

We have studied and applied the method of GA with a well appropriate and accurate model to calculate the optimal distribution of active power. For this purpose, we can say that the genetic algorithm method is more robust and efficient for solving the multivariable functions while comparing with the use of hessians method.

The application of AG led us to conclude that the cost and losses in standards and are better than those found by Hessian methods and there are very encouraging in the field of optimization. The Genetic algorithms seem to be very effective and are an important research topic in the context of optimizing the management of electrical networks.

Acknowledgements

We thank the entire team of the Research Laboratory for Simulation, Control, Analysis and Maintenance Electrical Network "SCAMRE", for his immense help in performing our work; we also thank the reviewers for their constructive suggestions expected.

References

[1] I. Papic, P. Zunko, D. Povh, M. Weinhold, “Basic control of unified power flow controller”. *IEEE Trans. Power Syst.*, vol. 12, no. 4, pp. 1734–1739, 1997.

[2] Farahat, M.A., Talaat, M., The using of curve fitting prediction optimized by genetic algorithms for short-term load forecasting, (2012) *International Review of Electrical Engineering (IREE)*, 7 (6), pp. 6209-6215.

[3] A Turgeon, “ Optimal from the principle of progressive optimality”, *Water resources research*, vol 17, pp 481-486, June 1981

[4] D G Luenberger,”*Linear and nonlinear programming*”, Addison-Wesley publisging company Inc, 1984.

[5] D P Bertsekas, “ *Nonlinear Programming*”, 2nd edition, Athena Scientific MIT, 2004

[6] Rahiel D- Répartition *Optimal power taking into account heuristics of a complex electrical system* - thesis - June 2009 USTOran.

[7] Rahiel, D., Khiat, M., Chaker, A., Haimour, R., Reactive power optimization in transmission power system using interior point method, (2010) *International Review of Electrical Engineering (IREE)*, 5 (2), pp. 614-618.

[8] Khiat M, Rahiel D, Chaker A, Frioui Z- Optimal Reactive power Dispatch and Voltage Control Using Interior Point Method- *Revue Acta Electronica*, volume 52, Number 2, 2011, pp 81-85.

[9] Abderrahmani, A., Chaker, A., Laoufi, A., Fuzzy-logic controller for STATCOM, (2012) *International Review of Electrical Engineering (IREE)*, 7 (6), pp. 6245-6251.

[10] Otsmani, Z., Khiat, M., Chaker, A., A genetic algorithm to minimize the periodic preventive maintenance cost in electrical system, (2011) *International Review of Electrical Engineering (IREE)*, 6 (3), pp. 1439-1445.

[11] Bracale, A., Caramia, P., Carpinelli, G., Meo, S., A low voltage Smart Grid control strategy with Power Quality issues, (2011) *International Review of Electrical Engineering (IREE)*, 6 (6), pp. 2704-2712.
[12] Damiano, A., Gatto, G., Marongiu, I., Meo, S., Perfetto, A., Serpi, A., Single-stage grid connected PV inverter with active and reactive power flow control via PSO-PR based current controlled SVPWM, (2012) *International Review of Electrical Engineering (IREE)*, 7 (4), pp. 4647-4654.
[13] Meo, S., Sorrentino, V., Discrete-time integral variable structure control of grid-connected PV inverter, (2015) *Journal of Electrical Systems*, 11 (1), pp. 102-116.
[14] Eslami, M., Shareef, H., Mohamed, A., Khajehzadeh, M., Damping of power system oscillations using genetic algorithm and particle swarm optimization, (2010) *International Review of Electrical Engineering (IREE)*, 5 (6), pp. 2745-2753.
[15] Jazebi, S., Jazebi, S., Rashidinejad, M., Application of a novel real genetic algorithm to accelerate the distribution network reconfiguration, (2009) *International Review of Electrical Engineering (IREE)*, 4 (1), pp. 114-121.
[16] Mohamed, F.A., Koivo, H.N., Multiobjective genetic algorithms for online management problem of microgrid, (2008) *International Review of Electrical Engineering (IREE)*, 3 (1), pp. 46-54.
[17] Bouslama-Bouabdallah, S., Tagina, M., A fault detection and isolation fuzzy system optimized by genetic algorithms and simulated annealing, (2010) *International Review on Modelling and Simulations (IREMOS)*, 3 (2), pp. 212-219.
[18] Rezaie Estabragh, M., Mohammadian, M., Rashidinejad, M., An application of elitist-based genetic algorithm for SVC placement considering voltage stability, (2010) *International Review on Modelling and Simulations (IREMOS)*, 3 (5), pp. 938-947.

Authors' information

[1]University Center AHMED ZABANA of RELIZANE Algeria.
Tel.: 213550670280.
E-mail: Khodja_1970@hotmail.com

[2]University Center AHMED ZABANA of RELIZANE Algeria.
Tel.: 213550232405
E-mail: benyssaad_y@yahoo.fr

[3]Department of Electrical Engineering at ENSET-Oran, Algeria.
Tel.: 213773201236
E-mail: mounir.khiat@enset-Oran.dz

[4]Department of Electrical Engineering at ENSET-Oran, Algeria.
Tel.: 213771385940
E-mail: chakeraa@yahoo.fr

Mohamed Khodja is a professor at the university center Ahmed Zabana of RELIZANE Algeria. He holds a magister in electrical engineering. He is a member of the laboratory ''SCAMRE'' His research focus is the optimization and modeling in the field of electrical systems.

Benyssaad Yssaad is a professor at the university center Ahmed Zabana of RELIZANE Algeria. He holds a doctorat in electrical engineering. He is a member of the laboratory ''SCAMRE'' His research focus is the optimization and modeling in the field of maintenance of electrical systems.

Abdelkader Chaker is a professor in the department of electrical engineering of the ENSET, in Oran, Algeria. He received a PhD degree in engineering systems from the university of Saint-Petersburg. He is a Director of "SCAMRE" laboratory. His search activities include the control of large power systems, multiconverter systems and unified power flow controller. His teaching includes neural process control and real time simulation of power systems.

Mounir Khiat is a professor in the Department of Electrical Engineering at the ENSET, Oran, in Algeria; he received a doctorate in Electrotechnics form the University of USTO, Oran. He is a member of the laboratory "SCAMRE". His research interests are: the maintenance of electrical systems, control systems, electric power, FACTS devices and HVDC systems.

Praise Worthy Prize

International Review of Automatic Control (I.RE.A.CO.), Vol. 8, N. 2
ISSN 1974-6059 *March 2015*

A Comparative Study between Dual Fuzzy Logic and Sliding Mode Control MPPT Techniques Applied to PV Pumping System

S. Abdourraziq, R. El-Bachtiri

Abstract – *The aim of this paper is to present a comparison investigation of the performance characteristics of two different Maximum Power Point Tracking (MPPT) techniques applied to photovoltaic (PV) pumping system. A dual fuzzy logic control technique and slide mode control command are developed and simulated by Matlab/Simulnk environment, the comparison is done to identifying the advantages and drawbacks of each technique for different values of radiation and temperature. The studied system consists of photovoltaic panel, dc-dc boost converter, a group motor-pump, and a storage tank. Simulation results obtained show the variation of the accuracy and speed response time with variation of condition atmospheric for each method, and verify their influence in the efficiency of the PV pumping system.* ***Copyright © 2015 Praise Worthy Prize S.r.l. - All rights reserved.***

Keywords*: PV Pumping System, MPPT, Dual Fuzzy Logic Control (DFLC), Slide Mode Control (SMC), Motor-Pump*

I. Introduction

To extract water from surface or underground, it is necessary to use pumps. The pumps need a source to be entrained.

Solar energy using as source to pump water has become one of the most promising applications of photovoltaic (PV) standalone systems, especially in rural areas that have a significant amount of solar radiation and do not have access to national grids. Depending on the state of the place, pumping water can be used in many applications such as domestic use, water for irrigation and village water supplies [1][2].

Different types of motors and pumps are available on the PV pumping market. Several studies have been done on the choice of the drive system, which suits PV source.

The most commonly pump used are: centrifugal or volumetric pump, depending on the state of the place. Single-stage centrifugal pumps are frequently used in PV shallow water pumping for low head applications. For PV subterranean water pumping and surface water pumping with higher heads, multistage centrifugal pumps are more suitable. Other types of pumps are used such as progressive cavity pumps [3], and piston pumps [4].

The PMDC motor and induction motor are the most type motor used in PV pumping system application. The choice of motor depends on several factors: the requirements of the size, efficiency, price, reliability and availability.

The power conditioning has a role to optimize the transferred energy between the PV generator and the motor-pump set. Power conditioning can be a DC/ AC inverter for an AC electric motor or a DC/DC inverter for a DC electric motor.

The Maximum Power Point Tracking (MPPT) command is a functional component of each PV systems; it allows to search the optimum operating point of the PV generator, for different weather conditions. In the literature, many techniques of maximum power point tracking (MPPT) have been proposed, the incremental conductance method (IncCond) [5], fraction of the short-circuit current [6], fraction circuit voltage open [6], fuzzy logic control [7] and other MPPT methods [8]-[9].

These methods vary in their complexity, reliability, cost, and their adaptation with variation of radiation and temperature. The improvement of MPPT algorithm optimize the efficiency of the PV panel, which aims to the maximization of the global efficiency, will lead consequently to maximize the drive speed and the water discharge rate of the coupled pump. In this paper, a simple and efficient photovoltaic water pumping system is presented. We proposed a comparative study between two different MPPT commands is done. The studied methods are dual fuzzy logic control [10]-[11] and slide mode control command [12], [17], [18], the choice of these methods is based on their robustness, their efficiency compared to traditional techniques, and low cost. The comparison allows to show the advantages and drawbacks of each method, and their influence in the efficiency of PV pumping system studied. The proposed MPPT techniques was tested in MATLAB/SIMULINK environment, under changed value of irradiance and temperature, to define the accuracy and speed response time of each method. The obtained results was compared and resumed in tables. The studied system consists of the PV array, the DC-DC boost converter, and the DC motor-pump. The block diagram of the PV pumping system proposed is shown in Fig. 1.

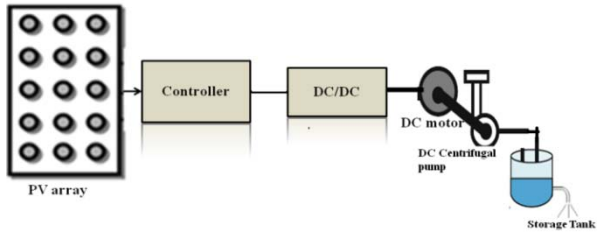

Fig 1. General configuration of a photovoltaic pumping system

II. PV Panel Model

PV panel is a p-n junction semiconductor, which converts light into electricity. In the literature, there are several mathematical models which describe the I − V characteristic [13]. The difference between these models is the procedure of the calculation, the intervening parameters number to compute the I –V characteristic and results accuracy. The equivalent circuit of a PV module is shown in Fig. 2. Based on this circuit model, the behavior of the PV array may be described by Eq. (4):

$$I = I_{ph} - I_d - I_p \tag{1}$$

with:

$$I_d = I_o\left(exp\left(\frac{V_j \cdot q}{K_o \cdot T}\right) - 1\right) \tag{2}$$

and:

$$I_p = \frac{V + R_s \cdot I}{R_p} \tag{3}$$

$$I = I_{ph} - I_o\left(exp\left(\frac{V_j \cdot q}{K_o \cdot T}\right) - 1\right) - \frac{V + R_s \cdot I}{R_p} \tag{4}$$

where:
V is the PV output voltage, I is the PV output current, I_{ph} is the photocurrent, I_0 is the saturation current, R_s is the series resistance, R_p is the shunt resistance, q is the electronic charge, n is the diode factor, K_o is the Boltzmann's constant, T is the junction temperature.

The output simulation results of the P-V and I-V curves of the PV cell for different values of radiation (G = 1000, 800, 600, 400 W/m²) are presented in Figs. 3(a), (b).

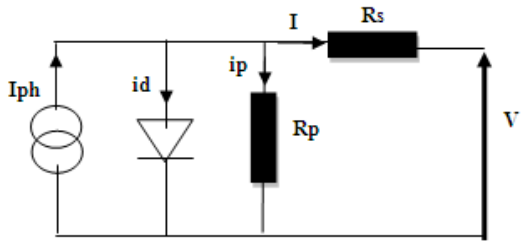

Fig. 2. Equivalent circuit of PV cell

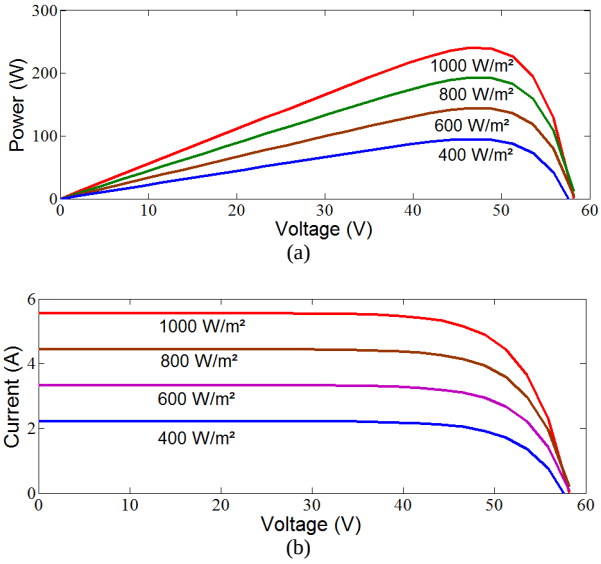

Figs. 3. Output characteristics of PV array (a) P-V, (b) I-V

III. Maximum Power Point Tracking (MPPT) Technique

In order to drive the load at the maximum supplied power of PV panel, a dc-dc boost converter is used for a better matching PV generator and motor-pump load around the optimal power is needed (Fig. 4).

The dc-dc boost converter [14] is an electronic power converter whose output voltage is higher than the input voltage. The expression of the output voltage depending on the input voltage and duty cycle is expressed as follow:

$$V_o = \frac{1}{1-\alpha} V_{pv} \tag{5}$$

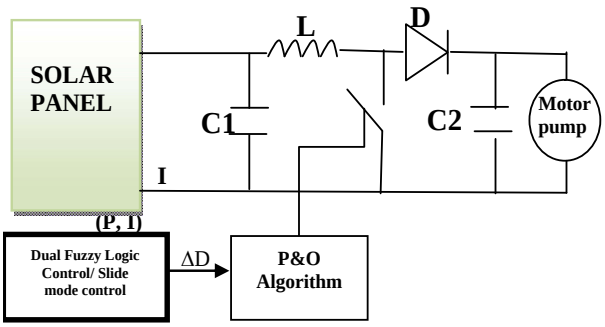

Fig. 4. Model of coupling PV generator with motor-pump load and MPPT command

The variation of duty cycle enables the PV generator to operate at the desired value. We note that the adaptation is performed when the output voltage V_{pv} and output current I_{pv} are equal to optimal voltage and current respectively.

In order to improve the efficiency, it is necessary to apply excellent MPPT technique to track the MPP of photovoltaic cell more stably and accurately.

The traditional MPPT techniques used in the literature, to extract MPP can't satisfy both performance requirements of fast dynamic response and good accuracy during the steady state at the same time.

The compared methods studied in this paper are characterized by a technique of search of MPP, with a variable step size allowing a good tracking of the MPP when atmospheric conditions change. A detailed description of each proposed method is shown in chapters bellow.

III.1. Dual Fuzzy Logic Controller MPPT Command

The fuzzy logic allows to define control laws of any process starting from a linguistic description of the control strategy to be adopted. The fuzzy logic controller technique has been used for tracking the MPP of PV systems since it has the advantages such as it is robust, relatively, not needing an accurate mathematical model, and does not require the knowledge of an exact model.

The dual fuzzy logic controller studied [10] can track the MPP of photovoltaic panel accurately and simultaneously with variation of weather conditions. When the operating point is far away from the MPP, the controller choose the Far tuning fuzzy control, the operating point track rapidly the MPP.

When the operating point is near from the MPP, the controller choose the near tuning mode control, the output power of the PV array is stable and more accurate. In other way, the two FLC intervene in different time.

The description of the principle of the method is presented Fig. 5.

The power is calculated from photovoltaic voltage and current:

$$P = V_{pv} \cdot I_{pv} \tag{6}$$

The dual mode control is categorized into three different sections. The principal elements of the DFLC systems are shown in Fig. 5. The input variables of the DFLC are (ΔP) and (ΔI) the variation in PV power and the variation of PV current, respectively; moreover the output of the DFLC is the variable step-size (ΔD) of the P&O algorithm.

The advantage of this method that the step-size using to track MPP are not fixed, it depends on positioning of optimum output power, under different values of radiation and temperature.

Which improve greatly the precision of search and the speed of response time.

III.2. Sliding Mode Control MPPT Command

In the literature, different papers are developed the sliding mode control technique [11]-[12], [17] to track the MPP of the PV generator. This method presents the advantages of robustness, simplicity and good performance. The control circuit adjusts the duty cycle of the switch with the different variation of radiation and temperature to track the MPP of the PV panel.

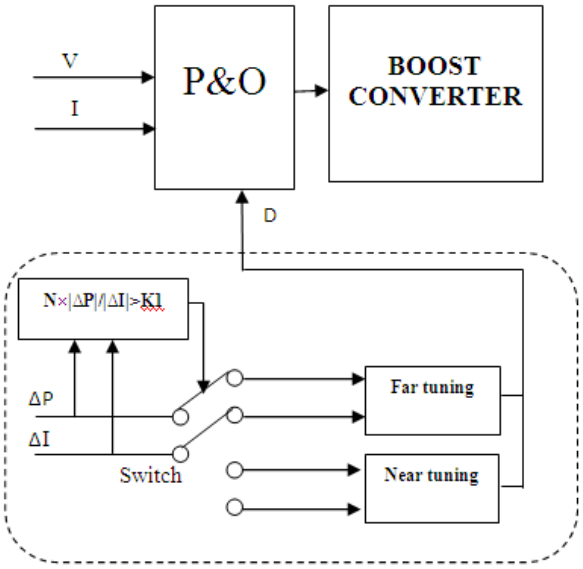

Fig. 5. Principle of FLC dual Control [10]

The traditional sliding mode control method use a limited surface to search the MPP, which causes a great oscillations and slow response time when atmospheric conditions change. The good choice of the surface can improve significantly the accuracy of tracking of MPP, and convergence time. We introduce the concept of the approaching control.

We select the sliding surface as:

$$\frac{dP_{pv}}{dV_{pv}\left(V_{pv}\right)} = 0 \tag{7}$$

$$\frac{dP_{pv}}{dV_{pv}} = \frac{d\left(V_{pv} \times I_{pv}\right)}{dV_{pv}} \tag{8}$$

$$\frac{dP_{pv}}{dV_{pv}} = I_{pv} + V_{pv}\frac{dI_{pv}}{dV_{pv}} \tag{9}$$

The sliding surface is given by the following equation:

$$\sigma = I_{pv} + V_{pv}\frac{dI_{pv}}{dV_{pv}} \tag{10}$$

The present paper develops a novel strategy of sliding mode control command, to track the MPP with more precision and a short response time. We choice from the curve of power-voltage two surfaces: large surface σ_L and small surface σ_S (Fig. 6).

The principle of search of the MPP is: if the reference power is far from the MPP of the PV generator, so we are in the large surface, the required of P_{ref} is maximized to the MPP, which will be reached in few steps. Thus, the track of the maximum power point is accelerated.

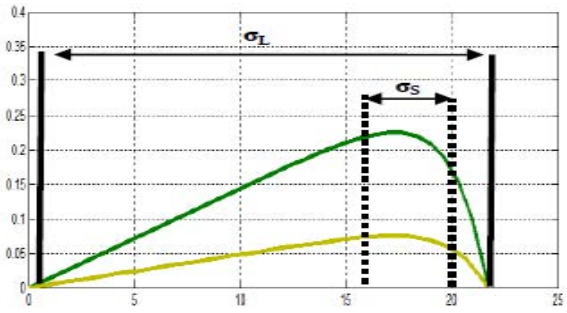

Fig. 6. The division of surface in the curve following a sudden change of insolation

Else if the P_{ref} is near to MPP, we are in the small surface, the required update of P_{ref} is minimized with a big accuracy of searching. The equation of P_{ref} is:

$$P_{ref} = N\frac{|\Delta P|}{|\Delta V|} \quad (11)$$

when P_{ref} is far from MPP. The proposed technique choose large surface, so the equations become:

The equivalent duty cycle must lies in $0.1<\alpha_{eq}<0.9$ The real controls signal α is proposed as:

$$\alpha = 0.9 \quad \text{if} \quad \alpha_{eq} + k\sigma \geq 0.9 \quad (12)$$

$$\alpha = \alpha_{eq} + k\sigma \quad \text{if} \quad 0.1 < \alpha_{eq} + k\sigma < 0.9 \quad (13)$$

$$\alpha = 0.1 \quad \text{if} \quad \alpha_{eq} + k\sigma \leq 0.9 \quad (14)$$

when P_{ref} is near from MPP. The proposed technique choose small surface, so the equations become:

The equivalent duty cycle must lies in $0.6<\alpha_{eq}<0.8$ The real controls signal α is proposed as [18]:

$$\alpha = 0.8 \quad \text{if} \quad \alpha_{eq} + k\sigma \geq 0.8 \quad (15)$$

$$\alpha = \alpha_{eq} + k\sigma \quad \text{if} \quad 0.6 < \alpha_{eq} + k\sigma < 0.8 \quad (16)$$

$$\alpha = 0.8 \quad \text{if} \quad \alpha_{eq} + k\sigma \leq 0.8 \quad (17)$$

The proposed equation of the reference power allows calculating of the novel power simultaneously with variation of insolation and temperature. It determines the position of the power at each moment, which facilities the task of tracking MPP. The simulation results of the proposed SMC technique compared to dual fuzzy logic command are presented in the next section; they show clearly the efficiency of each method with PV pumping system.

IV. Simulation Results

In order to evaluate the efficiency of each method, their advantages and drawbacks, and its influence on the reliability of the PV pumping system entrained by DC motor and coupled to a centrifugal pump, a simulation is realized in Matlab/Simulink environment, and the different results obtained are shown in the figures bellow

The PV generator source used is Shell SP75, it has the characteristics recorded in Table I. also, the parametric of the dc-dc Boost converter employed have been noted in Table I. The parameters of boost interface used are shown in Table II.

TABLE I
ELECTRICAL PARAMETERS OF SES96M

Maximum power(Pmpp)	240 W
Voltage at MPP(Vmpp)	48.5 V
Current at MPP(Impp)	4.95 A
Open circuit voltage(Voc)	58.2 V
Short circuit current(Isc)	5.55 A

TABLE II
PARAMETERS BOOST CONVERTER

C1	2mF
C2	800uF
L	10mH
R	100Ω

VI.1. Simulation Results with Fixed Radiation and Temperature

The output characteristics of the power and current of each method at G=1000w/m² and T =25°C are presented in figures below.

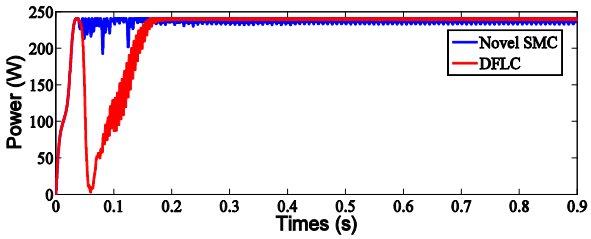

Fig. 7. Caracteristics of the output power of PV panel with DFLC and SMC

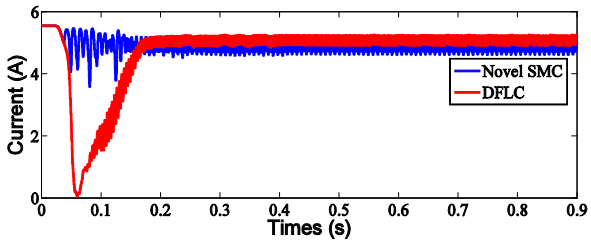

Fig. 8. Caracteristics of the output current of PV panel with DFLC and SMC

The Figs. 7, 8 show the output power and current of the PV panel, using two different MPPT techniques. We note that the dual fuzzy logic control method presented in red color has a perturbation at the start of the system till 0.2s, and its stabilize after with a good accuracy.

The sliding mode control expressed in blue color, has a speed response time, but a great oscillations compared to DFLC.

We can deduce that DFLC is characterized by a slow response time but a good accuracy. The SMC command has a problem of oscillation, which decreases the quality of tracking, but it presents a speed response time.

The output characteristics with variable values of temperature and radiation are presented in chapter bellow

VI.2. Simulation Results for Variable Radiation and Temperature

In this section, we present a comparison between proposed DFLC and SMC technique applied to PV water pumping system, at variable values of radiation (G=500, 1000, 600W/m²), and temperature (T=20, 30, 25°C).

The difference between two methods and the influence of proposed algorithm on system behavior is presented for different weather conditions in following figures.

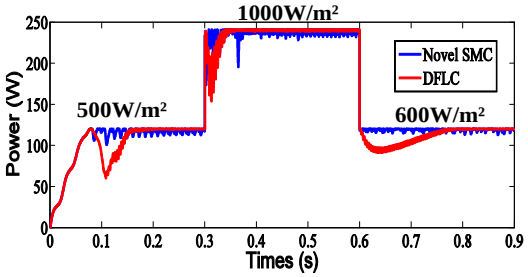

(a)

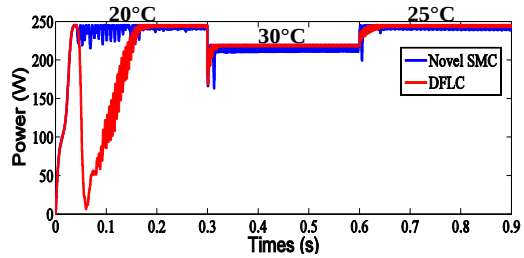

(b)

Figs. 9. The output behaviour of the power of the PV panel using DFLC and SMC for (a) variable radiation, (b) variable temperature

The simulation results for output power for irradiance changed from 500W/m², to 1000 W/m² at 0.3s, and from 1000 to 800W/m^2 at 0.6 are shown in Fig. 9(a).

We note that with each start, we obtain lateness with oscillation, but the curve stabilizes after. The DFLC presents a good accuracy with slow speed time. In the beginning, the output power don't stabilize till 0.15s, the same thing when the radiation changes to 1000W/m², and 600W/m². We can remark that the systems used DFLC MPPT technique are slow, but with good accuracy of searching of the MPP (Fig. 9(a)).

On the other side, the SMC MPPT method presents a speed response time, but a considerable oscillations and perturbations, which influence in the system stability.

The blue curve shows clearly the considerable oscillation compared to DFLC command. Fig. 9(b) presents the simulation results of the output power for temperature changed from 20°C, to 30°C at 0.3s, and from 30°C to 25°C at 0.6 are shown in Fig. 9(b). In each case, the solar irradiation is set as 1000W/m^2.

The output current of the PV panel for variable values of radiation at 25°C is shown in Fig. 10.

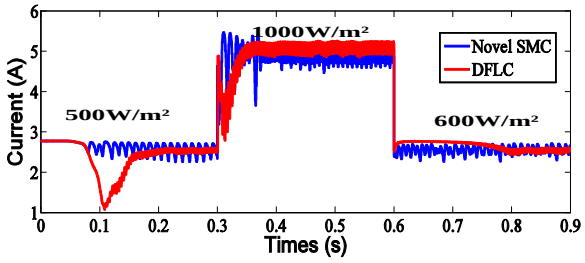

Fig. 10. The output characteristic of the current of the PV panel using DFLC and SMC for variable radiation

The response performance of each method with fixed radiation applied to PV water pumping system is resumed in Table III.

TABLE III
COMPARISON BETWEEN THE STUDIED MPPT FOR HIGH IRRADIATION (1000w/m², T=25°C)

MPPT	Response time	Ripple (A)	Mean value (240W)
Novel SMC	0.06s	0.8A	237.25
DFLC	0.16s	0.3A	239.82W

The comparison of the performance of each method apllied to PV pumping system at low temperature (T=20°C and G=1000W/m²) is presented in table below.

TABLE IV
COMPARISON BETWEEN THE STUDIED MPPT FOR LOW TEMPERATURE (1000w/m², T=20°C)

MPPT	Response time	Ripple (W)	Mean value (244W)
Novel SMC	0.04s	0.5A	242.42W
DFLC	0.16s	0.29A	244.2W

The tables show the differnce of response time, ripple and the value of the output power. For comparison, the values explain clearly the diference between the studied techniques.

The optimizationand the good choice of the MPPT technique allows to the maximization of the global efficiency, will lead consequently to maximize the drive speed and the water discharge rate of the coupled centrifugal pump.

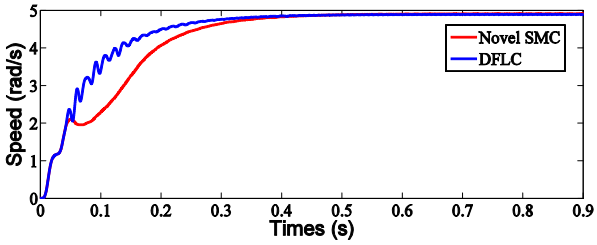

Fig. 11. Output speed of the DC motor driven by PV generator using DFLC and SMC MPPT techniques

The Figure 11 above shows the increase of the speed ω of the DC motor drived by PV generator.

The characteristics present the diference of the behavior of the speed in each case, whan we use DFLC MPPT technique and SMC command.

We can note that characteristic of the output speed track the behavior of the output power of the PV panel. The same remarks deduced from the output power are available to the speed. The improvement of accuracy and speed response time of the output power of photovoltaic pumping system compared with the traditional P&O method.

V. Conclusion

In this paper, a comparison study between two developed maximum power point tracking techniques applied to PV water pumping system driven by DC motor and coupled to a centrifugal pump has been presented. The comparison is done to defining the advantages and drawbacks of each method, to use the efficient method. The main concluding remarks are summarized as follows:

- The obtained simulation results of the dual fuzzy logic control MPPT technique has a slow speed response time, but a good accuracy,
- The sliding mode control method has a fast speed time with a considerable oscillations, which influence in the quality of the output power of the system,
- We can deduce that a combination between two methods lead to a good improvement of the performance of the system.

References

[1] Moussi, A. Torki, An improved efficiency permanent magnet brushless DC motor PV pumping system, *LARHYSS Journal*, N°.01, Mai 2002.

[2] Abdourraziq Sarah, El Bachtiri Rachid, Modeling of a photovoltaic pumping system using centrifugal pump and DC motor, *Sustainability in Energy and Buildings: Research Advances, Mediterranean Green Energy Forum* 2013 (MGEF-13): Vol.2 : pp.1-6 : mgf13s-002.

[3] A. Betka , A. Attal, Optimization of a photovoltaic pumping system based on the optimal control theory, *Solar Energy* 84 (2010) 1273–1283.

[4] Nejib Hamrouni , Moncef Jraidi, Theoretical and experimental analysis of the behaviour of a photovoltaic pumping system, , *Solar Energy* 83 (2009) 1335–1344.

[5] Guan-Chyun Hsieh, Hung-I Hsieh, Photovoltaic Power-Increment Aided Incremental-Conductance MPPT With Two-Phased Tracking, *IEEE Transactions on Power Electronics*, Vol. 28, No. 6, June 2013.

[6] Moacyr Aureliano Gomes de Brito, Luigi Galotto, Evaluation of the Main MPPT Techniques for Photovoltaic Applications, *IEEE Transactions on Industrial Electronics*, Vol. 60, No. 3, March 2013, pp 1156-1166.

[7] K. Benlarbi, L. Mokrani, A fuzzy global efficiency optimization of a photovoltaic water pumping system, *Solar Energy* 77 (2004) 203–216.

[8] Sreekanth.S, Jacob Raglend, A Comparitive AND Analytical Study OF Various Incremental Algorithms Applied IN Solar Cell, 2012 *International Conference on Computing, Electronics and Electrical Technologies [ICCEET]*, 2012 IEEE pp 452- 456.

[9] Sarah, A.; Rachid, E.B., A perturb and observe method using fuzzy logic control for PV pumping system, *IEEE Multimedia Computing and Systems* (ICMCS'14), pp 1608-1612.

[10] Abdourraziq, S., El Bachtiri, R., A novel MPPT dual fuzzy logic applied to resistive load and PV pumping system, (2014) *International Review of Automatic Control (IREACO)*, 7 (4), pp. 344-352.

[11] SARAH ABDOURRAZIQ, RACHID EL BACHTIRI, A Perturb and Observe Method using Dual Fuzzy Logic Control for Resistive Load, *Recent Advances in Environmental Science and Biomedicine*, ISBN: 978-960-474-391-9,pp 107- 112.

[12] Biel, D.; Fossas, E., "Application of sliding-mode control to the design of a buck-based sinusoidal generator", *Industrial Electronics, IEEE Transactions on* (Volume:48 , Issue: 3), p 563 – 571.

[13] Badia Amrouche, Abderrezak Guessoum, "A simple behavioural model for solar module electric characteristics based on the first order system step response for MPPT study and comparison", *Applied Energy* 91 (2012) 395–404.

[14] K. L. Rao and CH. Sibabu .*Theory of power Electronics.* First Edition. S.Chand& company Ltd, Newdelhi.

[15] Mohammed Ali Elgendy, Bashar Zahawi, "Comparison of Directly Connected and Constant Voltage Controlled Photovoltaic Pumping Systems", *IEEE Transactions on Sustainable Energy*, Vol. 1, No. 3, October 2010, pp 184- 192.

[16] Mrityunjaya Kappali, Dr. Uday Kumar R. Y., "*An Approach to Reduce the Size and Cost of PV Panel in Solar Water Pumping"*, 2010 5th *International Conference on Industrial and Information Systems*, ICIIS 2010, Jul 29 - Aug 01, 2010, India.

[17] Meo, S., Sorrentino, V., Discrete-time integral variable structure control of grid-connected PV inverter, (2015) *Journal of Electrical Systems*, 11 (1), pp. 102-116.

[18] Shouman, M., El Bayoumi, G., Adaptive Robust Control of Satellite Attitude System, (2015) *International Review of Aerospace Engineering (IREASE)*, 8 (1), pp. 35-42.

Authors' information

Sidi Mohammed Ben Abdellah University, LESSI Lab FSDM, REEPER Group, EST, Fez, Morocco.

Abdourraziq Sarah was born in Rabat, Morocco, on December 23, 1988. She received the Master's degree from Sidi Mohamed Ben Abdellah University, Faculty of Science and Technologies, she is PhD student at USMBA, with the LESSI Lab FSDM, REEPER Group, EST Fez, Morocco, From July, 2011
E-mail: Sarah.abdourraziq@usmba.ac.ma

Rachid El-Bachtiri, Professor at Sidi Mohammed Ben Abdellah University, LESSI Lab FSDM, REEPER Group, EST, Fez, Morocco
E-mail: Rachid.albachtiri@usmba.ac.ma

Praise Worthy Prize

International Review of Automatic Control (I.RE.A.CO.), Vol. 8, N. 2
ISSN 1974-6059 *March 2015*

Braking of Three Phase Induction Motors by Controlling Applied Voltage and Frequency Based on Particle Swarm Optimization Technique

Mahmoud M. Elkholy, M. A. Elhameed

Abstract – *Braking of three phase induction motors is required in many industrial applications. This paper introduces braking of three phase induction motors using particle swarm optimization (PSO) technique. The objective is to determine the optimum values of the applied voltage and frequency during braking to stop the motor in a certain time with minimum braking energy losses to limit any excessive thermal heating. The proposed technique is important and more useful in applications of repeated braking cycles. The results are compared with that obtained using plugging braking method and it's found that the proposed technique gives lower braking energy and shorter braking time. The braking energy losses with the proposed method are about 20% of the plugging braking energy losses with the same braking time. The proposed method determines the variation of optimal values of applied voltage and frequency to have a certain braking time of three phase induction motor at a certain load torque with minimum braking energy losses. The characteristics of the motor are simulated using SIMULINK/MATLAB.*

Keywords*: Braking, Induction Motor, Plugging, PSO, Regenerative Braking*

Nomenclature

u_{Sd}	d-axis stator voltage
u_{Sq}	q-axis stator voltage
i_{Sd}	d-axis stator current
i_{Sq}	q-axis stator current
i_{Rd}	d-axis rotor current
i_{Rq}	q-axis rotor current
λ_{Sd}	d-axis component of stator flux linkage
λ_{Sq}	q-axis component of stator flux linkage
λ_{Rd}	d-axis component of rotor flux linkage
λ_{Rq}	q-axis component of rotor flux linkage
R_S	Resistance of stator winding
R_R	Resistance of rotor winding referred to stator
L_S	Self inductance of stator winding
L_R	Self inductance of rotor winding
M	Mutual inductance between stator and rotor windings
θ	Rotor displacement
T_L	Load torque
J	Moment of inertia kg m^2
B	Rotor friction
p	Number of poles
p_{cu}	Motor copper losses
p_{iron}	Motor iron losses
I_S	Stator phase current
I_R	Rotor phase current referred to stator
V	Stator phase voltage
R_C	Core loss resistance

I. Introduction

Braking of three phase induction motors is an important issue especially in industrial applications that require multi stop in a definite time. Braking can be mechanical through friction or electrical. Mechanical braking results in waste of rotor stored kinetic energy and excessive heat.

Electrical braking has many methods such as plugging, regenerative and dynamic braking. Plugging depends on reversing the direction of the rotating field by changing the supply phase sequence, this results in an opposing torque that stops the motor.

Plugging results in high currents, serious overheating and the motor must be disconnected when the speed reaches zero otherwise it will revolve in the opposite direction. If the motor speed is greater than synchronous speed, the slip is negative. In this case the motor acts as a generator retuning the energy to supply, this is called regenerative braking.

Dynamic braking is achieved by disconnecting the supply and connecting external resistances across motor terminals, in this case rotor kinetic energy is converted into heat losses. Other braking methods can also be used such as DC injection, zero sequence, magnetic and capacitor self-excitation braking.

The issue of induction motor braking is discussed in literature, for example [1] deals with sensorless vector control of pulse width-modulated inverter-fed induction motor drives equipped with a three-phase diode rectifier.

An electronically controlled braking resistor across the dc link is not used, but instead, the power regenerated during braking is dissipated in the motor. In [2] braking of three phase induction motor is done using combination of two or more conventional methods, it is found that effective braking is obtained by applying different methods at different speed ranges, but this will result in complex circuit for braking. Braking torque in non-regenerative AC drives without the need of additional power circuits is discussed in [3]. In [4] conventional methods of braking, branch elimination method in conjunction with conventional tensor technique is used to establish a digital computer program to simulate the system. In [5], [6] two braking methods are examined to reduce motor current, one based on the injection of an AC voltage to the rotor winding during braking.

The injected voltage must have the same frequency, same phase shift and opposite in direction to the rotor induced voltage.

The second method depends on discrete variable frequency control using three phase inverter, AC thyristors monitored by a microcontroller PIC. Reducing energy loss during braking is examined by using direct torque control in [7], the method is investigated with constant and traction load toques.

Optimization of braking energy is a nonlinear problem; it is suitable to examine heuristic optimization techniques to solve this problem. PSO is used extensively to design, control and operate three phase induction motor [8]-[11]. The rule of the PSO in this paper is to find the suitable variation of voltage and frequency during a certain braking period to minimize energy losses in the motor, this will result in less heat and allow for frequent braking in a certain time.

II. Mathematical Model

The voltage equations of three phase squirrel cage induction motor in d-q frame are [12], [16]:

$$u_{Sd} = i_{Sd}R_s + \frac{d}{dt}\lambda_{Sd} - \dot{\theta_S}\lambda_{Sq} \tag{1}$$

$$u_{Sq} = i_{Sq}R_s + \frac{d}{dt}\lambda_{Sq} + \dot{\theta_S}\lambda_{Sd} \tag{2}$$

$$0 = i_{Rd}R_R + \frac{d}{dt}\lambda_{Rd} - \dot{\theta_R}\lambda_{Rq} \tag{3}$$

$$0 = i_{Rq}R_R + \frac{d}{dt}\lambda_{Rq} + \dot{\theta_R}\lambda_{Rd} \tag{4}$$

The flux linkages are defined by:

$$\lambda_{Sd} = L_S i_{Sd} + M i_{Rd} \tag{5}$$

$$\lambda_{Sq} = L_S i_{Sq} + M i_{Rq} \tag{6}$$

$$\lambda_{Rd} = L_R i_{Rd} + M i_{Sd} \tag{7}$$

$$\lambda_{Rq} = L_R i_{Rq} + M i_{Sq} \tag{8}$$

The electromagnetic torque equation is:

$$T_e = \frac{3}{2}\frac{p}{2}\frac{M}{L_R}(i_{Sq}\lambda_{Rd} - i_{Sd}\lambda_{Rq}) \tag{9}$$

The mechanical equation is:

$$T_e - T_L = J\frac{d\dot{\theta}}{dt} + B\dot{\theta} \tag{10}$$

The model of three phase squirrel cage induction motor is developed by SIMULINK /MATLAB to solve the above nonlinear equations and to study the dynamic performance characteristics of the motor.

The SIMULINK dynamic model of the motor is shown in Fig. 1. Energy lost in the motor is defined as:

$$w = \int_0^t (p_{cu} + p_{iron})\, dt \tag{11}$$

$$p_{cu} = 3I_S^2 R_S + 3I_R^2 R_R \tag{12}$$

$$p_{iron} = \frac{3V^2}{R_C} \tag{13}$$

The proposed method to optimize braking energy losses depends on changing motor input voltage and frequency according to the equations:

$$f = K_{f2} - K_{f1}t \tag{14}$$

$$V = K_V f \tag{15}$$

where; K_{f1}, K_{f2} and K_v are constants. The ratio of voltage to frequency K_V must be limited to prevent motor saturation.

Fig. 2 shows the SIMULINK model with these variable voltage and frequency.

III. Optimum Voltage and Frequency Variations Using PSO

In this part PSO is used to determine the constants K_v, K_{f1} and K_{f2} in Eqs. (14) and (15). The objective function is to minimize equation (11) at certain braking time with the following inequality constraint to prevent saturation in the motor:

$$\frac{V}{f} < 5$$

Fig. 3 shows the flow chart of PSO operation, for a certain load torque a swarm of 24 agents is initialized, for each agent the motor dynamic model is operated, and the objective function is evaluated.

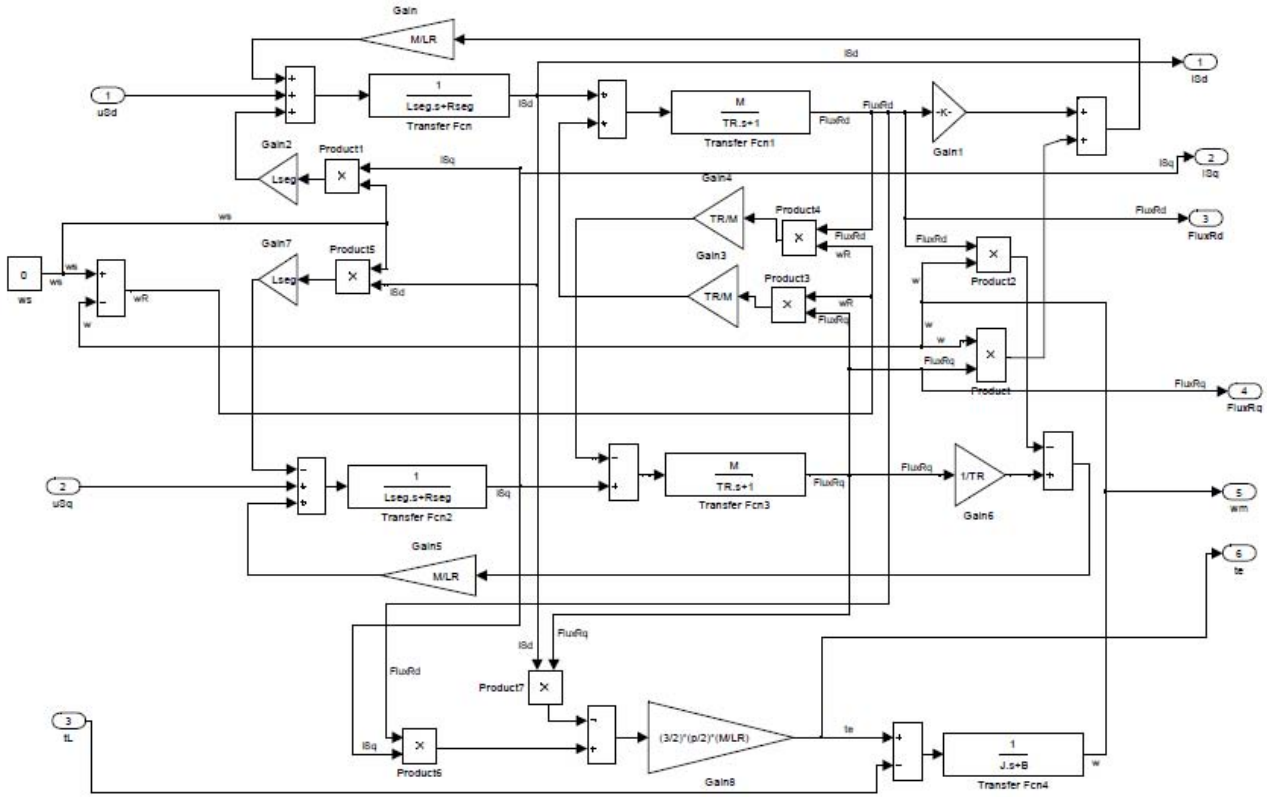

Fig. 1. Simulink Model of three phase induction motor

Agents are moved to their new position according to their velocities, their best position and the best position of the swarm. Agents velocity in swarm is updated according to the equation [13]:

$$v_i^{k+1} = wv_i^k + c_1 rand_1 \times \left(pbest_i - s_i^k\right) + \\ +c_2 rand_2 \times \left(gbest - s_i^k\right) \quad (16)$$

where v_i^k is velocity of agent i at iteration *k*, *w* is weighting function, c_j is weighting coefficients, rand is random number between 0 and 1, s_i^k is current position of agent i at iteration *k*, $pbest_i$ is best position of agent i, and gbest is best position of the swarm. The weighting function w is given by:

$$w = w_{max} - \frac{w_{max} - w_{min}}{iter_{max}} \times iter \quad (17)$$

where w_{max} is initial weight, w_{min} is final weight, $iter_{max}$ is maximum iteration number, and iter is current iteration number.

According to Shi and Eberhart [14], [15], the following parameters are appropriate and the values do not depend on problems:

$$c_i = 2,\ w_{max} = 0.9 \text{ and } w_{min} = 0.4 \quad (18)$$

Maximum number of iteration is $iter_{max}$ = 50. This process is repeated for a braking time of 4, 4.5 and 5 s at load torque of 0.5 N m.

IV. Results and Discussion

Simulation has been carried out using SIMULINK/MATLAB for 220/380 V, 1.1 kW, 50 Hz three phase induction motor having the following parameters:

R_S = 5.15 Ω R_R = 3.75 Ω
L_S =0.5887 H L_R =0.5887 H
M=0.5568 H p =2

In this section two groups of results are presented, the first one is the performance characteristics of the motor which is braked using conventional plugging method, by reversing two phases of the motor.

In the second case the motor is braked with the proposed method by controlling the applied voltage and frequency to stop the motor within certain time with minimum energy losses. All results are taken at load torque of 0.5 N m and the motor runs in motoring mode with rated voltage and frequency from 0 sec to 6 s, after that the motor is in braking mode.

IV.1. Plugging Method

The braking time with plugging is 5 s as shown in Fig. 4. The developed torque is reversed during plugging and reducing the motor speed in the same direction of load torque as shown in Fig. 5. Therefore, the speed is decreased from load speed to zero and to prevent rotation in reverse direction the applied voltage is removed.

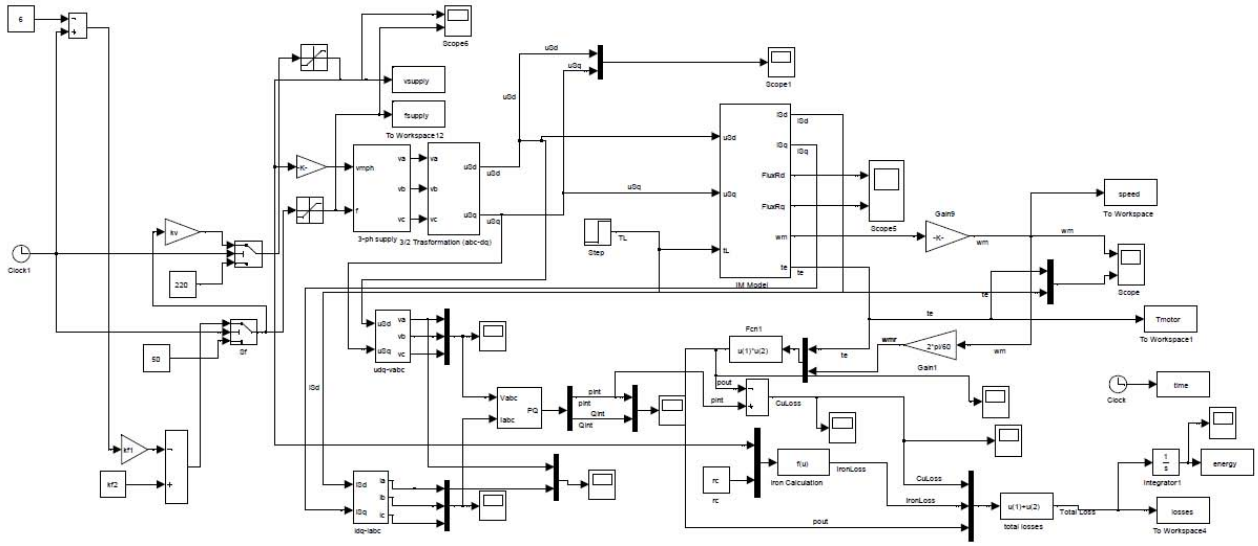

Fig. 2. SIMULINK system scheme

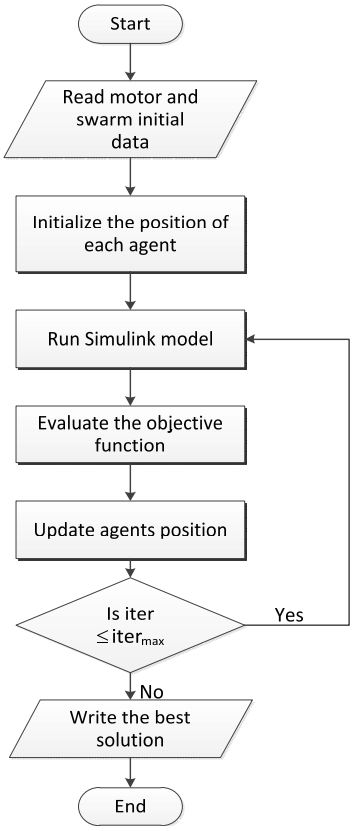

Fig. 3. Flow Chart of PSO

The motor current during plugging is higher than the starting current as shown in Fig. 6 because the motor slip during plugging is higher than 1 and hence the motor impedance is lower than that during stating. So the motor losses during plugging are higher than that during starting as shown in Fig. 7. Fig. 8 shows the variation of input and output powers with time.

The motor draws power from supply during motoring and plugging modes. The output power during plugging is reversed due to the reverse of torque direction.

During motoring mode the difference between input and output powers is converted into losses but during plugging both of input power and output power are converted into losses. Therefore the plugging losses are high. Fig. 9 shows the variation of energy losses during one cycle of operation of starting, running and braking.

The energy losses during braking with plugging are 14548 Joule within braking time of 5 s and this energy losses are converted into heat.

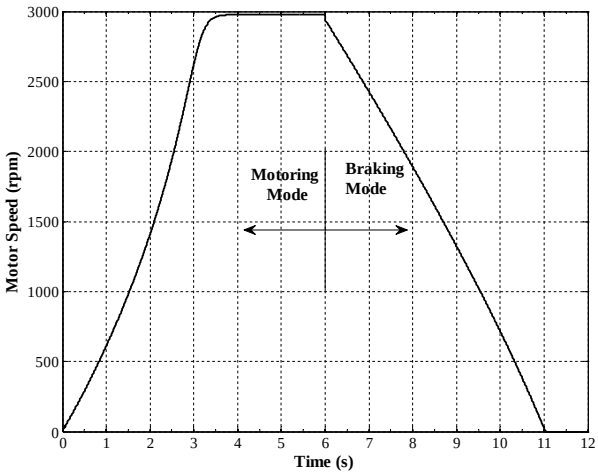

Fig. 4. Variation of motor speed with time (plugging method)

IV.2. Proposed Method

The performance characteristics of three phase induction motor with the proposed method of controlling both applied voltage and frequency to have minimum braking energy losses at certain braking time with PSO are shown in Figs. 10 to 17. Fig. 10 shows the variation of motor speed with time at different braking time of 4, 4.5 and 5 s using the proposed method. The braking developed torque with lower braking time is higher than that of higher braking time as shown in Fig. 11.

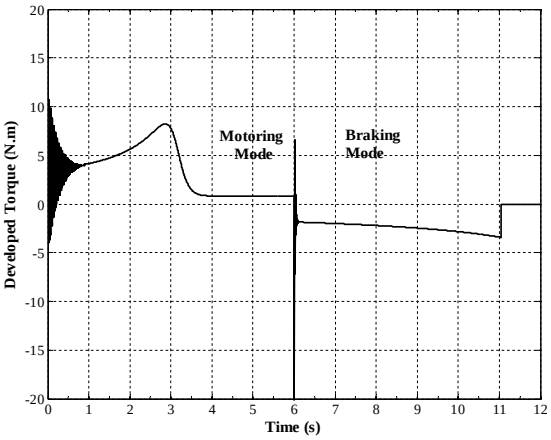

Fig. 5. Variation of developed torque with time (plugging method)

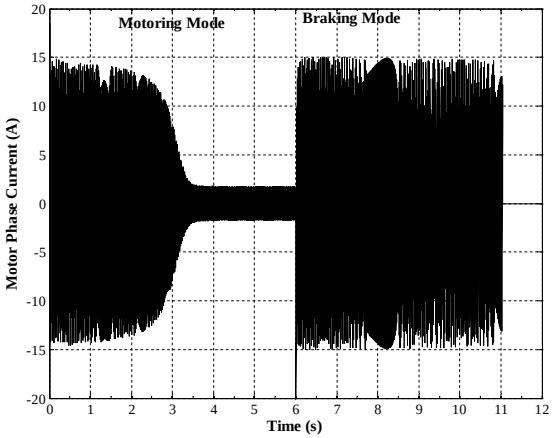

Fig. 6. Variation of motor phase current with time (plugging method)

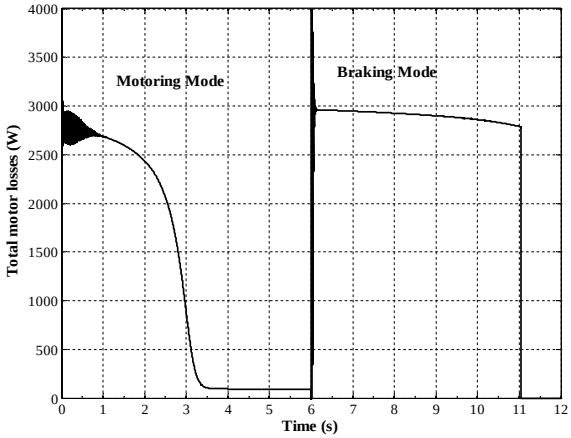

Fig. 7. Variation of total motor losses with time (plugging method)

Motor current in braking mode is lower than starting current and also lower than plugging braking current as shown in Fig. 12. Therefore, the motor losses and energy losses are reduced compared with of plugging method as shown in Fig. 13 and Fig. 14. The braking energy losses are 2884 Joule with braking time of 5 s, 2734 Joule with braking time of 4.5 s and 2944 Joule with braking time of 4 s. With the same braking time of 5 s, the braking energy losses with the proposed method are about 19.8 % of braking energy losses with plugging method. Therefore, the proposed method is more useful method to save energy for multi-braking applications.

With the proposed method, the motor can be braked with time shorter than plugging braking time with lower braking energy losses. In Fig. 15, the input power is the electrical power from supply and output power is the mechanical power.

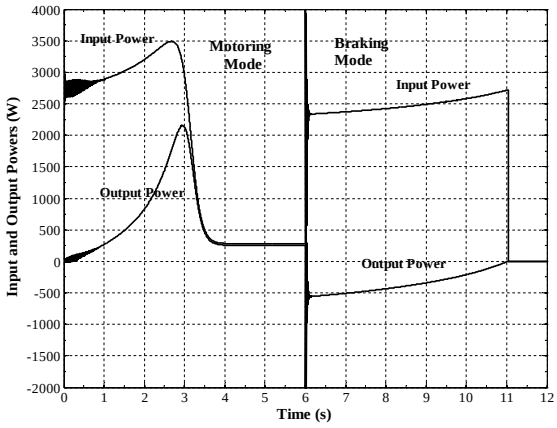

Fig. 8. Variation of input and output powers with time (plugging method)

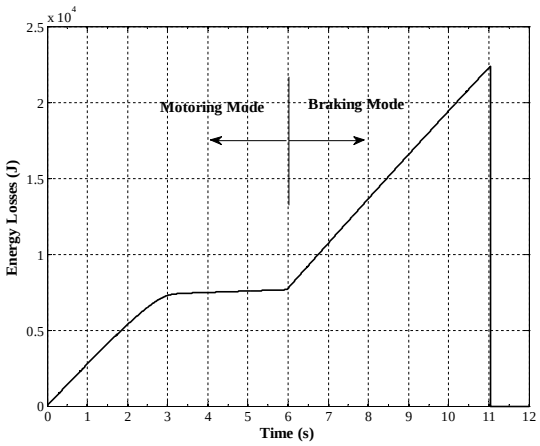

Fig. 9. Variation of energy losses with time (plugging method)

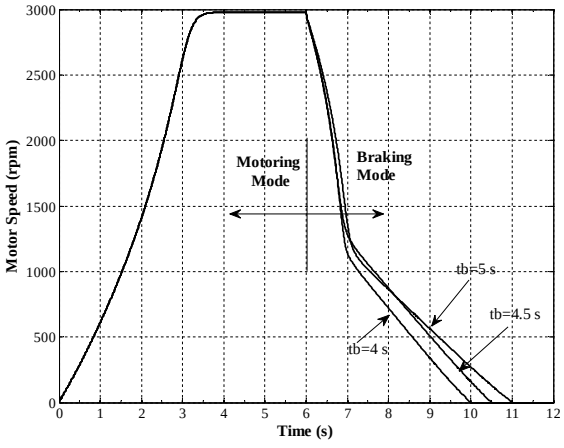

Fig. 10. Variation of motor speed with time (Proposed method)

The output power is reversed in braking mode because the developed torque reversed.

The input power during braking with the proposed method is returned to supply from motor during a part of braking period.

The optimum values of applied voltage and frequency to have certain braking time with minimum braking energy losses are obtained using PSO technique. The results and are shown in Fig. 16 and Fig. 17.

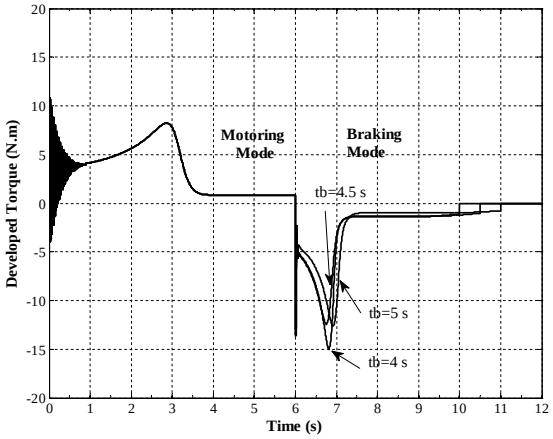

Fig. 11. Variation of developed torque with time (Proposed method)

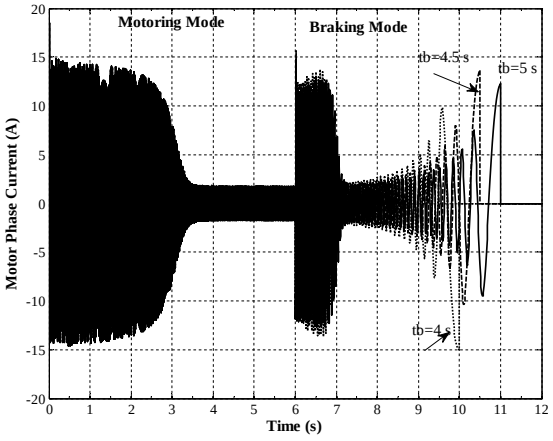

Fig. 12. Variation of motor phase current with time (Proposed method)

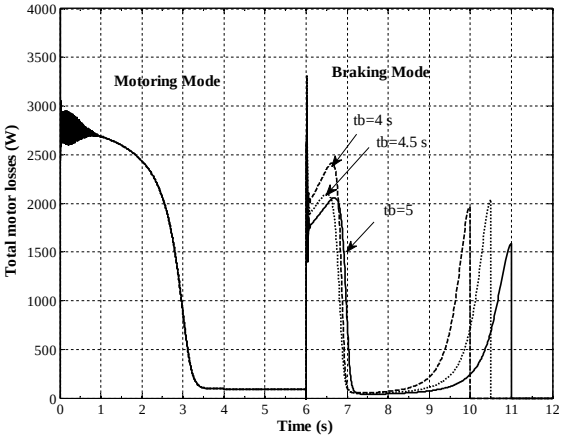

Fig. 13. Variation of total motor losses with time (Proposed method)

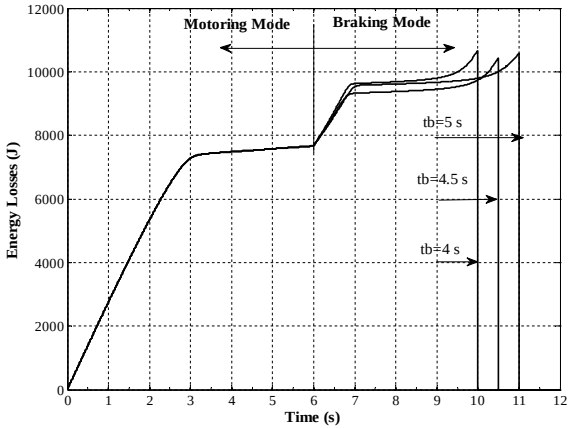

Fig. 14. Variation of energy losses with time (Proposed method)

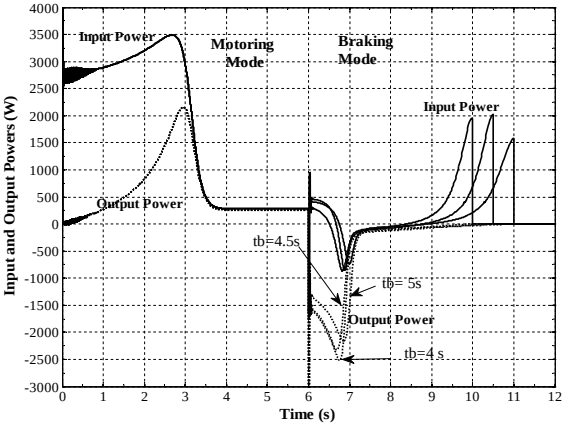

Fig. 15. Variation of input and output powers with time (Proposed method)

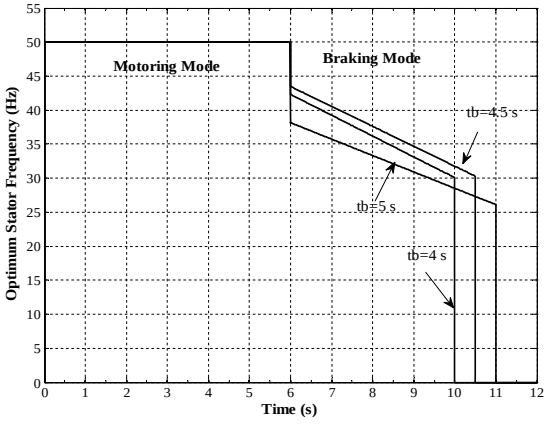

Fig. 16. Variation of optimum values of stator frequency with time (Proposed method)

V. Conclusion

Using the proposed braking method, three phase induction motors can be braked at a given braking time with minimum braking energy losses. The proposed method determines the optimum values of applied voltage and frequency to stop the motor within certain time with minimum braking energy losses by particle swarm optimization technique.

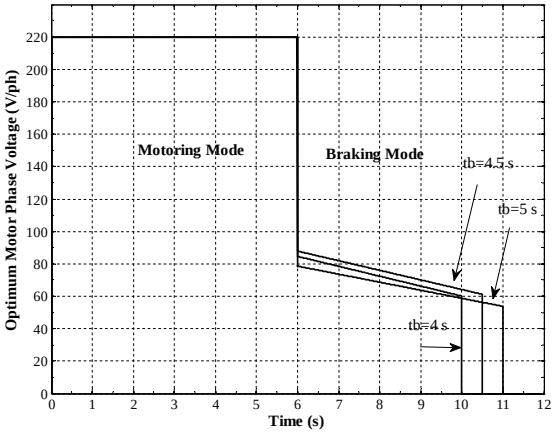

Fig. 17. Variation of optimum values of motor phase voltage with time (Proposed method)

The braking energy losses with the proposed method are about 20 % of plugging braking energy so that the proposed method is more useful for multi braking applications without any excessive overheating for the motor.

References

[1] Marko Hinkkanen and JormaLuomi, Braking Scheme for Vector-Controlled Induction Motor Drives Equipped With Diode Rectifier Without Braking Resistor, *IEEE Transactions on Industry Applications, Vol. 42(*No.5*):1257-1263, September/October 2006.*

[2] P.L. Rongmei, Shimi S.L, Dr. S. Chatterji and Vinod K. Sharma, A Novel Fast Braking System for Induction Motor, *International Journal of Engineering and Innovative Technology (IJEIT), Vol.1(*Issue 6*): 65-69, June 2012.*

[3] MukulRastogi and Peter W. Hammond, Dual-Frequency Braking in AC Drives, *IEEE Transactions On Power Electronics, Vol. 1:(*NO. 6*): 1032-1040, November 2002.*

[4] Bilal Abdullah Nasir, Braking Methods of Induction Motor Fed From A Current- Source Inverter, *Elsevier, Energy Procedia 14: 1819-1824, 2012.*

[5] Hairik, H.A. Thejel, R.H. Kadhem and W.A., Proposed scheme for plugging three-phase induction motor, *MELECON 2010 - 2010 15th IEEE Mediterranean Electrotechnical Conference, Valletta: 1-5, 26-28 April 2010.*

[6] Laabidi, M. Rebhi, B. Kourda, F. Elleuch and M. Ghodbani L., Braking of induction motor with the technique of discrete frequency control, *Systems Signals and Devices (SSD), 2010 7th International Multi-Conference, Amma: 1-6, 27-30 June 2010.*

[7] Sowilam, G.M.A., Korfly, M.I. and Hassan A.A., Braking methods of induction motor using direct torque control, *Power Systems Conference, MEPCON 2006, Eleventh International Middle East, vol.: 35 – 40 ,2006.*

[8] Amin, A.M.A., El Korfally M.I., Sayed, A.A. and Hegazy, O.T.M., Efficiency Optimization of Two-Asymmetrical-Winding Induction Motor Based on Swarm Intelligence, *Energy Conversion, IEEE Transactions, Vol 24(*Issue 1*): 12 – 20, 2009.*

[9] Ping Guo, Dagui Huang, Daiwei Feng, Wenzheng Yu and Hailong Zhang, Optimized design of induction motor parameters based on PSO (Particle Swarm Optimization), *Mechatronics and Automation (ICMA), International Conference , Chengdu: 837 – 842, 5-8 Aug. 2012.*

[10] Tofighi, E.M., Mahdizadeh, A. and Feyzi M.R., Online estimation of induction motor parameters using a modified particle swarm optimization technique, *Industrial Electronics Society, IECON 2013 - 39th Annual Conference of the IEEE: 3645 – 3650, 10-13 Nov. 2013.*

[11] Wei Hu, Gui Liu, Li Fu and Hongmei Zhang, Research of motor fault diagnosis based on PSO algorithm, *Control and Decision Conference (CCDC), 2013 25th Chinese, Guiyang, 25-27 May 2013.*

[12] John Chiasson, *Modelling and high performance control of electric machines* (John Wiley & Sons, Inc., 2005).

[13] Xin She Yang, *Natural Inspired Metaheuristic algorithm*, (Luniver Press, University of Cambrodge, United Kingdom, second edition, 2010).

[14] Shi Y, Eberhart R., A modified particle swarm optimizer, *Proceedings of IEEE International Conference on Evolutionary Computation (ICEC'98), Anchorage, IEEE Press: 69–73. , 1998.*

[15] Shi Y, Eberhart R. Parameter selection in particle swarm optimization, *Proceedings of the 1998 Annual Conference on Evolutionary Programming, San Diego, MIT Press, 1998.*

[16] Damiano, A., Gatto, G., Marongiu, I., Meo, S., Perfetto, A., Serpi, A., A predictive direct torque control of induction machines, (2012) *International Review of Electrical Engineering (IREE),* 7 (4), pp. 4837-4844.

Authors' information

Electrical Power and Machines Department, Faculty of Engineering, Zagazig University, Zagazig, Egypt.

Mahmoud Elkholy received Bachelor of Engineering (B.E) degree (with honor) from Zagazig University, Egypt in 1994 under the specialization of Electrical Machines and Power Engineering, Master of Science degree from Zagazig University, Egypt 1998 under the specialization of Electrical Machines and Doctor of Philosophy (Ph.d) in the year 2001 from Zagazig University, Egypt in the Dept. of Electrical power and Machines Engineering. He has 18 years of experience in academia and research at different positions. Currently he is an Assistant Professor, Faculty of Engineering, Zagazig University, Egypt.His interest includes control the steady state and dynamic performance of electrical machines and artificial intelligence.
E-mail: melkholy71@yahoo.com

Mohammed A. Elhameed received the B.E. degree (with honors) from Zagazig University-faculty of Engineering, Zagazig, Egypt in electrical power and machines engineering in 1996, Master degree in 2000 in the field of electrical power system from the same institute, and the Ph. D. degree from Zagazig University, Egypt, in 2004, in the field of electrical power system. He has been assistant professor, Faculty of Engineering, Zagazig University, Egypt. His current interest includes electrical machines modelling and control, artificial intelligence and power system control.
E-mail: m_a_elhameed@yahoo.com

International Review of Automatic Control (I.RE.A.CO.), Vol. 8, N. 2
ISSN 1974-6059 March 2015

Prediction of Glycemia Based on Diabetes Self-Monitoring Data

Marián Tárník, Vladimír Bátora, Tomáš Ludwig, Ivan Ottinger,
Eva Miklovičová, Ján Murgaš

Abstract – *This paper deals with the application of self-monitoring diabetes data that are supplemented by the continuous glucose monitoring for the blood glucose concentration prediction. The short-term predictor is designed and evaluated on three different datasets. A diabetes-specific metrics is used to evaluate the predictors. Standard Least Squares identification as well as an alternative identification method with constraints is considered.* ***Copyright © 2015 Praise Worthy Prize S.r.l. - All rights reserved.***

Keywords*: Diabetes, Glucose, Predictors, Least Squares Identification*

I. Introduction

The self-monitoring of glycemia plays an important role in treatment of Type 1 Diabetes Mellitus (T1DM). Typical blood glucose level self-monitoring is based on several fingerstick measurements of glucose samples. Routinely three or four glucometer measurements are made during the day. Such information serves only as a basic monitoring. In case of the insulin therapy adjustment, more frequent measurements are necessary to capture the glycemia evolution during the day. Typically eight or more fingerstick measurements are considered in these cases. In the recent decade systems for continuous glucose monitoring (CGM) have become commercially available. CGM provides information on the glucose concentration every 5 minutes, i.e. up to 288 measurements per day. In practice this means that a real time information on glucose concentration is available. An experienced diabetic patient can intuitively predict the future glycemic trend. The more complex information provided by the CGM can lead to better patient decisions.

Therefore it can improve the treatment of diabetes and prevent acute and long-term diabetic complications.

In this paper we address the use of routine diabetes self- monitoring data supplemented with the continuous glucose monitoring for the prediction of glycemia. Methods of the classical system identification and prediction [1] are used to design a blood glucose predictor. Prediction of the glucose concentration from the CGM data has been investigated previously [2].

In the recent years several blood glucose predictors have been proposed [2]-[7]. In general acceptable predictions are obtained for a prediction horizon up to 60 minutes. Therefore, the glucose predictors are often referred as a short-term predictors. A prediction horizon between 20 and 30 minutes is usually used for a predictive hypoglycemia alert. If the hypoglycemia is predicted ahead in time one can take an action to prevent it or mitigate its effects.

A longer prediction horizon can also be helpful in short-term decision-making. The predictions may be also taken into account in the planning of the future insulin delivery and carbohydrate intake.

In such case the predictor needs the information on future (planned) insulin and carbohydrate intake. [3], [5] and [6] present suitable predictors. In [5] part of the prediction model is fixed and the parameters are set to the average values known from the clinical studies. Particularly in [5] the slow- acting insulin has been modeled by Berger and Rodbard [8], and the fast-acting insulin has been modeled by the second order compartmental model.

The carbohydrate absorption has been modeled by compartmental models distinguishing the fast and slow carbohydrates. In [3] the carbohydrate absorption has been modeled using Chiara Dalla Man model [9]. The insulin concentration data are directly available, therefore modeling is unnecessary. The above-mentioned prediction models identify the remaining part as a black box model. In [6] whole model is considered as the black-box model.

Some predictors utilize only the glucose time series data [2], [4], [10]. These predictors use only the glucose signal, no information on insulin and carbohydrates is used. Therefore, planned insulin dose or carbohydrate intake does not affect the predicted glucose evolution.

Consequently, the decision support in this respect is limited. In this paper the aim of the prediction is to achieve a better decision on insulin dose for the planned carbohydrate intake. The standard diabetes self-monitoring data are considered in the prediction as described in Section II.

II. Self-monitoring Data and CGM

The purpose of this work is to study the possibilities of glycemia prediction based on the routine self-monitoring data not the data obtained in clinical studies.

We use data provided by one T1DM subject. However, three data acquisition sessions have been carried out in three different months in 2013, i.e. March, April and May. These data sets are considered as separate data sets.

The data acquisition has been based on the insulin pump which the subject has been using. A commercially available CGM has been augmented to the insulin pump. The data acquisition considers four basic signals, namely the glucose concentration, the basal insulin rate, the bolus insulin doses and the carbohydrate intake.

CGM provides the glucose reading every five minutes which determines the uniform sampling period used in the data processing specified below. The glucose meter readings have been also available. However, these values serves only as the calibration of CGM and have not been used in the prediction of glucose concentration. The insulin delivery data are automatically logged by the insulin pump. The basal insulin rate and the bolus doses are logged separately corresponding to the intensive insulin therapy. Finally the carbohydrate intake has been logged in the classical diabetic diary.

As mentioned above, three data acquisition sessions with one subject have been carried out in the three different months. Each session lasted for approximately four days. Figs. 1, 2 and 3 show the data corresponding to March, April and May session respectively.

To design the predictor of glycemia the data set of each session has been splitted to half to obtain the data for a prediction model identification (first half) and the data for the validation of the prediction model.

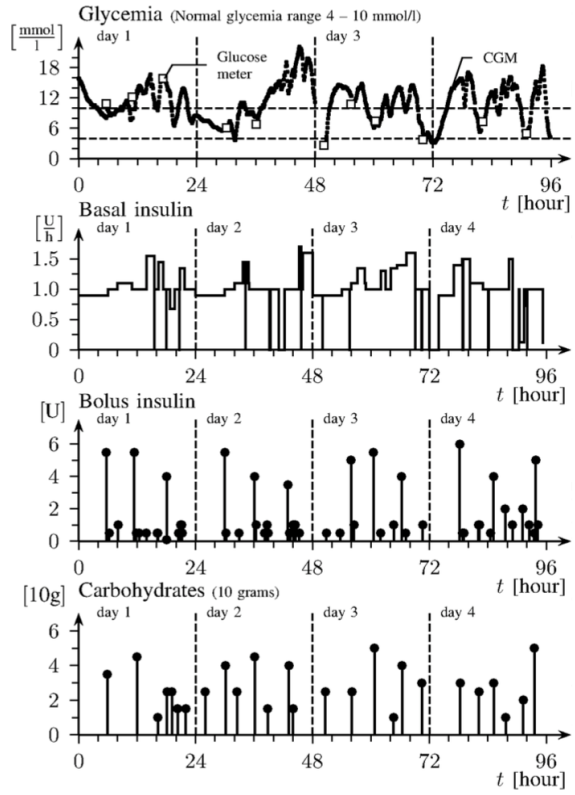

Fig. 1. Dataset — March

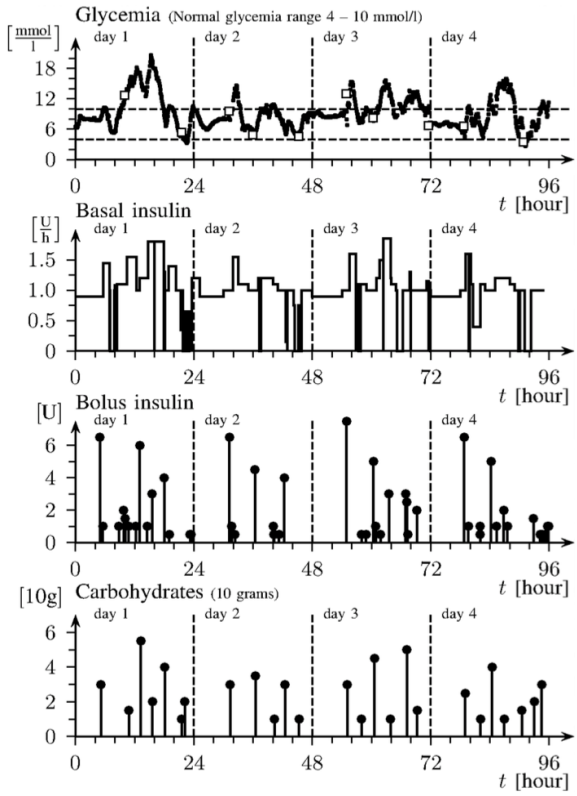

Fig. 2. Dataset — April

III. Methods

The raw data from the previous section have been pre-processed for further use. The data have been resampled with the sampling period T_S = 5 [min], which is determined by the CGM system. The missing glycemia data (gaps larger than 5 minutes) have been linearly interpolated. No filtration of CGM signal has been considered. We consider a prediction model consisting of two parts. A part with fixed structure and parameters set to the average population values and a part which is the subject of identification. [3], [5] use a similar approach as discussed in Section I. The first part part of data described in Section II is used for the identification and the glycemia predictor design. However, an impulse nature of the bolus insulin and carbohydrate intake data is not convenient for the identification purposes.

Therefore the first part of the model generates a couple of auxiliary signals that serve as an input to the second part of model. The first part corresponds to the carbohydrates and insulin absorption. We employ simple compartmental models [11] to describe the carbohydrate and insulin absorption. The carbohydrate absorption model has the form:

$$\dot{F}(t) = -\frac{1}{t_G} F(t) + \frac{1}{t_G} A_G d(t) \tag{1}$$

$$\dot{Ra}(t) = -\frac{1}{t_G} Ra(t) + \frac{1}{t_G} F(t) \tag{2}$$

where $Ra(t)$ [mg/kg/min] is rate of appearance of glucose in plasma and $F(t)$ is glucose appearance in the first compartment. The parameter A_G [unitless] is carbohydrate bioavailability and t_G [min] is the corresponding time constant. The signal $d(t)$ [mg/kg/min] has the form $d(t) = D(t)\delta(t)$, where $D(t)$ [mg/kg] is the amount of ingested carbohydrates and $\delta(t)$ is a Dirac impulse approximation (accounting the sampling frequency) at meal time. Both are determined by the carbohydrate data. The parameter values are t_G = 75 [min], A_G = 0.9. The body weight is BW = 75 [kg].

The insulin absorption model has the form:

$$\dot{S}_1(t) = -\frac{1}{t_I} S_1(t) + v(t) \tag{3}$$

$$\dot{S}_2(t) = -\frac{1}{t_I} S_2(t) + \frac{1}{t_I} S_1(t) \tag{4}$$

$$\dot{I}(t) = -k_I I(t) + \left(\frac{1}{t_I}\right)\left(\frac{1}{V_I}\right) S_2(t) \tag{5}$$

where $I(t)$ [μU/ml] is the plasma insulin concentration, $S_1(t)$ and $S_2(t)$ [μU/kg] represent the states of compartments and $v(t)$ [μU/kg/min] is the total subcutaneous insulin infusion rate including both basal and bolus insulin. The time constant t_I = 60 [min], the rate constant k_I = 0.2 [1/min] and the distribution volume of plasma insulin V_I = 20 [ml/kg] are the considered model parameters.

The second part of the prediction model is identified as an autoregressive exogenous (ARX) model with two inputs and one output. Particularly the rate of glucose appearance $Ra(t)$ and the insulin concentration $I(t)$ are the inputs and the glucose concentration $G(t)$ [mmol/l] (glycemia measured by CGM) is the output. The ARX model has the form

$$\begin{aligned} &A\left(z^{-1}\right) G(k) = \\ &= B_{Ra}\left(z^{-1}\right) Ra(k) + B_I\left(z^{-1}\right) I(k) + \xi(k) \end{aligned} \tag{6}$$

where $\xi(k)$ is the white noise disturbance and the polynomials have the standard form, i.e.

$$\begin{aligned} &A\left(z^{-1}\right) = 1 + a_1 z^{-1} + \ldots + a_{n_G} z^{-n_G},\ B_{Ra}\left(z^{-1}\right) = \\ &= b_{R1} z^{-1} + \ldots + b_{RnRa} z^{-nRa} \end{aligned}$$

and:

$$B_I\left(z^{-1}\right) = b_{I1} z^{-1} + \ldots + b_{In_I} z^{-n_I}$$

The second part of the considered model corresponds to the plasma glucose and insulin kinetics and the subcutaneous measurement of the glucose.

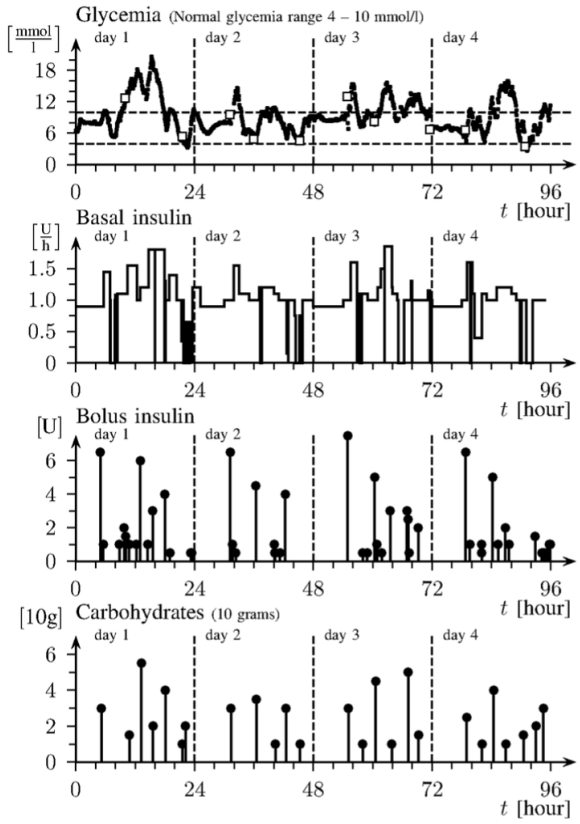

Fig. 3. Dataset — May

Relatively high order of the second part of the model is necessary. Namely the polynomial degrees n_G, n_{Ra} and n_I have to be chosen sufficiently high to capture the relevant model dynamics and time delays.

The quality of the glucose predictor can be accessed by several methods. The mathematical metrics such as a percentage fit or the root mean squared error can be used [3]. However in this case the diabetes-specific metrics is widely used. This metrics is based on the well-known Clarke error grid analysis (EGA) [12].

For the evaluation of the continuous glucose monitoring systems a continuous glucose – EGA (CG-EGA) has been introduced [13]. [7], [14] introduce modifications of the CG-EGA to evaluate the glucose predictions. The main difference between classical Clarke EGA and other mentioned is that the CG-EGA involves also the evaluation of the glucose rate of change, i.e. rate-error grid analysis (R-EGA). From the prediction point of view CG-EGA based evaluation can be viewed as a less conservative metrics compared to the classical Clarke EGA. Therefore in this work the classical Clarke EGA is considered for prediction evaluation.

IV. Results

A single prediction model has been designed or identified for each dataset separately. The first part of the models is the same in each case with the parameter values as reported in Section III.

IV.1. Identification

The second part of the model, i.e. ARX model is identified for each dataset. The polynomial degrees n_G, n_{Ra} and n_I have been chosen from the intervals 1–8, 1–16 and 1– 16 respectively. The choice of the degrees has been based on the best loss-function value criterion evaluated using the validation data. The chosen degrees of ARX model polynomials are reported in Table I.

TABLE I
ARX POLYNOMIALS DEGREES CHOSEN

Model	n_G	n_{Ra}	n_I
Model No.1 (Dataset - March)	8	2	1
Model No.2 (Dataset - April)	6	16	15
Model No.3 (Dataset - May)	7	4	3

The results of the identification for each dataset are as follows. Dataset — March (model No.1):

$$A\left(z^{-1}\right)=1-1.588z^{-1}+0.5878z^{-2}+ \\ +0.06326z^{-3}-0.1704z^{-4}+0.1585z^{-5}+ \\ -0.1149z^{-6}+0.1417z^{-7}-0.0675z^{-8} \quad (7a)$$

$$B_{Ra}\left(z^{-1}\right)=0.1546z^{-1}-0.1374z^{-2} \quad (7b)$$

$$B_I\left(z^{-1}\right)=-7.644e-5z^{-1} \quad (7c)$$

Dataset — April identification yields:

$$A\left(z^{-1}\right)=1-1.321z^{-1}+0.3713z^{-2}-0.183z^{-3}+ \\ +0.109z^{-4}+0.01887z^{-5}+0.01647z^{-6} \quad (8a)$$

$$B_{Ra}\left(z^{-1}\right)=-0.6099z^{-1}+1.509z^{-2}-2.141z^{-3} \\ +2.901z^{-4}-3.226z^{-5}+3.56z^{-6} \\ -3.467z^{-7}+2.585z^{-8}-1.581z^{-9} \\ +0.9933z^{-10}-1.611z^{-11}+2.679z^{-12} \\ -1.528z^{-13}-0.2004z^{-14}+0.8993z^{-15} \\ -0.7724z^{-16} \quad (8b)$$

$$B_I\left(z^{-1}\right)=0.00714z^{-1}+0.0076z^{-2}-0.0348z^{-3} \\ +0.04948z^{-4}-0.0593z^{-5}+0.0249z^{-6} \\ +0.05804z^{-7}-0.1168z^{-8}+0.099z^{-9} \\ -0.05z^{-10}-0.0107z^{-11}+0.0409z^{-12} \\ -0.0164z^{-13}-0.014z^{-14}+0.0154z^{-15} \quad (8c)$$

Finally the identification results for the dataset — May (Model No.3) are:

$$A\left(z^{-1}\right)=1-1.847z^{-1}+1.198z^{-2}-0.6547z^{-3} \\ +0.4265z^{-4}-0.2429z^{-5}+0.2651z^{-6}-0.1348z^{-7} \quad (9a)$$

$$B_{Ra}\left(z^{-1}\right)=0.2021z^{-1}-0.2227z^{-2}+ \\ -0.218z^{-3}+0.2352z^{-4} \quad (9b)$$

$$B_I\left(z^{-1}\right)=0.0162z^{-1}-0.03427z^{-2}+0.0187z^{-3} \quad (9c)$$

The residual autocorrelation analysis has been done to validate the models using validation data.

The representative example of residual analysis is shown in Fig. 4 which presents the results of model No.3 (dataset — May). The residuals correlation functions of all identified models indicates close to white noise correlation properties.

The other criterions for the degree choice, namely Akaike's information theoretic criterion (AIC) and Rissanen's minimum description length (MDL) criterion [1], suggest in general lower degrees of polynomials, especially n_G, with lower model percentage fit (not reported in the paper).

However the aim is the n_P–step ahead prediction, where n_P is circa eight, as discussed later. Therefore the higher polynomial degrees have been desired.

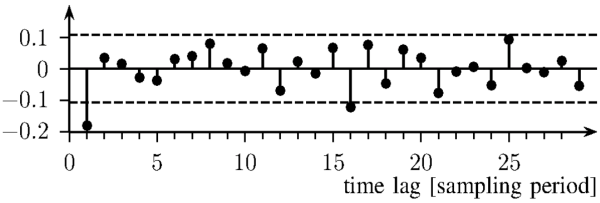

Fig. 4. Correlation function of residuals with 99% confidence interval. ARX model identified for the dataset — May (Model. No.3). Evaluated on the validation data

IV.2. Prediction

The prediction horizon approximately 20 to 30 minutes is usually considered in the glucose short-term prediction [3], [4], [14]. However, 120 minutes can be also considered as a short-term prediction depending on the sampling period, for example see [5].

In this paper we consider a prediction horizon of 40 minutes, which corresponds to 8-step ahead prediction, i.e. $n_P = 8$ since the sampling period $T_S = 5$ [min].

The results of prediction are shown in Fig. 5. For each validation dataset a separate predictor is used as discussed above. The predictors are assessed by means of Clarke EGA. Fig. 6 shows the assessment of results. Table III summarizes the results.

IV.3. The Model Gains

Consider the gain from the model first input $Ra(k)$ to the output $G(k)$, i.e. g_{Ra} [mmol/l/mg/kg/min]. Similarly the gain from the model second input $I(k)$ to the output $G(k)$ is g_I [mmol/l/μU/ml]. The values of these gains for models (7), (8) and (9) are reported in Table II in the column unconstrained least squares.

TABLE II
THE MODEL GAINS

	unconstrained least squares		constrained quadratic program	
Dataset	g_{Ra}	g_I	g_{Ra}	g_I
March	1.5931	-0.0071	3.1427	-0.0501
April	-0.8017	0.0083	1.8764	-0.0533
May	-0.3324	0.0601	5.7655	-0.0747

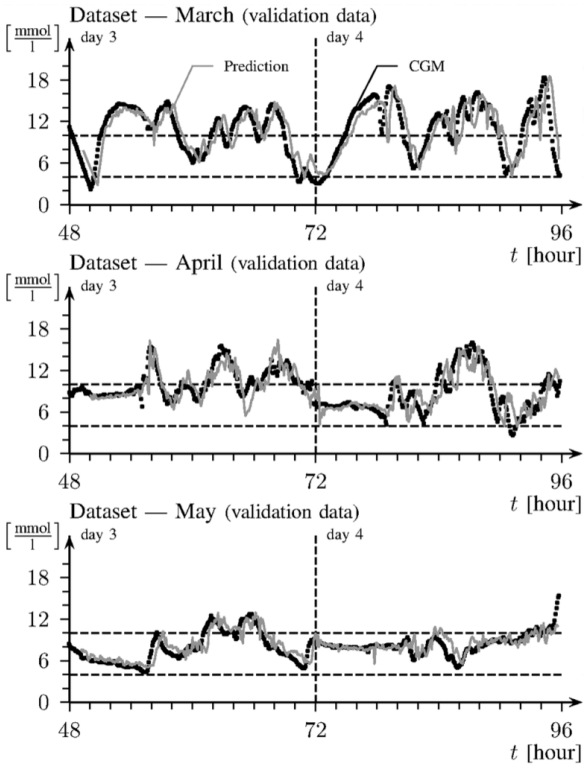

Fig. 5. Comparison of the original CGM data (black dots) with the predicted glucose concentration 40 minutes ahead (solid gray line)

The insulin lowers and carbohydrate intake increases the glucose concentration. Therefore g_I is expected to be negative and g_{Ra} positive. The identified model No.2 and No.3 have gains g_I and g_{Ra} which are not physiologic. Insulin boluses and carbohydrate intake are highly correlated as they occur almost at the same time, which is obvious since the pump and therefore the intensified insulin therapy is used in this case.

The correlation between bolus and carbohydrate intake can explain the unexpected model parameters such as the mentioned gains. To overcome this issue a sophisticated method for parameter identification should be used instead of common least squares.

We consider a constrained convex quadratic program in the form:

$$\begin{aligned} \min_{\Theta} \quad & \frac{1}{2}\Theta^T H^T H\Theta - y^T H\Theta \\ \text{subject to} \quad & G\Theta \le h \end{aligned} \tag{10}$$

where $\Theta \in \mathbb{R}^{n_G+n_{Ra}+n_I}$ is the estimated parameters vector containing the coefficients of polynomials A, B_{Ra} and B_I.

$y \in R^N$ consist of the measured samples and N is the number of the samples. The matrix H is composed so that the vector $\hat{y} = H\Theta, \hat{y} \in \mathbb{R}^N$ is a one-step ahead prediction of measured glucose concentration (vector y) – Table III. Further the inequality constraint matrices has the form:

$$G = \begin{bmatrix} I_{nG} & 0 & 0 \\ 0 & -I_{n_{Ra}} & 0 \\ 0 & 0 & I_{nI} \end{bmatrix} \tag{11}$$

where $I_{n_G} \in \mathbb{R}^{1\times n_G}, I_{nRa} \in \mathbb{R}^{1\times n_{Ra}}, I_{n_I} \in \mathbb{R}^{1\times n_I}$ are the vectors of ones. Finally the vector $h = \begin{bmatrix} 1 & 0 & -0.0005 \end{bmatrix}^T$ is considered in this particular case.

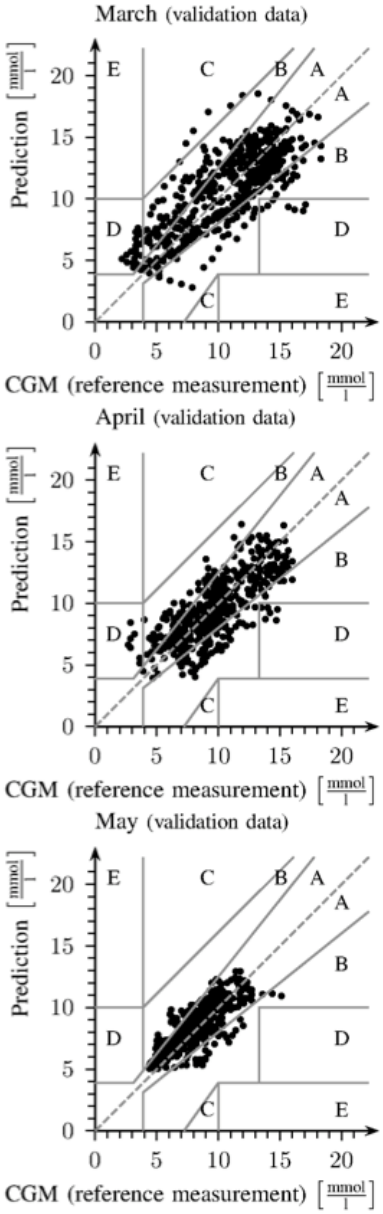

Fig. 6. Clarke error grid analysis

TABLE III
EVALUATION OF PREDICTION MODELS PERFORMANCE
ON 40 MINUTES PREDICTION HORIZON (VLAIDATION DATA)

Model	zona A	zone B	zone C	zone D	zone E
No.1	70.6093	22.4014	1.0753	5.914	0
No.2	77.6364	20	0	2.3636	0
No.3	89.6243	10.3757	0	0	0

Percentage of points falling within EGA zones

Same model polynomial degrees have been used as in the previous unconstrained least squares method. Solving the quadratic program yields the model gains (g_{Ra} and g_I) as reported in Table II in the column constrained quadratic program. In general the prediction results are almost same as obtained with previous method. Fig. 7 illustrates the prediction results for May dataset.

The results of this alternative identification method are summarized in Table IV.

TABLE IV
CLARKE EGA OF PREDICTION MODELS IDENTIFIED BY MEANS
OF CONSTRAINED QUADRATIC PROGRAM

dataset	zona A	zone B	zone C	zone D	zone E
March	72.58	20.43	0.89	6.09	0
April	77.09	20.54	0	2.36	0
May	90.34	9.66	0	0	0

Percentage of points falling within EGA zones

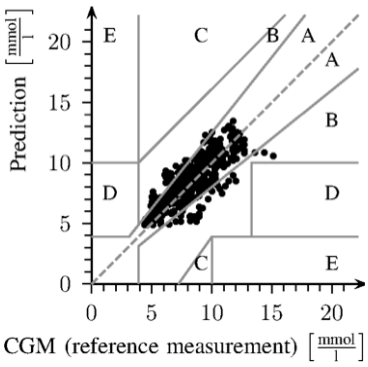

Fig. 7. Clarke EGA of prediction results obtained by means of constrained quadratic program, dataset May

V. Conclusion

In this paper we designed the prediction models for the short-term prediction of the glycemia with the prediction horizon of 40 minutes. The design is based on the routine diabetes self-monitoring data and CGM data measured in real-life conditions.

The standard identification method does not provide acceptable model gains. Therefore, we proposed and evaluated an alternative identification method. The results of the diabetes-specific evaluation metrics based on the Clarke error grid analysis show a good quality of the proposed prediction models.

Acknowledgements

This work has been supported by Slovak scientific grant agency through grant VEGA-1/2256/12.

This paper is the result of implementation of the project: "Centre of competence for intelligent technologies for computerization and informatization of systems and services" (ITMS: 26240220072) supported by the Research & Development Operational Programme funded by the ERDF.

The paper is one of the outcomes of the research work for the project entitled "Research center for severe diseases and related complications", "ITMS: 26240120038". "This project is being co-financed by the European Union. We support research activities in Slovakia". Podporujeme výskumné aktivity na Slovensku. Projekt je spolufinancovaný zo zdrojov EÚ.

References

[1] L. Ljung, *System Identification (2nd Ed.): Theory for the User*. Saddle River, NJ, USA: (Prentice-Hall PTR, 1999).

[2] G. Sparacino, F. Zanderigo, S. Corazza, A. Maran, A. Facchinetti, and C. Cobelli, Glucose concentration can be predicted ahead in time from continuous glucose monitoring sensor time-series, *Biomedical Engineering, IEEE Transactions on, vol. 54*, no. 5, pp. 931–937, May 2007.

[3] M. Cescon and R. Johansson, Glycemic trend prediction using empirical model identification, in *Decision and Control, 2009* held jointly with the *2009 28th Chinese Control Conference. CDC/CCC 2009*. Proceedings of the 48th IEEE Conference on, Dec. 2009, pp. 3501–3506.

[4] M. Eren-Oruklu, A. Cinar, and L. Quinn, Hypoglycemia prediction with subject-specific recursive time-series models, *Journal of Diabetes Science and Technology, vol. 4, no. 1, pp. 25–33*, Jan. 2010. [Online]. Available: http://www.ncbi.nlm.nih.gov/pmc/articles/ PMC2825621/

[5] F. Stahl and R. Johansson, Diabetes mellitus modeling and short-term prediction based on blood glucose measurements, *Mathematical Biosciences, vol. 217, no. 2, pp. 101–117, 2009*. [Online]. Available: http://www.sciencedirect.com/science/article/pii/S0025556408001648

[6] F. Ståhl, R. Johansson, and E. Renard, Post-prandial plasma glucose prediction in type i diabetes based on impulse response models, in *Engineering in Medicine and Biology Society (EMBC), 2010 Annual International Conference of the IEEE, Aug. 2010, pp. 1324–1327*.

[7] F. Zanderigo, G. Sparacino, B. Kovatchev, and C. Cobelli, Glucose prediction algorithms from continuous monitoring data: Assessment of accuracy via continuous glucose error-grid analysis, *Journal of Diabetes Science and Technology, vol. 1, no. 5, pp. 645–651, Sep. 2007*. [Online]. Available: http://www.ncbi.nlm.nih.gov/pmc/articles/ PMC2734107/pdf/dst-01-0645.pdf

[8] M. Berger and D. Rodbard, Computer simulation of plasma insulin and glucose dynamics after subcutaneous insulin injection, *Diabetes Care, vol. 12, no. 10, pp. 725–736, 1989.* [Online]. Available: http://care.diabetesjournals.org/content/12/10/725.abstract

[9] C. Dalla Man, M. Camilleri, and C. Cobelli, A system model of oral glucose absorption: Validation on gold standard data, *IEEE Transactions on Biomedical Engineering, vol. 53, no. 12, pp. 2472–2478, Dec. 2006.* [Online]. Available: http://ieeexplore.ieee.org/ xpls/abs_all.jsp?arnumber=4015600

[10] S. Pereverzyev and S. Sampath, Regularized learning algorithm for prediction of blood glucose concentration in no action period,

in *1st International Conference on Computational & Mathematical Biomedical Engineering, R. L. Perumal Nithiarasu and R. van Loon, Eds., 2009, pp. 395–398.* [Online]. Available: http://www.compbiomed.net/2013/cmbe-proceedings.htm

[11] P. Herrero, P. Georgiou, N. Oliver, M. Reddy, D. Johnston, and C. Toumazou, A composite model of glucagon-glucose dynamics for in silico testing of bihormonal glucose controllers, *Journal of Diabetes Science and Technology, vol. 7, no. 4, pp. 941–951, Jul. 2013*. [Online]. Available: http://jdst.org/worldpress/index.php?s=Volume+7%2C+Issue+4%3A+941+2013

[12] W. L. Clarke, D. Cox, L. A. Gonder-Frederick, W. Carter, and S. L. Pohl, Evaluating clinical accuracy of systems for self-monitoring of blood glucose, *Diabetes care, vol. 10, no. 5, pp. 622–628, 1987*. [Online]. Available: http://care.diabetesjournals.org/content/10/5/622. Abstract

[13] B. P. Kovatchev, L. A. Gonder-Frederick, D. J. Cox, and W. L. Clarke, Evaluating the accuracy of continuous glucose-monitoring sensors continuous glucose–error grid analysis illustrated by therasense freestyle navigator data, *Diabetes Care, vol. 27, no. 8, pp. 1922–1928, 2004*. [Online]. Available: http://care.diabetesjournals. org/content/27/8/1922.full.pdf

[14] S. Sivananthan, V. Naumova, C. Dalla Man, A. Facchinetti, E. Renard, C. C., and S. Pereverzyev, Assessment of blood glucose predictors: The prediction-error grid analysis, *Diabetes Technology & Therapeutics, vol. 13, no. 8, pp. 787–796, Aug. 2011*. [Online]. Available: http://people.ricam.oeaw.ac.at/v.naumova/pdf/article2.pdf

Authors' information

Institute of Robotics and Cybernetics, Faculty of Electrical Engineering and Information Technology, Slovak University of Technology in Bratislava, Slovak Republic.

Marián Tárník (MSc. PhD.) was born in Levice, Slovakia in 1986. He received Bachelor of Science degree from the Faculty of Electrical Engineering and Information Technology, Slovak University of Technology in Bratislava in 2008, Master of Science degree in technical cybernetics in 2010 and PhD. degree in 2013 at the same place where he is from 2013 until now doing further research as a researcher. He is interested in Adaptive Control, Lyapunov design approach and modeling and control of type one diabetes mellitus.
E-mail: marian.tarnik@stuba.sk

Vladimír Bátora (MSc.) was born in Bánovce nad Bebravou, Slovakia in 1990. He received Bachelor of Science degree from the Faculty of Electrical Engineering and Information Technology, Slovak University of Technology in Bratislava in 2011 and Master of Science degree in technical cybernetics in 2013 from the same university where he is since 2013 until now a PhD. student. He is interested in modeling and control of type one diabetes mellitus and Model Predictive Control.

Tomáš Ludwig (MSc), born in 1988, graduated in robotics and cybernetics in 2012 form the Faculty of Electrical Engineering, Slovak University of Technology in Bratislava. He is currently a postgraduate student focused on bio cybernetics with the specialization in modeling diabetes.

Ivan Ottinger (MSc), born in 1987, graduated in robotics and cybernetics in 2012 form the Faculty of Electrical Engineering, Slovak University of Technology in Bratislava. He is currently a postgraduate student focused on bio cybernetics with the specialization in adaptive control.

Eva Miklovičová obtained the MSc. in 1990 and the PhD. in Automation in 1997, both from the Slovak University of Technology in Bratislava. Currently she is with the Institute of Robotics and Cybernetics at the Faculty of Electrical Engineering and Information Technology, STU in Bratislava. Her research interests include predictive control, adaptive control, system modeling and identification.

Ján Murgaš (Prof, MSc, PhD), born in 1951, graduated in control engineering in 1975 and received the PhD degree in 1980 form the Faculty of Electrical Engineering, Slovak University of Technology in Bratislava. Since 1996 he has been Full Professor for control engineering. His research interests include adaptive and non-linear control, large-scale systems. He is a member of the IEEE, of the American Mathematical Society and of the Slovak Society for Cybernetics and Informatics.

Praise Worthy Prize

International Review of Automatic Control (I.RE.A.CO.), Vol. 8, N. 2
ISSN 1974-6059 *March 2015*

Reactive Compensation in Long Lines Through the Joint Effect of Transformer Tap and Shunt Compensation: a Parametric Plane Study

Nakka Lakshmi Srinivasa Rao, G. Govinda Rao, S. Sivanagaraju

Abstract – *This paper investigates the steady state performance of long line with reactive compensation provided through transformer tap control on one side and shunt compensation provided on the other side. Constant voltage contours in the parametric plane are obtained. Also the voltage profile over the line together with the flatness index is determined. Results of case studies are presented and analyzed. This study can make a foundation to build up an expert system through which the voltage at the load end can be controlled by suitably designed parameters of both the compensators.*

Keywords*: Joint Control, Reactive Compensation, Transmission Line, Flat Voltage Profile, Expert System*

I. Introduction

The control of reactive power flow in a transmission line and hence the voltage profile over transmission line by using a tap changing transformer and/or the shunt compensation at the load end is very popular and is exhaustively studied by several researchers ([1]-[22]).

An optimal power flow program is used to improve the voltage by coordinating the voltage control elements such as capacitor and transformer taps in several papers [1], [2] and also proposed expert systems for voltage and reactive power control [3]-[6]. An expert system is proposed for voltage corrections for different conditions by using switchable shunt reactive compensation and transformer tap settings [7] to improve the performance over the conventional optimization methods. Voltage stability aspect is also studied by changing the transformer tap and shunt capacitor injection [8].

However, in order to provide relatively a free hand to the operator at the sending end to control the said variables, an investigative research is still needed to study the individual and joint effect of tap changing transformer at the sending end and shunt compensation at the receiving end or load end. The tap and the shunt compensation being the control variables a look-up table of these parameters for constant voltage/constant reactive power also needed to assist the system operator for regulating the said variables. This kind of study is also necessary to design an expert system or to design an online controller.

II. TapChanging Transformer Modeling

A transformer can be represented as an ideal transformer with turns ratio '*a*' in series with transformer series impedance Z_t (where $Z_t = 1/Y_t$), neglecting the magnetizing circuit. Fig. 1 represents the model of the tap changing transformer. Tap '*a*' is a real number in case of voltage or reactive power control and complex number in case of active power control.

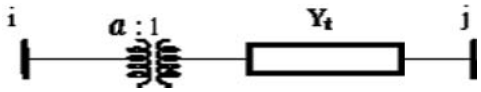

Fig. 1. Representation of transformer with tap setting ratio *a* : 1

Here the tap exists on non-unity side and it is called tap side and the series admittance is connected on the unity side. The equivalent Π circuit for this can easily be derived from the elementary voltage-current relationships [9]. This equivalent circuit is shown in Fig. 2.

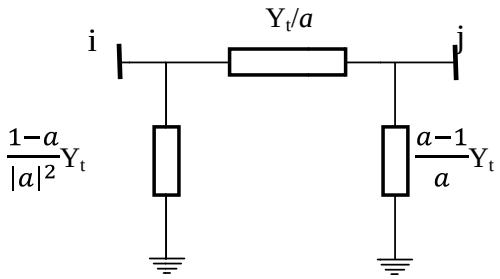

Fig. 2. Equivalent Π circuit of a tap changing transformer

III. Joint Effect of Transformer Tap and Shunt Compensation

In order to study the steady state performance of the long line with reactive compensation provided jointly with tap changing transformer and shunt compensation, the scheme shown in Fig. 3 is considered.

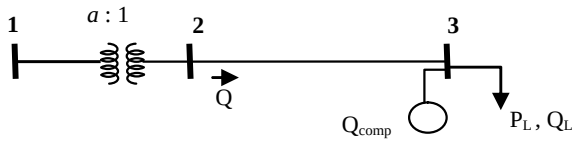

Fig. 3. Transmission line with joint compensation

Tap changing transformer is connected at sending end of the transmission line and shunt compensation is provided at the receiving end of the line. A load-flow is conducted on the transmission line for various values of tap settings and shunt compensation.

The sending end (bus 1) is considered as slack bus, the non-tap side of transformer (bus 2) is considered as PQ bus with P=0, Q=0, and receiving end (bus 3) as PQ bus with P_L, Q_L, and shunt compensator Q_{comp} connected to it.

IV. Case Study

For the case study, the transmission line and transformer parameters are taken as follows.

Line parameters:

Series resistance = 0.04699 pu

Series reactance = 0.19797 pu

Half line shunt susceptance = 0.0219 pu

Transformer parameters:

Series reactance = 0.20912 pu

The load details at the bus 3 are P_L = 0.5 pu, Q_L = 0.19 pu and Q_G = 0.4 pu. Transformer tap is varied from 0.8 to 1.2 and the reactive compensation is varied from -0.4 pu (-40 MVAr) to +0.4 pu(40 MVAr). The control variables (in this case transformer tap at sending end and reactive compensator at the receiving end) are varied such that a constant voltage is always maintained at the receiving end.

A look-up table (Table I) is prepared to show the various combinations of both the control variables (transformer tap and reactive compensation) in order to keep the receiving end (bus 3) voltage at a constant value. The constant voltage contours are also plotted on the parametric plane (Fig. 4).

IV.1. Voltage Variation

It is clear that the voltage varies with both transformer tap and shunt compensator. The voltage value for different tap values and shunt compensator values are shown in the Table II.

The same is displayed in Figs. 5, 6, and 7. As it is well known the voltage magnitude increases with the reactive compensation moving from more inductive to less inductive and more capacitive, Fig. 5 depicts the same.

The transmission line is on the non-tap side, so voltage magnitude is decreased with increase in tap and vice-versa, Fig. 6 shows this.

TABLE I
LOOK-UP TABLE FOR CONSTANT VOLTAGE

	Q_{comp}(MVAr)						
Tr. Tap / Voltage, pu	0.85	0.9	0.95	1.0	1.05	1.1	1.15
0.8	-	-	-	-	-	-32.07	-23.75
0.85	-	-	-	-	-32.97	-23.3	-14.57
0.9	-	-	-	-34.62	-23.6	-13.44	-4.098
0.95	-	-	-37.55	-24.52	-12.87	-2.287	7.773
1.0	-	-	-26.8	-13.17	-0.9078	10.46	20.68
1.05	-	-30.46	-14.74	-0.4347	12.32	23.98	35.08
1.1	-36.29	-18.12	-1.669	13.17	26.63	39.29	-
1.15	-23.37	-4.25	12.74	28.5	-	-	-
1.2	-9.22	10.61	28.47		-	-	-

TABLE II
VOLTAGE VALUES FOR DIFFERENT TAP AND SHUNT COMPENSATOR VALUES

	Voltage at receiving end, pu								
Tr. Tap / **Q_{comp}(MVAr)**	0.8	0.85	0.9	0.95	1.0	1.05	1.1	1.15	1.2
-40	1.1684	1.0845	1.0079	0.9372	0.8709	0.8077	0.7461	0.6838	0.6164
-35	1.1872	1.1050	1.0304	0.9620	0.8983	0.8384	0.7811	0.7251	0.6684
-30	1.2054	1.1248	1.0519	0.9853	0.9239	0.8666	0.8124	0.7605	0.7096
-25	1.2230	1.1438	1.0725	1.0076	0.9480	0.8927	0.8410	0.7920	0.7449
-20	1.2401	1.1622	1.0922	1.0287	0.9707	0.9172	0.8675	0.8207	0.7763
-15	1.2568	1.1800	1.1112	1.0490	0.9924	0.9404	0.8922	0.8472	0.8049
-10	1.2730	1.1973	1.1296	1.0686	1.0131	0.9623	0.9155	0.8720	0.8313
-5	1.2887	1.2141	1.1474	1.0874	1.0330	0.9833	0.9377	0.8954	0.8561
0	1.3042	1.2304	1.1646	1.1056	1.0521	1.0034	0.9588	0.9176	0.8794
5	1.3192	1.2463	1.1814	1.1232	1.0706	1.0228	0.9790	0.9388	0.9015
10	1.3340	1.2618	1.1977	1.1403	1.0885	1.0414	0.9985	0.9590	0.9225
15	1.3484	1.2770	1.2136	1.1569	1.1058	1.0595	1.0172	0.9785	0.9427
20	1.3625	1.2918	1.2291	1.1731	1.1226	1.0769	1.0353	0.9972	0.9621
25	1.3764	1.3064	1.2443	1.1888	1.1390	1.0939	1.0529	1.0154	0.9808
30	1.3900	1.3206	1.2591	1.2042	1.1549	1.1104	1.0699	1.0329	0.9989
35	1.4034	1.3346	1.2736	1.2193	1.1705	1.1265	1.0865	1.0499	1.0164
40	1.4166	1.3482	1.2878	1.2340	1.1857	1.1421	1.1026	1.0665	1.0334

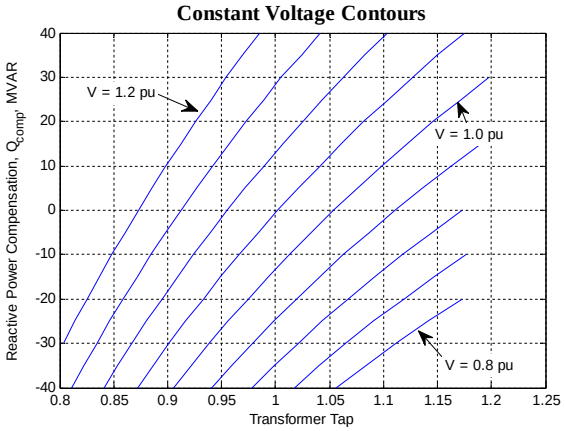

Fig. 4. Constant voltage contours

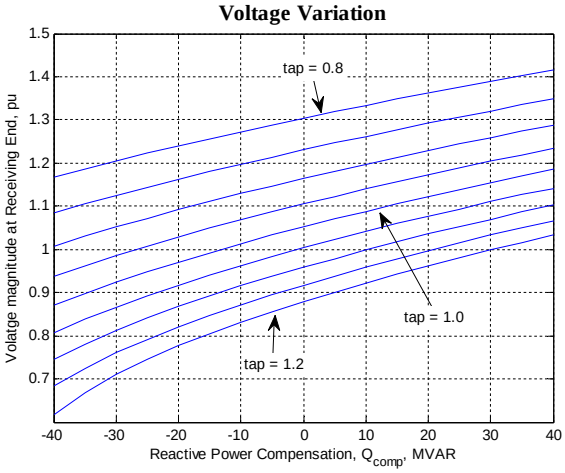

Fig. 5. Receiving end voltage variation with shunt compensation

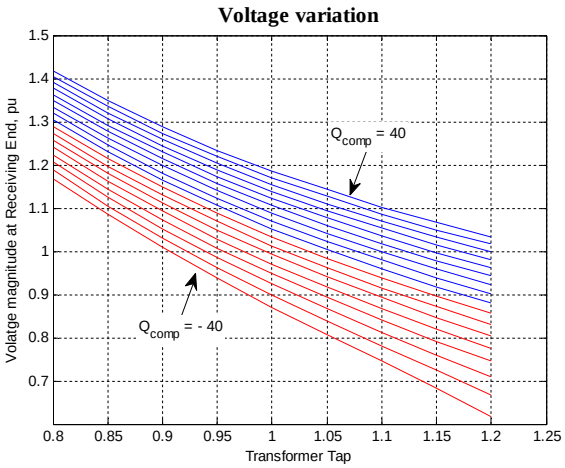

Fig. 6. Receiving end voltage variation with transformer tap

From the data in Table II and figures it is interesting to observe that, for a given compensation the effect of voltage variation with respect to variation in tap setting is almost the same as the variation of the voltage with respect to compensation for a given tap setting. This observation, of course is subject to the reactive power limits that are imposed on the compensation.

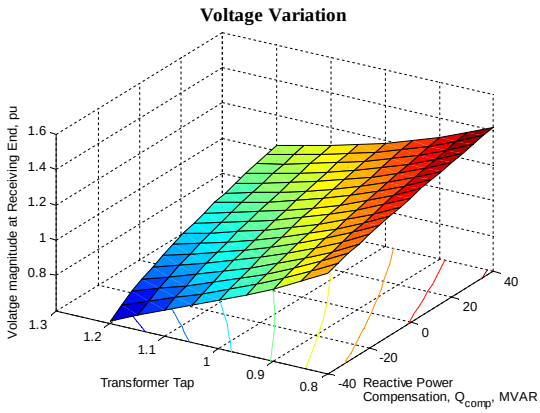

Fig. 7. Receiving end voltage variation with tap and shunt compensation

But in case of receiving end voltage angle it is different. At lower tap values the change in shunt compensator has no effect on voltage angle. At higher tap values there is a minor change in angle (approximately 6^0 in this case) with the change in shunt compensator value varying from -40 to +40 MVAr. These voltage angle changes are shown in Figs. 8, 9 and 10.

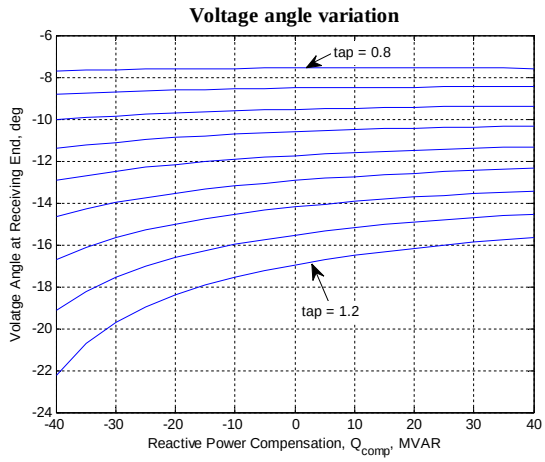

Fig. 8. Receiving end voltage angle variation with tap and shunt compensation

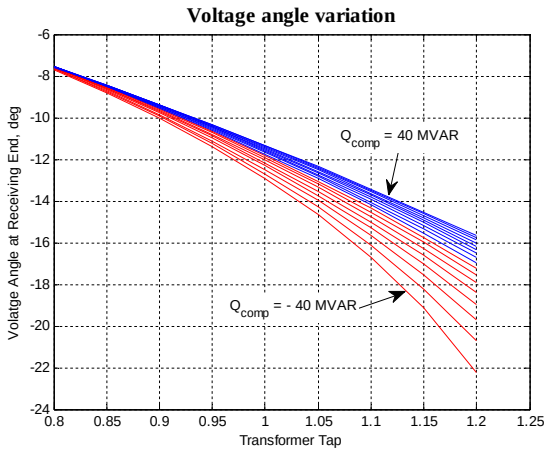

Fig. 9. Receiving end voltage angle variation with transformer tap

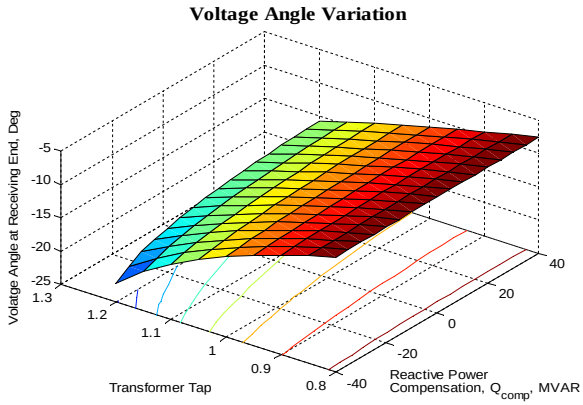

Fig. 10. Receiving end voltage angle variation with tap and shunt compensation

IV.2. Reactive Power Flow In Line

The reactive power flow variation with both the control parameters is also observed. It is interesting to note that the reactive power variation with tap change is around 0.1 pu irrespective of the shunt compensation value. On the other hand a significant change in reactive power flow in the line is observed with the change in shunt compensator value at any tap. This is shown in Figs. 11, 12, and 13

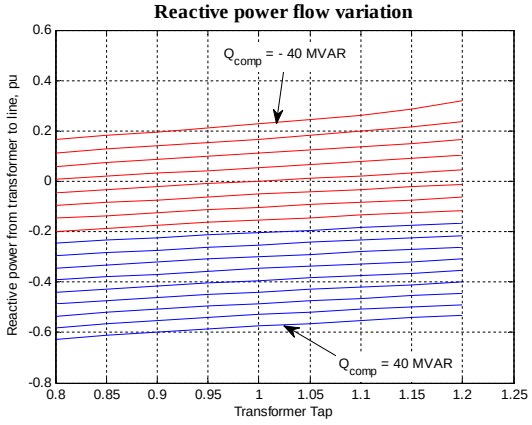

Fig. 11. Reactive power variation with tap

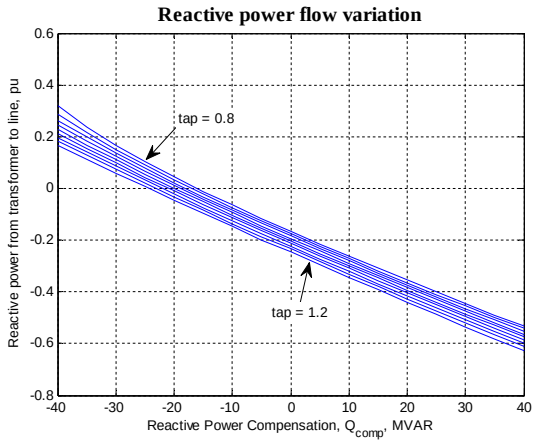

Fig. 12. Reactive power variation with shunt compensation

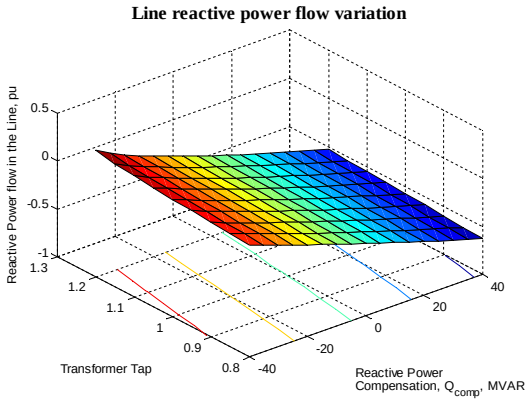

Fig. 13. Reactive power variation with tap and shunt compensation

A look-up table for constant reactive power flow in the line is formed. The values in the Table III show the required shunt reactive compensation value at the receiving end for a given tap and line reactive power flow.

For example, in order to keep the line reactive power flow at the sending end of the line at -0.2 pu, the shunt compensation value is 1.606 MVAr at tap 0.9 and -2.402 MVAr at tap 1.1.

The values are shown in Table III and the corresponding constant reactive power flow lines are displayed in Fig. 14.

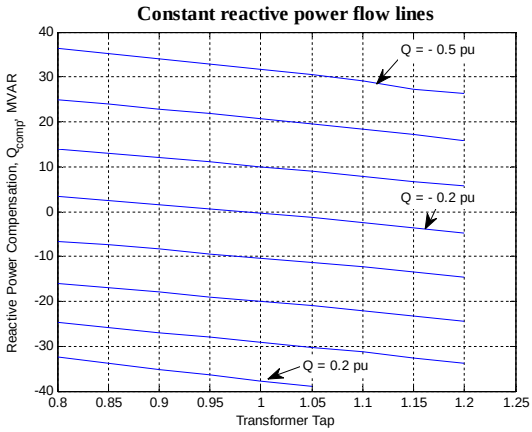

Fig. 14. Constant reactive power flow lines

IV.3. Real Power Flow in Line

As expected the real power flow variation in this case is very minimal because the model has slack bus and PQ bus in a single line. As the load bus is a PQ bus, any change in line flow reflects in the line losses.

From Fig. 15 and Fig. 16 this can be observed. The maximum change in the real power is approximately 0.027 pu at any combination of tap and shunt compensator value. Plots are also drawn in PQ plane for the real and reactive powers at the sending end of the line for various tap and shunt compensator values. These are shown in Figs. 17 and 18.

TABLE III
LOOK-UP TABLE FOR CONSTANT REACTIVE POWER FLOW IN LINE

Tr. Tap \ Q in Line, pu	Q_{comp} (MVAr) -0.5	-0.4	-0.3	-0.2	-0.1	0	0.1	0.2
0.8	36.3	24.96	14.01	3.474	-6.554	-15.99	-24.7	-32.41
0.85	35.16	23.93	13.04	2.552	-7.485	-16.98	-25.83	-33.86
0.9	34.03	22.88	12.07	1.606	-8.42	-17.96	-26.93	-35.22
0.95	32.88	21.82	11.07	0.657	-9.37	-18.95	-28.02	-36.48
1.0	31.68	20.71	10.04	-0.3277	-10.34	-19.96	-29.12	-37.74
1.05	30.44	19.58	8.981	-1.337	-11.32	-20.97	-30.22	-38.99
1.1	29.15	18.39	7.862	-2.402	-12.37	-22.03	-31.34	
1.15	27.29	17.13	6.678	-3.536	-13.49	-23.16	-32.53	
1.2	26.34	15.76	5.836	-4.783	-14.71	-24.39	-33.8	

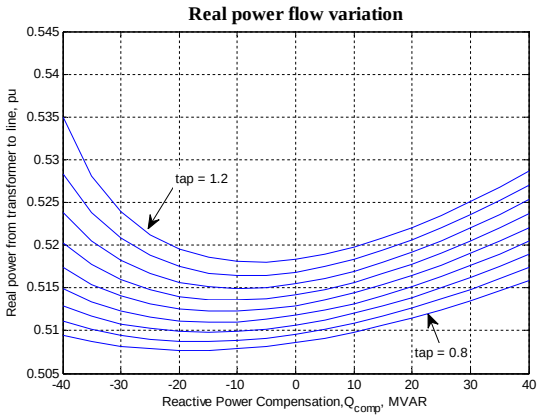

Fig. 15. Real power flow variation with reactive compensation

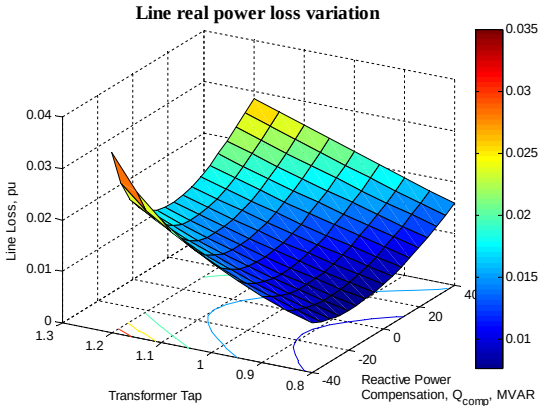

Fig. 16. Real power loss variation with tap and shunt compensation

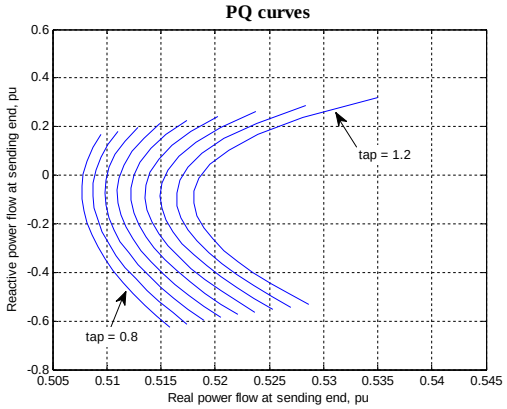

Fig. 17. PQ curves for various taps

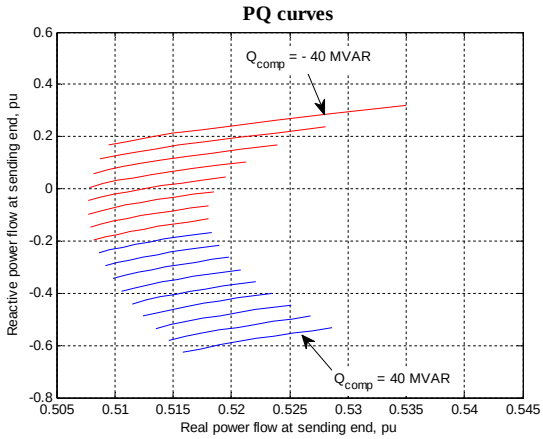

Fig. 18. PQ curves for different shunt compensation

IV.4. Voltage Profiles

At each combination of tap and shunt compensator values the voltage profile along the line is observed. As is in the model both the ends of the line (bus 2 and bus 3) are considered as PQ buses; hence the voltage magnitude varies. The voltage profiles along the line for some values, (depending on the system under study, in this case tap varies from 0.8 to 1.2 in steps of 0.2 and Q_{comp} is varied from -40 to +40 in steps of 20), are shown in Fig. 19.

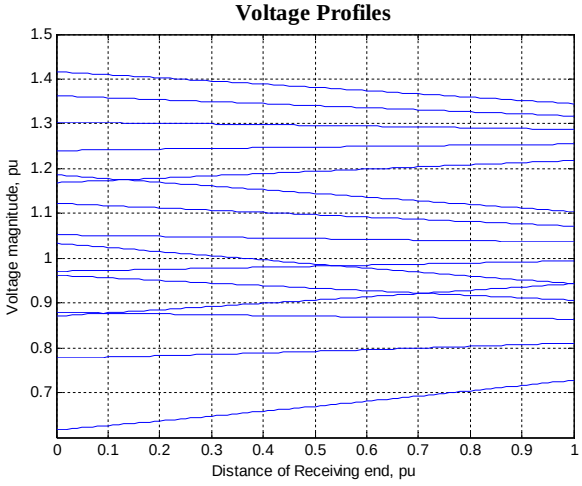

Fig. 19. Voltage profiles along the line

The voltage magnitudes at both ends are at different values. It is not possible to keep both the voltage magnitudes at any same desired value. However with the available controls, both ends of the line can be maintained at the same voltage magnitude only in some cases. But some of these values are beyond the allowable voltage levels. If the allowable voltage limits are considered as 0.95pu and 1.05 pu, there are only two valid rows which are in bold. Those details are shown in Table IV. The voltage profiles for the two valid cases are shown in Figs. 20 and 21.

TABLE IV
VALUES OF TAP AND Q_{comp} FOR SAME VOLTAGE ON LINE BOTH ENDS

Tap	Q_{comp} MVAr	Voltage magnitude at receiving end, pu	Voltage angle at receiving end, deg	Voltage magnitude at sending end, pu	Voltage angle at sending end, deg
0.8	-10.91	1.27	-7.582	1.27	-3.836
0.85	-10.3	1.196	-8.564	1.196	-4.336
0.9	-9.719	1.131	-9.608	1.131	-4.869
0.95	-9.191	1.072	-10.72	1.072	-5.437
1	**-8.655**	**1.018**	**-11.9**	**1.018**	**-6.038**
1.05	**-8.148**	**0.9701**	**-13.14**	**0.9701**	**-6.676**
1.1	-7.656	0.9259	-14.46	0.9259	-7.351
1.15	-7.168	0.8853	-15.86	0.8853	-8.065
1.2	-6.655	0.8478	-17.34	0.8478	-8.821

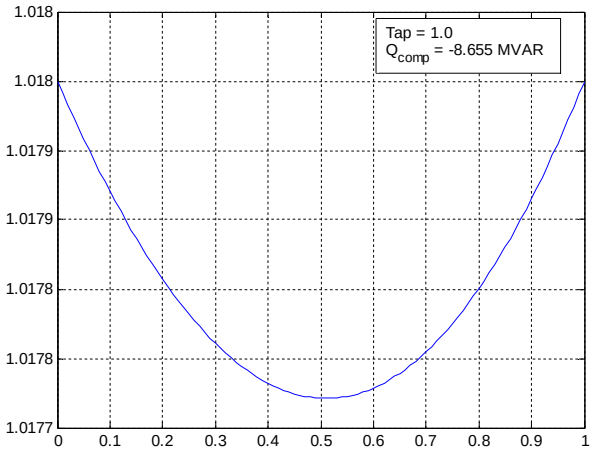

Fig. 20. Voltage profile at tap=1.0 and Q_{comp} = -8.655 MVAr

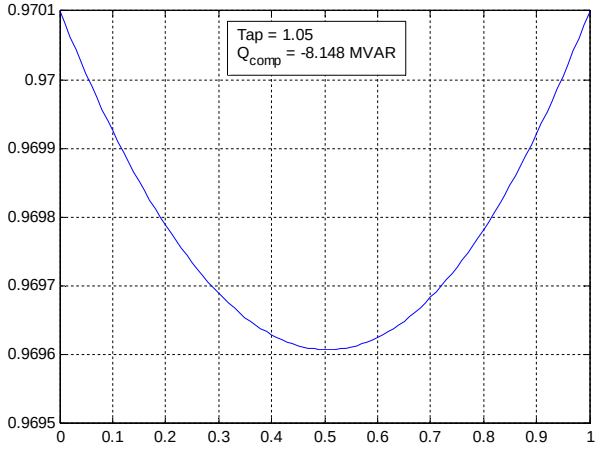

Fig. 21. Voltage profile at tap=1.05 and Q_{comp} = -8.148 MVAr

As the voltage angle difference is very less (5.862^0 and 6.464^0), the voltage all along the line is almost at the same value, hence exhibiting a flat voltage profile [10].

V. Conclusion

The combined effect of transformer tap and shunt compensation on the voltage profile of a transmission line has been investigated. In particular, constant voltage contours in the parametric plane (like phase plane curves) have been plotted and analyzed. Similarly constant reactive power plots have also been drawn in the similar parametric plane.

These investigations help in designing an expert system situated at the sending end to maintain nearly a constant voltage profile over the transmission line. It is observed that, while both the tap and shunt compensator influence both the voltage magnitude and reactive power, the tap controls more of voltage than reactive power and the shunt compensator controls more of reactive power than the voltage magnitude.

References

[1] Bridenbaugh, C.J.; DiMascio, D.A.; D'Aquila, R. "Voltage control improvement through capacitor and transformer tap optimization"*IEEE Transactions on Power Systems, 1992, pp 222-227.*

[2] Pablo Frıas, Tomas Gomez, David Soler, "Voltage Control and Reactive Power Support in the Spanish Transmission Network", *IEEE Mediterranean Electrotechnical Conference, MELECON 2006, pp. 916 - 919.*

[3] C. C. Liu and K. Tomsovic, "An expert System Assisting Decision-Making of Reactive Power/Voltage Control", *IEEE, vol. PWRS-1, no. 3, pp.195 -201 1986*

[4] S.J.Cheng, O.P.Malik and G.S.Hope, "An Expert System for Voltage and Reactive Power Control of a Power System", *IEEE Transactions on Power Systems, Vol.3, No.4, November 1988, pp. 1449-1455*

[5] J.L. Martinez Ramos et al., "A Hybrid Tool to Assist the Operator in Reactive Power/Voltage Control and Optimization", *IEEE Trans. on PWRS, Vol. 10, No. 2, May 1995, pp. 760-768*

[6] Taylor, G.A., Rashidinejad, M., Song, Y.-H. ; Irving, M.R., Bradley, M.E.; Williams, T.G. "Algorithmic techniques for transition-optimised voltage and reactive power control", International Conference on Power System Technology Proceedings, PowerCon 2002, IEEE-PES/CSEE, Kunming, China, Volume: 3, pp. 1660 – 1664

[7] Bansilal D. Thukaram; K. Parthasarathy, "An Expert System for Voltage Control in a Power System Network", *International Conference on Energy Management and Power Delivery, Proceedings of EMPD'95, 1995, pp 364-369.*

[8] Pyone Lai Swe, WannaSwe and KyawMyo Lin, "Effects of Tap Changing Transformer and Shunt Capacitor on Voltage Stability Enhancement of Transmission Networks", *World Academy of Science, Engineering and Technology 51,2011, pp 555-558.*

[9] John J. Grainger and William D. Stevenson, *Power System Analysis* (Tata McGraw-Hill, 2003).

[10] Srinivasa Rao N.L., Govinda Rao G., Sivanagaraju S., "Beta (phase constant) compensation for flat voltage profile in a transmission line", International Journal of Electrical Power Systems Research (EPSR, ELSEVIER), Volume 104, November 2013, pp. 35–41

[11] Baum, W.U.; Frederick, W.A., "A Method of Applying Switched and Fixed Capacitors for Voltage Control", *IEEE Transactions on Power Apparatus and Systems, Volume: 84,* Issue 1, *1965, pp 42-48.*

[12] Edward W. Kimbark, "A New Look at Shunt Compensation",

IEEE Transactions on Power Apparatus and Systems, Vol. PAS-102, No.1, *January 1983, pp 212-218.*

[13] Rao, N.L.S., Govinda Rao, G., Sivanagaraju, S., An extension to the theory of the transmission lines, (2012) *International Review on Modelling and Simulations (IREMOS)*, 5 (5), pp. 2348-2354.

[14] Timothy J. E. Miller, *Reactive Power Control in Electric Systems* (Wiley-India Edition, 2010).

[15] HadiSaadat, *Power System Analysis*(Tata McGraw-Hill, New Delhi, 2010).

[16] P. Kundur,*Power System Stability and Control*, (McGraw-Hill, New York. 1994,).

[17] G. Anderson et al., "Causes of 2003 Major Grid Blackouts in North America and Europe, and Recommended Means to Improve System Dynamic Performance", *IEEE Transactions on Power Systems, Vol.20, no.4, Nov 2005, pp. 1922-1928.*

[18] Mohamed Mostafa Saied,"Optimal Long Line Series Compensation",IEEETransactions on Power Systems, Vol. PWRD-1, No. 2, April 1986, pp 248-253.

[19] Dixon, J., Moran, L., Rodriguez, J., Domke, R., "Reactive Power Compensation Technologies: State-of-the-Art Review",proceedings of the IEEE (Volume:93 , Issue: 12), Dec. 2005, pp 2144 – 2164.

[20] N.J.Balu, R.Adapa, G. Cauley , M. Lauby and D.J. Maratukulam "Review of Expert Systems in Bulk Power System Planning and Operation", Proceedings of the IEEE, vol.80, no.5, 1992, pp.727 - 731.

[21] Shakeri, J., Abbasi, A.H., Shayegani, A.A., Mohseni, H., A new method for partial discharge localization using multi-conductor transmission line model in transformer winding, (2009) *International Review of Electrical Engineering (IREE)*, 4 (3), pp. 470-476.

[22] Porkar, S., Poure, P., Abbaspour-Tehrani-fard, A., Saadate, S., Distributed generation planning for losses, voltage profile, line congestion and total system cost improvement, (2009) *International Review of Electrical Engineering (IREE)*, 4 (3), pp. 434-440.

Authors' information

Dr. **Nakka Lakshmi Srinivasa Rao** is born at Visakhapatnam, Andhra Pradesh, India. He obtained B.E. (Electrical and Electronics Engg) and M.E. (Power Systems) from Andhra University, Visakhapatnam, India. He received Ph.D. from JNTU, Kakinada. He started his career as an Electrical Engineer with M.N.Dastur&Co Ltd and worked 4+ years at Visakhapatnam Steel Plant site. Later he joined GITAM University as faculty member and worked for 8 years. Since 2000, he has been working in AT&T at NJ, USA. He presented and published 11 papers in Conferences and Journals of National and International repute. His research interests are in Transmission Lines and Reactive Power Management. Dr. Srinivas is a Member of Institution of Engineers (India), Society of EMC Engineers (India) .

Dr. **G. Govinda Rao** is born at Srikakulam, Andhra Pradesh, India on 19th January, 1939. He obtained B.E.(Electrical Engg.) and M.E.(Power Systems) from Andhra University, Visakhapatnam, India and Ph.D. in the area of Long Term Dynamics in Power Systems from IISc, Bangalore, India. Working after a short while as an Electrical Engineer, he joined on the Teaching Faculty of Andhra University College of Engg., Visakhapatnam, India and served for more than 40 years in different positions. After relinquishing his service there, he worked as Professor at ANITS, Visakhapatnam for 4 years. After working for a semester at Southern Polytechnic State University, South Marietta, USA as a Visiting Professor, he is presently working as a Senior Professor in the GVP College of Engg., Visakhapatnam, India, putting forth a total service of over 55 years. He presented and published more than 62 Papers in Conferences and Journals of National and International Repute. He was awarded the Best Teacher Award by the A.P. State Government. His research interests are in fundamentals of Circuit Analysis, Power System Dynamics, Voltage Stability and Reactive Power Management. Prof. Govinda Rao is a Fellow of Institution of Engineers (India) (FIE), and a Member of Society of Technical Education (India).

Dr. **S. Sivanagaraju** obtained B.E.(Electrical and Electronics Engg) in 1998 from Andhra University, M.Tech in 2000 from IIT, Kharagpur and Ph.D. from J.N.T. University in 2004. He joined the faculty of JNTU, Ananthapur, India in Oct. 1999 and currently working as Professor and Board of Chairman, Dept. of Electrical Engg., JNTU, Kakinada, Andhra Pradesh, India. He presented and published 60+ publications in National and International Conferences and Journals. He has received two National awards (Pandit Madan Mohan Malaviya memorial prize award and Best paper prize award) from the Institute of Engineers (India) for the year 2003-04. He is referee for IEE Proceedings-Generation, Transmission and Distribution, and International Journal of Emerging Electric Power Systems. His areas of interest are in Distribution Automation, Genetic Applications to Distribution Systems and Power Systems.

International Review of Automatic Control (I.RE.A.CO.), Vol. 8, N. 2
ISSN 1974-6059 March 2015

State-Feedback Control in TCP Network: Geometric Approach

K. Lefrouni, R. Ellaia

Abstract – *In this paper, we study the problem of congestion of a router, initially, we propose a model of TCP based on the fluid flux model and, secondly, considering frequency-domain approach, we synthesize a state-feedback control to ensure the stability of our system. This study is essentially based on the analysis of the stability of the characteristic equation associated to closed loop system with consideration of communication delays. Finally, simulation results are provided to validate the proposed methodology.*

Keywords*: Congestion Control, TCP Network, Delay Systems, Geometric Approach*

Nomenclature

TCP	Transmission Control Protocol
AQM	Active Queue Management
QoS	Quality of Service
SISO	Single Input Single Output system
PI	Proportional Integral
R	Round-Trip Time (RTT)
W	TCP window size
N	Number of TCP sessions
T_p	Propagation delay
C	Link capacity
p	Probability of dropping packets
q	Queue length
K	State feedback gain
$x(t)$	State vector
τ_1	Delay time from the source to the router
τ_2	Delay time from the router to the source via the receiver
τ^*	Critical delay
ω_0	Critical crossing frequency
Ω	Set of crossing frequency

I. Introduction

We were interested in this paper at the problem of congestion of a router in TCP Network, more precisely, we have focused on the determination of stability regions of the closed-loop system, and on the development of a state feedback control based on Active Queue Management (AQM) mechanism. Implemented in the router, this control law will allow TCP traffic regulation and, at the same time, maintaining a certain level of Quality of Service (QoS). Several control laws have been developed to regulate congestion in the router [1]-[4].

However, most of these studies have been based on temporal approaches that can grouped into two categories, the first category uses the state prediction techniques [5]-[6] and the second, the Lyapunov-Krasovskii functionals [7]-[9] and the Lyapunov-Razumikhin functions [10]-[11].

Although interesting in theory, these methods requiring multiple matrix calculations and are difficult to use in practice. Studies that are interested in solving a problem using frequency approaches are very few, and are based generally on the smith predictor [12]-[13], a technique that is only valid when the communication delays from the source to the router and from the router to the source are identical, and when the system is stable in the open loop. Motivated by synthesis techniques in the frequency domain, we propose to develop a state feedback control law by using a so-called geometric approach (see [14]-[16]). This technique allows to determine the system stability region in the control parameter space with asymmetric communication delays.

Thus allowing to choose the parameters of the control law belonging to the stability region and satisfying the desired requirements. The remaining of the paper is organized as follows. In section 2, we introduce a fluid flow model of TCP network, section 3 is dedicated to the synthesis of a state feedback control law ensuring the stabilization of the closed loop system. Section 4 presents an example extracted from the literature and simulations validate the proposed methodology. Finally, we present our conclusions in section 5.

II. TCP Network Modeling

The majority of research examining the control of congestion in TCP network have used a model based on the fluid mechanics, and which was developed by Misra et al [17]-[18].

II.1. Preliminaries

Considering the network parameters: TCP window size, number of TCP sessions, link capacity, probability

of dropping packets and the queue length (*W*, *N*, *C*, *p* and *q* respectively), the fluid model of TCP network is the following:

$$\begin{cases} \dot{W}(t) = \dfrac{1}{R(t)} - \dfrac{W(t)W\left(t-R(t)\right)}{2R\left(t-R(t)\right)} p\left(t-R(t)\right) \\ \dot{q}(t) = \dfrac{W(t)}{R(t)} N(t) - C \\ R(t) = \tau_1(t) + \tau_2(t) \end{cases} \quad (1)$$

where $R(t)$, τ_1 and τ_2 are respectively, the round-trip time (RTT), the delay time from the source to the router and the delay time from the router to the source via the receiver.

Remark 1. The communication between the router and the different sources can be considered as a single input single output system (SISO).

Indeed the TCP flow model (1) considers the flow from N TCP sessions without specifying the source of each session.

In this paper, we consider that the delays are constant and asymmetric.

II.2. The Linearized TCP Fluid Model

The linearization of the model (1) requires firstly the determination of the operating point, this point is defined by the two equations $\dot{W} = 0$ and $\dot{q} = 0$.

After calculation, we find:

$$W_0^2 p_0 = 2 \text{ and } W_0 = \frac{R_0 C}{N} \quad (2)$$

Thus, the linear model around the operating point is defined by:

$$\begin{cases} \delta\dot{W}(t) = -\dfrac{2N}{R_0^2 C}\delta W(t) - \dfrac{R_0 C^2}{2N^2}\delta p\left(t-\tau_1(t)\right) \\ \delta\dot{q}(t) = \dfrac{N}{R_0}\delta W(t) - \dfrac{1}{R_0}\delta q(t) \end{cases} \quad (3)$$

For more details about the linearization, see [19]. As a result, the state space model of TCP network can be written as follows:

$$\begin{cases} \dot{x}(t) = Ax(t) + Bu\left(t-\tau_1(t)\right) \\ y(t) = Cx(t) \end{cases} \quad (4)$$

where $x(t) = \left[\delta W(t)\ \delta q(t)\right]^T$ is the state vector, $u(t) = p(t)$ is the input, and:

$$A = \begin{bmatrix} a_1 & 0 \\ a_2 & a_3 \end{bmatrix},\ B = \begin{bmatrix} b_1 \\ 0 \end{bmatrix}, C = \begin{bmatrix} 0 & 1 \end{bmatrix}$$

with:

$$a_1 = \frac{-2N}{R_0^2 C},\quad a_2 = \frac{N}{R_0},\quad a_3 = \frac{-1}{R_0},\quad b_1 = \frac{-R_0 C^2}{2N^2}$$

III. State-feedback Control Law

This section will be devoted to the synthesis of a state feedback control ensuring the stability of the closed loop system.

As is mentioned in the introduction, we conducted a study in the frequency domain based on a geometric approach [16], which allows to determine in the control parameter space, the areas where the stability is assured.

III.1. Principle of Geometric Approach

The geometric approach is a frequency method allowing, firstly, the determination of stability regions during the synthesis of a control law, and secondly, the determination of the regions where the estimation error converges to zero during the synthesis of an observer.

This approach goes through several stages. For example, during the synthesis of a control law.

First, assuming a zero delay, we determine the conditions for which the closed loop system is stable, which amounts to determine the conditions where the characteristic polynomial of the closed loop system is Hurwitz.

Then, in the second step, we determine the set of points for which the characteristic equation associated to the closed loop system has at least one pure imaginary root for a fixed value of the delay, the set of these points is called crossing curve.

Finally, we determine the direction of crossing which represents the direction of evolution of crossing points when the parameters of correction vary. This allows to know if these parameters have a stabilizing effect (roots cross the imaginary axis from the right to the left) or destabilizing effect.

Several studies are based on this approach, in particular, the authors of [20] have developed a PI controller stabilizing a linear system with delayed input.

In the following, we present only the necessary points for solving our problem.

III.2. Stability Study

We will now apply the different steps mentioned in the previous paragraph, to find the stability regions of the closed loop system.

The state feedback control law has the following form:

$$u(t) = -Kx(t) \quad (5)$$

where K is the state feedback gain to ensure the stability of the closed loop system (4) for any $\tau_1 < \tau^*$ (where τ^* is the maximum value of the delay τ_1, beyond which the closed loop system becomes unstable).

Under the assumption that the pair (A, B) is controllable, the problem then is to determine the gain K, such that the characteristic equation associated to the closed-loop system:

$$H\left(s,e^{-\tau_1 s}\right) = det\left(sI_2 - \left(A - BKe^{-\tau_1 s}\right)\right) = 0 \qquad (6)$$

is Hurwitz for any $\tau_1 < \tau^*$. By introducing the Laplace transform, our system can be written as the following form:

$$\begin{cases} sx(s) = Ax(s) + Bu(s)e^{-\tau_1 s} \\ y(s) = Cx(s) \end{cases} \qquad (7)$$

Also, the control law takes the form:

$$u(s) = -Kx(s) \qquad (8)$$

where s is the Laplace variable, and $K = [k_1, k_2]$ is the state feedback gain. The characteristic equation associated to the closed loop system is then defined by:

$$H(s,k_1, k_2,\tau_1) = Q(s) + P(s)e^{-\tau_1 s} = 0 \qquad (9)$$

where $Q(s)$ and $P(s)$ are two polynomials with real coefficients defined by:

$$\begin{aligned} Q(s) &= s^2 - (a_1 + a_3)s + a_1 a_3 \\ P(s) &= b_1(a_2 k_2 - a_3 k_1 + k_1 s) \end{aligned} \qquad (10)$$

Remark 2. The characteristic Eq. (9) has real coefficients, therefore, if s is a root of (9) then its conjugate $\bar{s} = -s$ is also a root.

Additionally, if s is purely imaginary, we have $\bar{s} = -s$. Thus, if there are characteristic roots located on the imaginary axis, then it verify the following system:

$$\begin{aligned} H(s,k_1, k_2,\tau_1) &= Q(s) + P(s)e^{-\tau_1 s} = 0 \\ H(-s,k_1, k_2,\tau_1) &= Q(-s) + P(-s)e^{\tau_1 s} = 0 \end{aligned} \qquad (11)$$

Consider first the case of a closed loop system with zero delay, and seeking conditions on the parameters of the corrector to ensure the stability of the closed loop system (4). In this case, so that the characteristic polynomial $H(s,k_1, k_2,0) = 0$ defined by (9) is Hurwitz.

That is, all its roots are located in the complex left half plane, it is necessary that:

$$k_1 < \frac{a_1 + a_3}{b_1}, k_2 < \frac{a_3}{a_2}k_1 - \frac{a_1 a_3}{b_1 a_2} \qquad (12)$$

which represents a first condition on the parameters of the corrector. Furthermore, the determination of conditions to ensure the stability of the closed loop system in the presence of a non-zero delay will be the subject of the following sections.

III.3. Crossing Curves

In order to determine the parameters of the state feedback gain K ensuring the distribution of the roots of the characteristic Eq. (6) in the complex left half plane, it is necessary, first, to determine the K parameters for which the characteristic Eq. (6) has at least one pure imaginary root. This amounts to solving the following equation:

$$\forall \omega > 0, \quad \tau^* \in R^+, \quad H\left(j\omega,e^{-j\omega\tau^*}\right) = 0 \qquad (13)$$

The K parameters for which (13) is satisfied, that is, for which the system is at the limit of stability, define what is called the crossing points. Which then allows to generate the crossing curves in the space defined by the K parameters for a fixed value of the delay τ^*.

In view of our system (4) we can then determine all the crossing points in the space of parameters (k_2, k_1) as follows:

Proposition 1. For a delay $\tau^* > 0$ and $\omega \in \Omega$, the crossing points (k_2, k_1) satisfy the following relations:

$$k_1 = \frac{a_1 + a_3}{\beta}\omega + \frac{\left[\omega^2 - \frac{\alpha}{\beta}(a_1 + a_3)\omega - a_1 a_3\right] sin\left(\omega\tau^*\right)}{\alpha\, sin\left(\omega\tau^*\right) + \beta\, cos\left(\omega\tau^*\right)} \qquad (14)$$

$$k_2 = \frac{\omega^2 - \frac{\alpha}{\beta}(a_1 + a_3)\omega - a_1 a_3}{a_2 b_1\left[\frac{\alpha}{\beta} sin\left(\omega\tau^*\right) + cos\left(\omega\tau^*\right)\right]} \qquad (15)$$

with:

$$\begin{aligned} \alpha &= b_1\omega\, sin\left(\omega\tau^*\right) - b_1 a_3\, cos\left(\omega\tau^*\right) \\ \beta &= b_1 a_3\, sin\left(\omega\tau^*\right) + \omega b_1\, cos\left(\omega\tau^*\right) \end{aligned}$$

where Ω is the set of crossing frequency $\omega \in R^+$ such that there is at least one pair (k_2, k_1) for which $H\left(j\omega,k_1, k_2,\tau^*\right) = 0$ is satisfied.

Proof: By rewriting the characteristic Eq. (13) as follows:

$$-\omega^2 - (a_1 + a_3)\, j\omega + a_1 a_3 + \\ + b_1 (a_2 k_2 - a_3 k_1 + j\omega k_1) e^{-j\omega\tau^*} = 0$$

Then, by separating the real and imaginary parts, we obtain:

$$k_1 \alpha + k_2 a_2 b_1 \cos(\omega \tau^*) = \omega^2 - a_1 a_3$$
$$k_1 \beta - k_2 a_2 b_1 \sin(\omega \tau^*) = (a_1 + a_3)\omega$$

The direct resolution of these two equations leads to the relations (14) and (15).

Remark 3. The restriction of the study to the positive frequencies arises from the remark 2, which, stipulates that:

$$H(j\omega, k_1, k_2, \tau^*) = 0 \Leftrightarrow H(-j\omega, k_1, k_2, \tau^*) = 0$$

Thus, considering the numerical example presented in [3], and different values of $\tau^* \in \{0.3, 0.5, 0.7\}$, we get, for positive values of ω, the crossing curves shown in Fig. 1, Fig. 2 and Fig. 3.

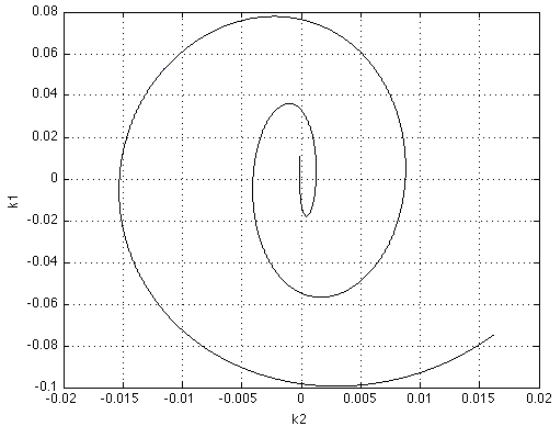

Fig. 1. Crossing curves for the closed loop system with $\tau^* = 0.3$

Remark 4. When ω tends to infinity, the parameters k_1 and k_2 given by (14) and (15) also tends to infinity.

But, in the context of our study, we are interested in determining the crossing points (k_1, k_2) such as k_1 and k_2 are finite. So subsequently, we will assume that the set of crossing frequency Ω consists of a finite number of finite length intervals.

III.4. Crossing Direction

The crossing curves defined by (14) and (15) are continuous.

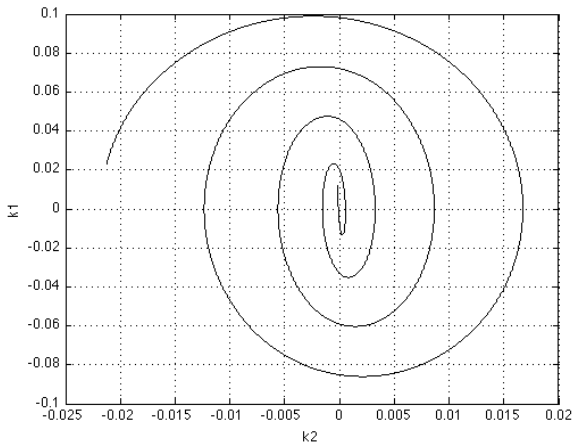

Fig. 2. Crossing curves for the closed loop system with $\tau^* = 0.5$

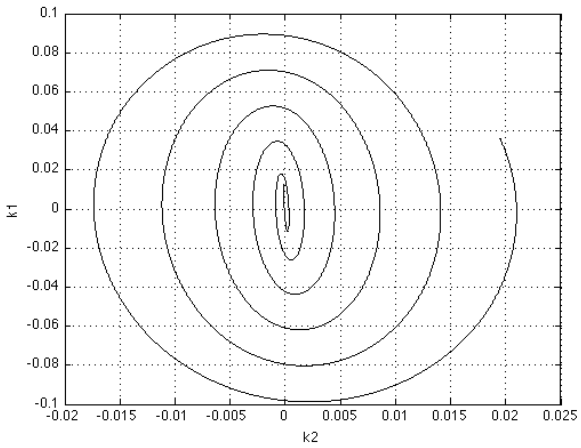

Fig. 3. Crossing curves for the closed loop system with $\tau^* = 0.7$

So by using the approach described in [20] and [15], we can determine the crossing direction. For that, consider the real numbers R_i and I_i, $i \in \{1, 2, 3\}$ defined by:

$$R_0 + jI_0 = j \left. \frac{\partial H(s, k_1, k_2, \tau^*)}{\partial s} \right|_{s=j\omega}$$
$$R_1 + jI_1 = -\frac{1}{s} \left. \frac{\partial H(s, k_1, k_2, \tau^*)}{\partial k_2} \right|_{s=j\omega} \qquad (16)$$
$$R_2 + jI_2 = -\frac{1}{s} \left. \frac{\partial H(s, k_1, k_2, \tau^*)}{\partial k_1} \right|_{s=j\omega}$$

Proposition 2. The crossing curve is regular everywhere except at the points where $s = j\omega$ is a multiple solution of $H(s, k_1, k_2, \tau^*) = 0$.

Proof: By applying the implicit function theorem, the tangent crossing curve is defined by:

$$\begin{pmatrix} \frac{dk_2}{d\omega} \\ \frac{dk_1}{d\omega} \end{pmatrix} = \frac{1}{R_1 I_2 - R_2 I_1} \begin{pmatrix} R_1 I_0 - R_0 I_1 \\ R_0 I_2 - R_2 I_0 \end{pmatrix} \quad (17)$$

provided that:

$$R_1 I_2 - R_2 I_1 \neq 0 \quad (18)$$

It follows that the crossing curve is regular everywhere except for the points where (18) is not satisfied, that is:

$$\frac{dk_1}{d\omega} = \frac{dk_2}{d\omega} = 0 \quad (19)$$

thus, $R_0 = I_0 = 0$, which implies:

$$\left. \frac{\partial H\left(s, k_1, k_2, \tau^*\right)}{\partial s} \right|_{s=j\omega} = 0 \quad (20)$$

In view of (20) and (17), and given that $H\left(j\omega, k_1, k_2, \tau^*\right) = 0$, it appears that $s = j\omega$ is a multiple solution. Now, based on the concepts introduced in [15], we can determine the crossing direction, which is, by definition, the direction in which the roots cross the imaginary axis as (k_1, k_2) deviates from the crossing curve.

When (k_1, k_2) traverses the crossing curve from the right to the left, a pair of solution of $H\left(j\omega, k_1, k_2, \tau^*\right) = 0$ crosses the imaginary axis from the left to the right, which translates into the inequality:

$$R_2 I_1 - R_1 I_2 > 0$$

In our case, by a simple calculation, we find:

$$R_2 I_1 - R_1 I_2 = \frac{-b_1^2 a_2}{\omega} < 0 \quad (21)$$

Thus, we deduce that the crossing direction is to the left.

III.5. Stability Regions

Based on the results of the previous paragraphs, we will determine the stability regions of the closed loop system. In other words, the set of values of the state feedback gains, for which the characteristic Eq. (6) has all its roots in the left half plane for any τ_1 belongs to $\left[0, \tau^*\right]$.

As we have seen, the condition (12) must be satisfied to ensure that all the roots of $H(s, k_1, k_2, 0) = 0$ have strictly negative real parts. In addition, we found that $R_2 I_1 - R_1 I_2 < 0$, which implies that the crossing is to the left.

Thus, for $\tau^* = 0.5$, we obtain the stability region, shown in Fig. 4.

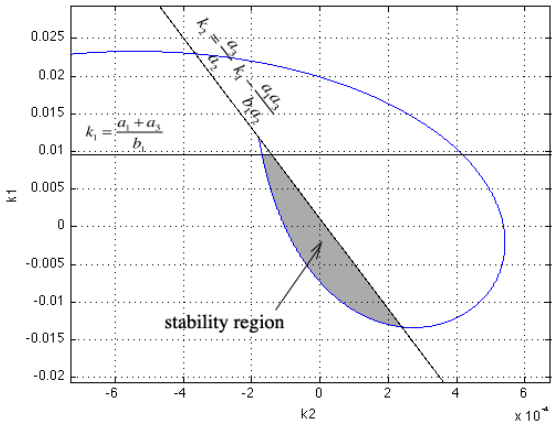

Fig. 4. Stability region for the closed loop system with $\tau^* = 0.5$

Any pair of parameters (k_1^*, k_2^*) belonging to the stability region of the closed loop system, corresponds to a state feedback gain $K^*=[k_1^*, k_2^*]$ for which the characteristic equation:

$$H\left(s, k^*_1, k^*_2, \tau_1\right) = 0 \quad (22)$$

is Hurwitz for any $\tau_1 < \tau^*$, where τ^* is an upper bound on the delay τ_1, beyond which the closed-loop system will become unstable.

It therefore seems important to determine the critical value of the delay, from which the stability is not preserved.

Proposition 3. Critical delay

The state feedback control law $u(t) = -K^* x(t)$, with $K^*=[k_1^*, k_2^*]$, asymptotically stabilizes the closed loop system (4) for any $\tau_1 < \tau^*$, such as τ^* is defined by:

$$\tau^* = \frac{1}{\omega} arc\cos\left[\frac{\left[\begin{array}{l} a_1\left(\omega^2 + a_3^2\right)k^*_1 + \\ +a_2\left(\omega^2 - a_1 a_3\right)k^*_2 \end{array} \right]}{\left[\begin{array}{l} b_1\left(a_2 k_2^* - a_3 k^*_1\right)^2 + \\ +b_1\left(k^*_1 \omega\right)^2 \end{array} \right]} \right] \quad (23)$$

Proof: Suppose that the characteristic Eq. (22) has an imaginary root $s = j\omega$, then we find the following equation:

$$Q(j\omega)+P(j\omega)e^{-j\omega\tau^*}=0 \qquad (24)$$

with:

$$P(j\omega)=b_1\left(a_2k^*_2-a_3k^*_1+j\omega k^*_1\right)$$

$$Q(j\omega)=-\omega^2-(a_1+a_3)\,j\omega+a_1a_3$$

We can rewrite (24) as follows:

$$e^{-j\omega\tau^*}=\frac{-Q(j\omega)}{P(j\omega)}$$

Using the Euler's formula, we obtain:

$$cos\left(\omega\tau^*\right)-j\,sin\left(\omega\tau^*\right)=-\frac{-\omega^2-(a_1+a_3)\,j\omega+a_1a_3}{b_1\left(a_2k^*_2-a_3k^*_1+j\omega k^*_1\right)}$$

By separating the real and imaginary parts, and by focusing on the real part, we find the result (23).

Proposition 4. Critical crossing frequency

The crossing frequency ω_0 corresponding to the critical delay τ^* is defined by:

$$\omega_0=\sqrt{\frac{\alpha_1+\sqrt{\alpha^2_1+4\alpha_0}}{2}} \qquad (25)$$

with:

$$\alpha_0=b_1^2\left(a_2k^*_2-a_3k^*_1\right)^2-\left(a_1a_3\right)^2$$

$$\alpha_1=\left(b_1k^*_1\right)^2-a^2_1-a^2_3$$

Proof: From the Eq. (24), we can write:

$$e^{-j\omega\tau^*}=\frac{-Q(j\omega)}{P(j\omega)},\ e^{j\omega\tau^*}=\frac{-Q(-j\omega)}{P(-j\omega)}$$

By multiplying the terms of these two equations, we find the following equation:

$$Q(j\omega)Q(-j\omega)-P(j\omega)P(-j\omega)=0$$

Then, by substituting $Q(j\omega)$ and $P(j\omega)$ by their values, we find a quadratic equation in ω^2:

$$\omega^4-\alpha_1\omega^2-\alpha_0=0 \qquad (26)$$

The resolution of this equation leads to a single positive root ω_0 defined by (25).

IV. Simulation

This section aims to illustrate the various developments presented in the previous sections. We consider the system presented in [7], whose dynamics are described by (4) with: q_0 = 175 packets, T_p = 0.2s, C = 3750 packets/s and for N = 60 TCP sessions, we have W_0 = 15 packets, p_0 = 0.008, τ_1 = 0.5. Therefore, by taking into consideration the stability region shown in Fig. 4, we arbitrarily choose a pair (k_1^*, k_2^*) = (-0.0097, 0.00015) in this region:

$$i.e. \qquad K=10^{-3}\begin{bmatrix}-9.7 & 0.15\end{bmatrix} \qquad (27)$$

Then, using Eqs. (23) and (25), we determine the critical values of the delay and of the crossing frequency:

$$\tau^* = 1.3451 \quad \text{and} \quad \omega_0 = 2.0672$$

This means that the state feedback gain (27) stabilizes the system (4) for any delay τ_1 belongs to $[0,1.3451)$.

We obtain then the Fig. 5, which illustrates the temporal evolution of the size of the queue. Now, choose another pair (k_1, k_2) always belonging to the region of stability, namely:

$$K=10^{-3}\begin{bmatrix}-11 & 0.18\end{bmatrix} \qquad (28)$$

We thus find the temporal evolution shown in Fig. 6, and the critical values:

$$\tau^* = 0.7948 \quad \text{and} \quad \omega_0 = 3.2729$$

By comparing the results from these two examples, we notice that a slight increase in the state feedback gain causes, on the one hand, the increase in the critical value of the delay τ^*, which enlarge the interval of allowed values for the delay τ_1 and, on the other, the increase of the oscillations.

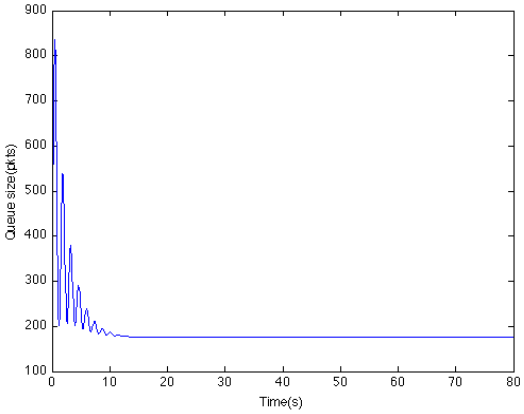

Fig. 5. Temporal evolution of the queue length with the state feedback gain (27) and the desired length q_0 = 175 packets

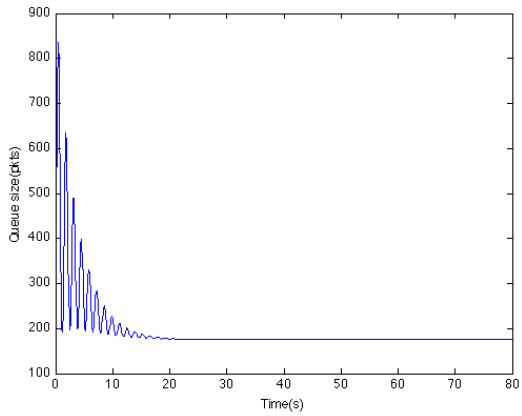

Fig. 6. Temporal evolution of the queue length with the state feedback gain (28) and the desired length q_0 = 175 packets

It therefore appears that the choice of the gain in the stability region is not an easy task. It would be, then, interesting to develop a method to choose the best pair of gain (k_1, k_2), taking into consideration the requirements of the specifications.

V. Conclusion and Future Works

In this paper, we have discussed the phenomenon of congestion of router in the TCP network. By considering the case of constant and asymmetric delays and based on a geometric approach, we have designed a state feedback controller, ensuring the stability of our system.

Then, we have illustrated the viability of this approach through a simulation study. However, our hypothesis of a constant delay with a zero lower bound is unrealistic which can lead to a certain conservatism of the results achieved.

Future works will first focus on the reduction of this conservatism, and then the implementation of the Luenberger observer, with consideration of the delay that occurs in the measurement loop.

References

[1] C.K. Chen, Y.C. Hung, T.L. Liao, and J.J. Yan, Design of robust active queue management controllers for a class of tcp communication networks. *Information Sciences, 177(*19*):4059–4071, 2007.*

[2] Y. Ariba, Y. Labit, and F. Gouaisbaut, Congestion control of a single router with an active queue management. *International Journal on Advances in Internet Technology, 2(*1*), 2009.*

[3] H. S. Low, F. Paganini, and J. C. Doyle, Internet congestion control. *IEEE Control Systems Magazine, 22:28–43, Feb 2002.*

[4] Y. Ariba, F. Gouaisbaut, and Y. Labit, Controle de congestion d'un routeur par retour d'état. *Conference International Francophone d'Automatique (CIFA'08), July 2008.*

[5] Z. Artstein, Linear systems with delayed controls: A reduction. *IEEE Trans. Aut. Control, 27(*4*):869-879, 1982.*

[6] E. Witrant, D. Georges, C. Canudas-de-Wit, M. Alamir, On the use of state predictors in networked control system. *In Lecture notes in control and information sciences: Vol. 352. Applications of time delay systems (pp. 17–35). New York: Springer, 2007.*

[7] N.E. Alami, R. Ellaia, and K. Lefrouni, State feedback controller and observer design for TCP network with consideration of UDP flow, *Journal of Theoretical and Applied Information Technology, Vol. 55 (*1*), pp. 14, September 2013.*

[8] A. Seuret., F. Michaut, J.-P. Richard, and T. Divoux, Networked control using gps synchronization, *Proc. of ACC06, American Control Conf., Mineapolis, USA, June 2006.*

[9] E. Fridman, New Lyapunov-Krasovskii functionals for stability of linear retarded and neutral type systems, *Systems & Control Letters, vol. 43, pp. 309–319, 2001.*

[10] M. Yu, L. Wang, and T. Chu, An LMI approach to network control systems with data packet dropout and transmission delays, *MTNS '04 Proc. of Mathematical Theory Networks and Systems, Leuven, Belgium, 2004.*

[11] Y. Y. Cao, and P. M. Frank, Stability analysis and synthesis of nonlinear time delay systems via linear Takagi-Sugeno fuzzy models, *Fuzzy Sets and Systems, vol. 124, pp. 213-229, 2001.*

[12] W. Michiels, S.-I. Niculescu, On the delay sensitivity of smith predictors, *International Journal of Systems Science 34(8-9), 543-552. 2003.*

[13] O. J. M. Smith, Closer control of loops with dead time, *Chem. Eng. Prog., vol. 53, pp. 217–219, 1959.*

[14] K. Gu, S.-I. Niculescu, and J. Chenc, On stability crossing curves for general systems with two delays, *J. Math. Anal. Appl. 311, 231–253, 2005.*

[15] K. Gu, S.-I. Niculescu, and J. Chen, On stability crossing curves for general systems with two delays, *J. Math. Anal. Appl., vol. 311, pp.231-253, 2005.*

[16] C.-I. Morˇarescu, C.-M. Barrios, S.-I. Niculescu, and K. Gu, Stability Crossing Boundaries and Fragility Characterization of PID Controllers for SISO Systems with I/O Delays, *American Control Conference on O'Farrell Street, San Francisco, CA, USA, June 29 - July 01, 2011.*

[17] C. V. Hollot, V. Misra, D Towsley, and W. Gong. A control theoretic analysis of red. *IEEE INFOCOM, pp.1510–1519, April 2001.*

[18] V. Misra, W.-B. Gong, and D. Towsley. Fluid-based analysis of a nerwork of AQM routers supporting TCP flows with an application to red, *Proc. ACM SIGCOMM, pages 151–160, 2000.*

[19] H. S. Low, F. Paganini, and J. C. Doyle. Internet congestion control. *IEEE Control Systems Magazine, 22:28–43, Feb 2002.*

[20] C.-I. Morˇarescu, S.-I. Niculescu, and K. Gu, On the geometry of pi controllers for SISO systems with input delays, *In Proc. of IFAC Time Delay Systems, 2007.*

Authors' information

Khalid Lefrouni was born in 1985 in Azrou, Morocco. He received his Diploma degree in electrical engineering from Mohammed V University, Mohammadia School of Engineers, Rabat, in 2009. Currently, he is a Ph.D. student at Laboratory of Study and Research for Applied Mathematics, Mohammed V University. His research interests include Time-delay systems, quality of services in TCP network, congestion control and AQM techniques.

Rachid Ellaia is a full professor at Mohammed V University, Mohammadia School of Engineers in Rabat. He received his doctorat 3ème cycle from Toulouse University in Applied Mathematics and Optimization, and Ph.D. degree in1992 in Applied and Computational Mathematics. He has held visiting professor positions at Toulouse university, Chile university, INSA of Rouen , Nice Sophia Antipolis University, Haute Alsace University and INRIA Lille. His interests are in Metaheuristics and Nature Inspired Computing, Optimization and Uncertainties, Finance, Global Optimization. Actually, he is President of the Moroccan society of Nature-Inspired Computing and Meta-heuristics (METAH).

Praise Worthy Prize

International Review of Automatic Control (I.RE.A.CO.), Vol. 8, N. 2
ISSN 1974-6059 *March 2015*

Using D-STATCOM in Voltage Regulation of Future Distribution Systems

Y. Bot, A. Allali

Abstract – *Due to the development of Distributed Generation (DG), which is installed in Medium-Voltage Distribution Networks such as generators based on renewable energy, voltage control is currently a very important issue. The voltage is now regulated at the MV bus bars acting on the On-Load Tap Changer (OLTC) of the HV/MV transformer. This method does not guarantee the correct voltage value in the network nodes when the distributed generators deliver their power. In this study, the problem of using OLTC for the voltage regulation of a radial distribution feeder will be solved by using reactive power compensation using D-STATCOM at the DG connected bus. Simulation results reveal that the proposed control method is capable of maintaining the system voltage within the permitted range in the worst scenarios of the test system.*

Keywords: *Smart Grids, Distribution Systems, Distributed Generation, FACTS, D-STATCOM*

Nomenclature

AND	Active Distribution Network
ANM	Active Network Management
AVC	Automatic Voltage Control
DG	Distributed Generation
FACTS	Flexible Alternating Current Transmission System
GTO	Gate Turn-Off Thyristor
HV	High Voltage
MV	Medium Voltage
MVDN	Medium-Voltage Distribution Network
OLTC	On-Load Tap Changer
D-STATCOM	Distribution-Static Compensator
VSC	Voltage Source Converter

I. Introduction

Distributed Generations (DGs) are mentioned usually to the production of electricity using small generators located in power distribution systems or the power load centers [1]-[27]. Due to the development of DG, which is installed in Medium-Voltage Distribution Networks (MVDNs) such as generators based on renewable energy (*e.g.*, wind energy or solar energy), voltage control is currently a very important issue [2].

In some areas, the installed generation power is significantly higher than the consumption. Distributed generation (DG) causes altered power flow patterns. Thus, the power flow may even become bidirectional.

The temporary reversal of the power flow can provoke voltage rises away from the substation, especially at remote feeder ends. If the voltage exceeds the tolerance of usually 10 % above nominal voltage, other devices and equipment might be damaged [3].

The voltage of MVDNs is now regulated acting only on the On-Load Tap Changer (OLTC) of the HV/MV transformer [4]. The OLTC control is typically based on the compound technique, and this method does not guarantee the correct voltage value in the network nodes when the generators deliver their power [5].

According to [6], an active distribution network (ADN) is defined as a distribution network with systems capable of controlling distributed energy resources consisting of generators and storage.

An ADN should also be able to adopt the integration of control and communication technologies for the effective management of the new distribution network by DNOs [7]. Hence, an active network management (ANM) scheme is needed to provide control and coordination to power system operation. According to [8], ANM is the use of real-time control and communication systems to provide a means to better integrate renewable distributed generators.

DNOs consider three worst-case operating scenarios in ensuring that their network and their customers will not be adversely affected. These scenarios are categorized into: i) no generation and maximum system demand, ii) maximum generation and maximum system demand, and iii) maximum generation and minimum system demand. As increasing the generation reverses the power flow along the line from the generator to the substation, the voltage rises and becomes more severe in the absence of demand because all local generation is exported back to the primary substation. Hence, the issue of voltage rise calls for a management scheme that can alleviate excessive voltage rise issues.

Voltage rise caused by DG can be decreased by allowing the generator to absorb reactive power. Using synchronous generators, the control of reactive power is

usually realized by an excitation system that consists of an AC or DC exciter, controller and voltage measurement components [9]. However, these generators have limitations on control of voltage and reactive power in distribution systems and therefore it requires additional compensating devices to ensure that the voltage level is acceptable.

The applications of several end users or local compensation methods have proven to be a promising solution. These methods have several advantages in terms of efficiency, flexibility, reliability and scalability.

A device such as STATCOM has the advantage of providing solution in fast response time, thus providing dynamic voltage control in the systems [24]-[27]. When the STATCOM is applied in distribution system is called D-STATCOM (Distribution-STATCOM) and its configuration is the same. In this paper, in order to maximize the benefits of OLTC action and D-STATCOM response, a new voltage control method is proposed. The main idea is to concentrate the response of each controller in its most suited working ranges and to consequently use each controller in the defined voltage range which corresponds to its merits.

II. Modelling of DGs in Load Flow Studies

The DG is noticed by two models when it is injected in networks:

- Participating DGs (PV model).
- Non-participating DGs (PQ model).

II.1. DG Modelled as PV Node

Some types of DGs which can be modelled as PV nodes, like micro turbines, fuel cells and so on. It has to be dealt with separately because it does not match the back/forward sweep algorithm [10]. The model is Eq. (1):

$$\begin{cases} P = -P_g \\ U = U_g \end{cases} \quad (1)$$

II.2. DG Modelled as PQ Node

This type of DGs, a compared with PQ type load, has opposite power flows. Therefore, there is nothing to handle but invert the sign of power when dealing with PQ type DGs, as Eq. (2) shows.

In the distribution power flow calculation, the vast majority of nodes are PQ nodes [11]:

$$\begin{cases} P = -P_g \\ Q = -Q_g \end{cases} \quad (2)$$

III. Static Compensator

III.1. Modeling of STATCOM

The static synchronous compensator, or STATCOM, is a shunt connected FACTS device [21]-[22].

The configuration of STATCOM used in this paper is shown in Fig. 1.

It generates a balanced set of three phase sinusoidal voltages at the fundamental frequency, with rapidly controllable amplitude and phase angle. This type of controller can be implemented using various topologies.

However, the voltage-sourced inverter, using GTO thyristors in appropriate multi-phase circuit configurations, is presently considered the most practical for high power utility applications. A typical application of this type of controller is voltage support [12].

In addition to this, this controller has a coupling transformer and a dc capacitor. The control system can be designed to maintain the magnitude of the bus voltage constant by controlling the magnitude and/or phase shift of the VSC output voltage [13].

Few papers address the issue of how to model STATCOM for load flow calculation. It is traditionally modeled for power flow analysis as PV or PQ bus depending on its primary application. The active power is either set to zero (neglecting the StatCom losses) or calculated iteratively.

In a load flow calculation, a STATCOM is typically treated as a shunt reactive power controller assuming that it can adjust its injected reactive power to control the voltage at the StatCom terminal bus.

Fig. 2 depicts a STATCOM and the traditional simple model used in this paper for load flow calculation. In this model reactive power load at bus i (jQ_i), is combined with STATCOM reactive power output $jQ_c$and therefore power varies as $|V_i|$. This model is essentially a PV bus with the STATCOM's active power output set to zero [14].

III.2. Modal Analysis

The modal analysis technique utilized in this paper involves the computation of Eigenvalue and the associated eigenvectors of a reduced power system steady state Jacobian matrix, which retains the Q-V relationship in the network and participation factor for minimum Eigenvalue which identify weakest buses.

By using the reduced Jacobian matrix, the relationship between the incremental change in bus voltage magnitude and incremental change in bus reactive power injection can be examined.

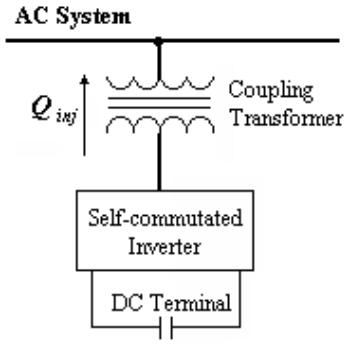

Fig. 1. Configuration of STATCOM

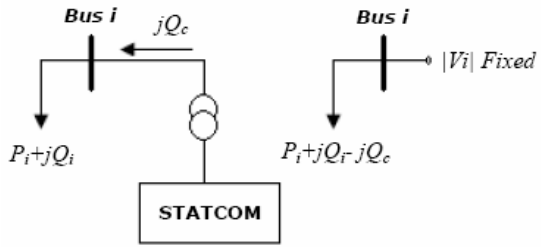

Fig. 2. Model of STATCOM in load flow calculation

Since voltage stability is essentially of a steady-state nature, therefore, static analysis can be effectively used to determine stability margins which show how close the current operation point of power system is to the voltage collapse point. Voltage stability is affected by both real and reactive load power.

However, at each operating point real power (P) can be kept constant and evaluate voltage stability by considering the incremental relationship between reactive power (Q) and voltage magnitude (V). The effects of changes in system load or power transfer levels are taken into account by studying incremental relationship between (Q) and (V) at different operating conditions.

As the power flow method is implemented for voltage stability analysis, the Jacobian matrix of solved load flow equations, by Newton-Raphson method, can be used.

The linearized steady-state system power voltage equation is expressed as [15]:

$$\begin{bmatrix}\Delta P\\ \Delta Q\end{bmatrix}=\begin{bmatrix}J_{P\theta} & J_{PV}\\ J_{Q\theta} & J_{QV}\end{bmatrix}\begin{bmatrix}\Delta\theta\\ \Delta V\end{bmatrix} \quad (3)$$

where:
ΔP = incremental change in bus real power.
ΔQ= incremental change in bus reactive power.
$\Delta\theta$ = incremental change in bus voltage angle.
ΔV= incremental change in bus voltage magnitude.

To express the relation between ΔQ and ΔV for a small change in real power, ΔP=0 can be assumed, this yields:

$$\Delta Q = \left[J_{QV} - J_{Q\theta}J_{P\theta}^{-1}J_{PV}\right]\Delta V \quad (4)$$

Rearrange Eq. (4), then:

$$\Delta V = J_R^{-1}\Delta Q \quad (5)$$

where:

$$J_R = \left[J_{QV} - J_{Q\theta}J_{P\theta}^{-1}J_{PV}\right] \quad (6)$$

J_R is called the reduced Jacobian matrix of the system; it relates the bus voltage magnitude and reactive power injection.

IV. Simulation Results

In order to validate the proposed voltage regulation scheme, a distribution System is considered which is shown in Fig. 3.

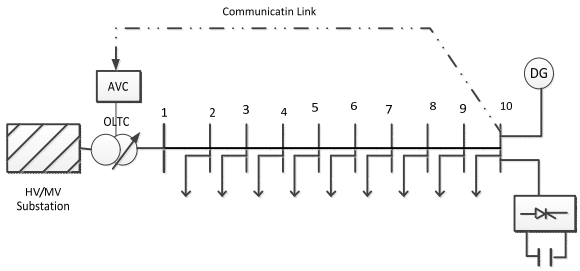

Fig. 3. The investigated system

The system under study consists of a DG unit which is located at the end of the feeder where D-STATCOM also installed. The OLTC mechanism is installed on the secondary side of the HV/MV transformer (60/20 kV)

The parameters of the investigated system are as follow:

- The line and bus data are same as IEEE 10 bus distribution system.
- Total loads of the feeder are 12.368 MW and 4.186 MVAR.
- Maximum power of DG unit (P_{DG})= 4 MW.

In this paper, a worst case in the voltage regulation of the investigated system is simulated. The simulations are carried out by using a Newton–Raphson algorithm based load flow program written in MATLAB.

Fig. 4 shows the voltage at the bus 10 as a function of demand of the load and power of DG unit.

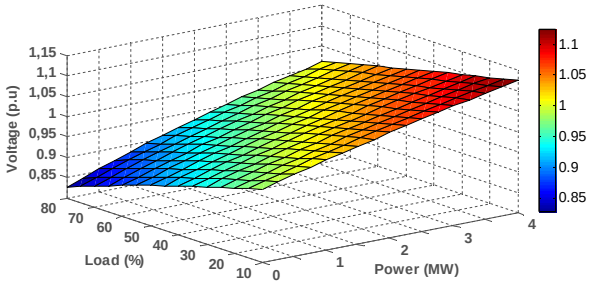

Fig. 4. Voltage at bus 10 with variations of demand of the load and power of DG

We can see that the worst case of voltage rise is when DG generates its maximum power (P_{DG}= 2.5 MW) and the demand of the load is minimal (20% of the nominal load) and that the worst case of voltage drop is when DG generates its minimum power (P_{DG}= 0) and the demand of the load is maximal (100% of the nominal load).

IV.1. Case 1

The first test case is when DG generates its maximum power and the demand of the load is minimal (20% of the nominal load). Fig. 5 shows the profile of the voltage along the feeder in this situation. As the voltage rise at bus 10 is more than the permitted range of the voltage (± 5%). The single action of OLTC cannot manage the voltage rise along the feeder. The single action of the OLTC leads to a voltage drop at the sending point of the

feeder (92% at bus 1) as in Fig. 6. Fig. 7 show that the D-STATCOM controls the voltage of the regulated point by adapting the amount of absorbed reactive power. As long as the exchanged reactive power stays within the maximal limits, the voltage is regulated at the target voltage value.

Fig. 8 shows that the proposed idea is capable of managing the extreme voltage rise at bus 10.

As it can be seen, without any controller, the voltage rise at bus 10 is about 12% and based on the proposed idea, 5% of this voltage rise was managed by OLTC action and the rest of the voltage rise (7%) was compensated by D-STATCOM response. In this case, the absorbed reactive power of D-STATCOM is 1.3 MVAr (inductive mode).

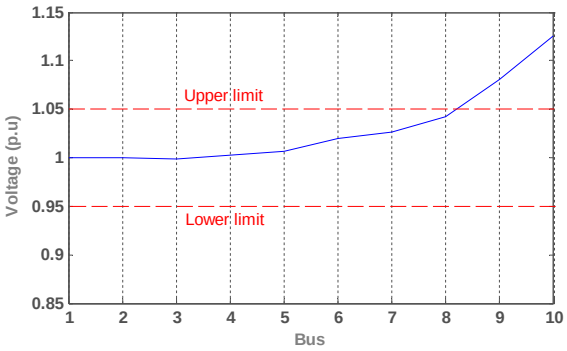

Fig. 5. Voltage profile of the system buses in the case 1 without any controller

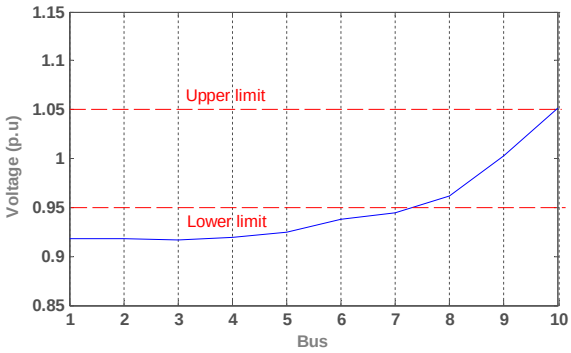

Fig. 6. Voltage profile of the system buses in the case 1 with single action of OLTC

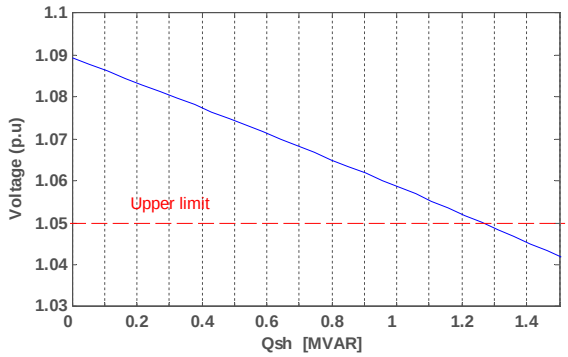

Fig. 7. Voltage at bus 10 in the case 1 with the variation of D-STATCOM reactive power

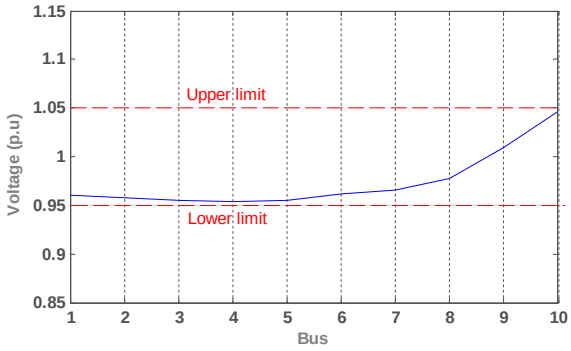

Fig. 8. Voltage profile of the system buses in the case 1 with the proposed idea

IV.2. Case 2

The second worst case is considered when the injected power of DG is minimal (PDG= 0) and the demand of the load is maximal (100% of the nominal load). Fig. 9 shows the profile of the voltage along the feeder in this situation. Like the previous case, the single action of OLTC Fig. 10 cannot effectively manage the voltage drop at bus 10 (more than 6%).

Fig. 11 show that the D-STATCOM controls the voltage of the regulated point by adapting the amount of injected reactive power. As long as the exchanged reactive power stays within the minimal limits, the voltage is regulated at the target voltage value.

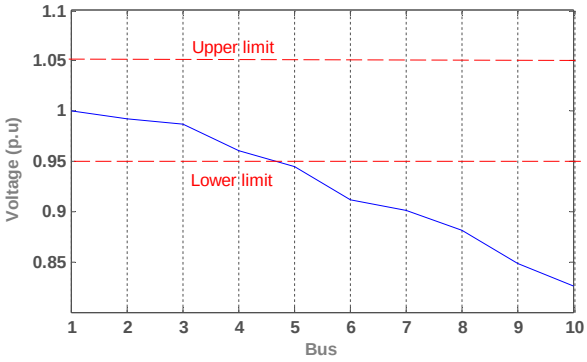

Fig. 9. Voltage profile of the system buses in the case 2 without any controller

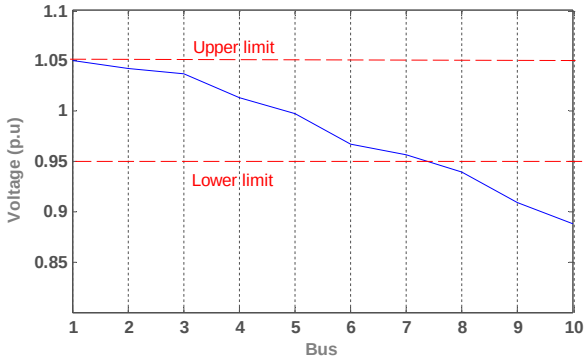

Fig. 10. Voltage profile of the system buses in the case 2 with single action of OLTC

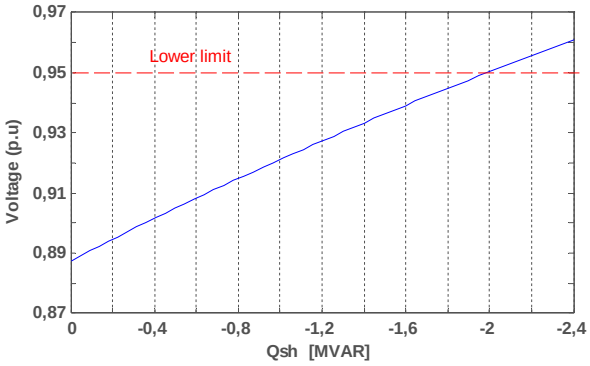

Fig. 11. Voltage at bus 10 in the case 2 with the variation of D-STATCOM reactive power

The proposed idea with the combination of OLTC action and D-STATCOM response is able to keep the voltage of all buses within the predefined limits Fig. 12.

In this case, the reactive power of D-STATCOM is equal to -2.1 MVAr (capacitive mode).

Based on the simulation results, it can be concluded that the proposed method is able to keep the voltage of the all buses within the limits.

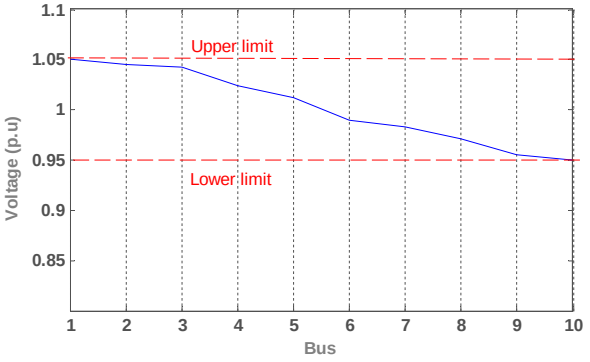

Fig. 12. Voltage profile of the system buses in the case 2 with the proposed idea

V. Conclusion

In this paper, a new idea for the voltage regulation of radial distribution systems with DG unit at the transformer bus was presented. The proposed idea was based on the combination of two different control methods which are OLTC action and static compensator.

The idea was to use the OLTC action in the predefined range (based on the permitted range of voltage) and allow D-STATCOM to manage the rest of the voltage violations. Simulation results revealed that the proposed method enables us to efficiently manage the voltage control problem of a radial MV distribution system in the worst working conditions.

Moreover, as the D-STATCOM is only used in the extreme voltage conditions (when OLTC cannot work anymore), it does not considerably increase network losses. In future research, a practical evaluation and the cost of implementation of the proposed method will be investigated.

References

[1] H. Manafi, N. Ghadimi, M. Ojaroudi and P. Farhadi, Optimal Placement of Distributed Generations in Radial Distribution Systems Using Various PSO and DE Algorithms, *Elektronikair Elektrotechnika*, vol. 19, no. 10, pp. 53–57, 2013.

[2] Yousfi, A., Allaoui, T., Chaker, A., Harmonic Current Compensation and Reactive Power Based on Three-Level Shunt Active Filter Controlled by Fuzzy Logic Connected to a Photovoltaic Source, (2015) *International Review of Automatic Control (IREACO)*, 8 (1), pp. 56-62.

[3] P. Esslinger, and R. Witzmann, "Experimental study on voltage dependent reactive power control Q(V) by solar inverters in low-voltage networks," *22nd International Conference on Electricity Distribution*, Stockholm , Sweden, June 10-13, 2013.

[4] R. Marconato, "Electric Power Systems," Vol. 2, CEI, Milano, 2008.

[5] Y. Rosales Hernandez and T. Hiyama, "Distance Measure Based Rules for Voltage Regulation with Loss Reduction", *Journal of Electromagnetic Analysis and Applications (JEMAA)*, Vol. 1, No. 2, pp. 85-91, June 2009.

[6] A. Jupe and G. Abbey, Global Survey on Planning and Operation of Active Distribution Networks,*20thInternational Conference and Exhibition on Electricity Distribution*,Prague, June 8-11, 2009.

[7] R. Hidalgo, C. Abbey, G. Joo, A review of active distribution networks enabling technologies, *IEEE Power and Energy Society General Meeting*, July 25-29, 2010, pp. 1-9.

[8] T. Sansawatt. L. F. Ochoa and G.P. Harrison, Integrating distributed generation using decentralised voltage regulation, *IEEE Power and Energy Society General Meeting*, July 25-29, 2010, pp. 1-6.

[9] K. Turitsyn, P. Sulc, S. Backhaus, and M. Chertkov, Local Control of Reactive Power by Distributed Photovoltaic Generators, *First IEEE International Conference on Smart Grid Communications*, 2010, pp. 79-84.

[10] J.H.Teng, Modelling distributed generations in three-phase distributed load flow, *IET Gener. Transm. Distrib.*, Vol.2, No.3, pp.330-340, 2008

[11] A.E. Feijoo, J. Cidras: Modeling of wind farms in the load flow analysis, *IEEE Trans. Power Syst.*,Vol. 1, No. 15, pp. 110–115, 2000

[12] M. L. Pranesh Rao, Crow,*YZ*hiping,STATCOM Control for Power System Voltage Control Applications, *IEEE Trans. On Power Delivery*, Vol. 15, No. 4, pp. 1311-1317, October 2000.

[13] N. Mithulananthan, A.C. Canizares, J. John Reeveand Graham. Rogers,Comparison of PSS, SVC, and STATCOM Controller for Damping Power System Oscillations, *IEEE Trans. On Power system*, Vol. 18, No. 2, pp. 786-792, May 2003.

[14] Boudiaf, M., Moudjahed, M., Rahli, M., Improvement of transient stability and damping power by means of IPFC and STATCOM - A comparative study, (2013) *International Review of Automatic Control (IREACO)*, 6 (4), pp. 410-418.

[15] F.A. El-Sheikhi, Y.M. Saad, S.O. Osman, K.M. El-Arroudi, Voltage Stability Assessment Using Modal Analysis of Power Systems including Flexible AC Transmission System (FACTS), *Power Engineering, 2003 Large Engineering Systems Conference*, 7-9 May 2003, pp 105 -108.

[16] Bracale, A., Caramia, P., Carpinelli, G., Meo, S., A low voltage Smart Grid control strategy with Power Quality issues, (2011) *International Review of Electrical Engineering (IREE)*, 6 (6), pp. 2704-2712.

[17] Damiano, A., Gatto, G., Marongiu, I., Meo, S., Perfetto, A., Serpi, A., Single-stage grid connected PV inverter with active and reactive power flow control via PSO-PR based current controlled SVPWM, (2012) *International Review of Electrical Engineering (IREE)*, 7 (4), pp. 4647-4654.

[18] Meo, S., Sorrentino, V., Discrete-time integral variable structure control of grid-connected PV inverter, (2015) *Journal of Electrical Systems*, 11 (1), pp. 102-116.

[19] Meo, S., Sorrentino, V., Zohoori, A., Vahedi, A., Second-order sliding mode control of a smart inverter for renewable energy system, (2014) *International Review of Electrical Engineering (IREE)*, 9 (6), pp. 1090-1096.

[20] Porkar, S., Poure, P., Abbaspour-Tehrani-fard, A., Saadate, S., Distributed generation planning for losses, voltage profile, line congestion and total system cost improvement, (2009) *International Review of Electrical Engineering (IREE)*, 4 (3), pp. 434-440.
[21] Baghaee, H.R., Mirsalim, M., Kashefi-Kaviani, A., Gharehpetian, G.B., Optimal allocation of Multi-type FACTS devices to improve security and reduce the losses and fault level using multi-objective particle swarm optimization, (2009) *International Review of Electrical Engineering (IREE)*, 4 (6), pp. 1326-1335.
[22] Laifa, A., Boudour, M., Multi-objective particle swarm optimization for FACTS allocation to enhance voltage security, (2009) *International Review of Electrical Engineering (IREE)*, 4 (5), pp. 994-1004.
[23] Laaksonen, H., Kauhaniemi, K., Stability of microgrid with different configurations after islanding due to fault in the utility grid, (2008) *International Review of Electrical Engineering (IREE)*, 3 (3), pp. 498-512.
[24] Kamarposhti, M.A., Alinezhad, M., Effects of STATCOM, TCSC, SSSC AND UPFC on static voltage stability, (2009) *International Review of Electrical Engineering (IREE)*, 4 (6), pp. 1376-1384.
[25] Jin, P.K., Dahidah, M.S.A., Recent advances in multilevel voltage source converters based STATCOM technology, (2009) *International Review of Electrical Engineering (IREE)*, 4 (6), pp. 1164-1181.
[26] Hemeida, A.M., Mobarak, Y.A., Mousa, M.R., Power systems stabilization using svc and statcom, (2010) *International Review on Modelling and Simulations (IREMOS)*, 3 (5), pp. 900-910.
[27] Maya, G., Cheriyan, E.P., Jacob, J., Stability enhancement of a multimachine system using STATCOM with supplementary controller, (2013) *International Review on Modelling and Simulations (IREMOS)*, 6 (2), pp. 480-489.

Authors' information

LDDEE, Laboratory Sustainable Development of Electrical Energy, Department of Electrotechnical, Faculty of Electrical Engineering, USTO-MB, University of Sciences and Technology of Oran-Mohamed Boudiaf, Algeria.

Y. Bot was born on 08.11.1979. In 2004 he graduated at the Electrotechnical Department at Tiaret University in Algeria. He defended his "Magister"from the University of Sciences and Technology of Oranin the field of IPFCload flow in 2011; his thesis title was "Influence of FACTS on load flow calculates using IPFC". His scientific research is focusing on load flow and real time simulation of power systems, and study of the future networks electrical supply.

A. Allali was born in Mecheria in Algeria in July 3rd 1960. In 1987 he graduated at the electrotechnics Department of the Faculty of Electrical Engineering at the University of Sciences and Technology of Oran in Algeria. He received the M.Sc. and the PhD degrees from the University of Sciences and Technology of Oran, Algeria in 1990 and 2006 respectively all in electrical engineering. Director LDDEE laboratory, Sustainable development of electrical energy.His main research interests are in the field of a control and real time simulation of power systems, and the study and the location of FACTS and their influence on the electricity network and renewable energy (solar and wind).

Praise Worthy Prize

International Review of Automatic Control (I.RE.A.CO.), Vol. 8, N. 2
ISSN 1974-6059 *March 2015*

Dynamic Mathematical Design and Modelling of Autonomous Control of All-Terrain Vehicles (ATV) Using System Identification Technique Based on Pitch and Yaw Stability

Mohd Shahrieel Mohd Aras, Mohd Khairi Mohd Zambri, Mohd Zamzuri Ab Rashid, Fadilah Abdul Azis, Alias Khamis

Abstract – *This research describes the dynamically mathematical design and modelling of autonomous control of all-terrain vehicles (ATV) using system identification technique based on pitch and yaw stability. The modelling of ATV using dynamic mathematical method based on single track model which the left and right tires for both front and rear have the same characteristics.*

The main difficulty of the ATV control is the steering control which could not rotate easily and need higher forces to control the ATV movement manually. The movement is very limited when driving the ATV manually, since it requires a strong thrust to move the steering. Therefore, the design of wireless control system is use to solve the problem which could control the rotation angle of 45° to the left and right with precision, and accuracy on the steering control. First, the modelling of ATV will be derived using Newtonian formulation, and also design the controller of the ATV with accordance to the path-following planning motion method.

The results for stability of ATV is validate using a model generated by MATLAB system identification toolbox.

The best fit for yaw estimation is 92.7% and whereas pitch estimation is 69.76% respectively. As a conclusion, the yaw estimation shows that the ATV achieved its stability at the angle 45° and verify simulated of yaw axis part.

Keywords: *Autonomous Control, All-Terrain Vehicles, System Identification, Yaw and Pitch Stability*

Nomenclature

K_{steer}	Steering ratio; ratio between the turn of the steering wheel and the angular displacement of the wheel
$C1$ or C_f	Cornering stiffness front
$C2$ or C_r	Cornering stiffness rear
I	Moment of inertia about vertical axis
β	Sideslip angle
a_y	Lateral acceleration
δ	Angle steering
a	Distance of front axle to Centre gravity
b	Distance of rear axle to Centre gravity
I_z	Yaw of inertia
l_f, l_r	Distances from the centre of gravity to the front and rear axles respectively
F_F	Lateral tire force front
F_R	Lateral tire force rear
U or u	Velocity forward
r	Yaw of velocity
M or m	Mass
N	Rotational Speed

I. Introduction

Nowadays, constructions workers have discovered that the usage of All-Terrain Vehicle (ATV) gives much benefit to their work field which dedicated to huge driveability on irregular ground track as well as in paved road. ATV is one of the vehicle type that much lighter than other four-wheel vehicles and it is popular among the expert drivers.

This vehicle is also known as a quad bike or four-wheeler or can be defined as a vehicle that travels on low pressure tires. When taking corners, it is more challenging than rugged four-wheel vehicle since the current ATV's stabilizing mode is more difficult. ATV performance keep improving for the design and materials used, so as the performance. Hence, better knowledge is needed to improve the characteristics of the ATV parameters. The aim of this research is to improve the dynamic mathematical modelling of the ATV and also to design the controller for the ATV [1]-[28].

The modelling of ATV used based on the single track model or also known as *Bicycle* model will explained in the next section.

At the first stage, the controller will be designed using a wireless controller and aimed to obtain the performance improvement in terms of stability and workability. Wireless controller system design needs some knowledge about the fundamental of wireless system such as transmitter/receiver radio controller suitable for an ATV. Wireless remote control technology normally use for wireless control, automation and telemetry in a variety of applications industry. Anything that can be changed for examples: on/off, up/down or that can send and receive data; can be wireless. Remote control technology is the global leader in wireless solutions industry, provides a wide range of uses, the use are more focused in engineering and systems integration capabilities [1]-[3]. In the mathematical modelling design, it involves a description of the relation among inputs to the process, its state variables, and its output. This description is called the model of the system. The model can be represented as a set of transfer functions for linear time invariant systems or other relationships for non-linear or time variant systems [4]. Modelling of complex systems may be very difficult task.

II. ATV Overview

Before we go further about the mathematical modelling of the ATV, the overview of ATV part will be discussed to understand the operations of ATV system. Fig. 1 shows the overview of ATV such as engine part, brake system, power terrain, steering system (handle bar), and also tires.

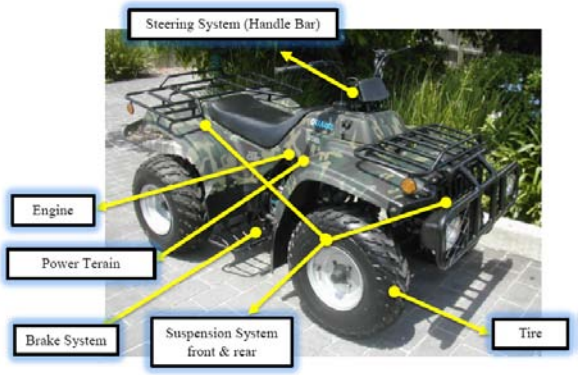

Fig. 1. ATV Components

The path-following route test that are selected to conduct the experiment in this project are climb u and lane change course according to paper [5] and [6] whereby the test procedure and track test is presented in next section. Then, the design controller for the tracking path-following route is by using wireless controller since several researches in paper [7]-[10] that wireless controller make better in term of stability controllable and dynamic performance. This controller will be further discussed on another section. In addition, the technique of system identification shall be used to get the best fit of the result as proposed in paper [11]-[14]. The system identification technique is been exercised for the validation of the result as to estimate the movement of the ATV whether it is follow the path-following planning that has been conducted when the data is collected. Besides, the noise and disturbance in result section need to be screened as to get a better result.

Thus, to filter the noise, complementary filter is used as proposed in paper [15] and [16] because of it works for the angle estimate is responsive and accurate and much easier to explain the theory rather than the unscented and extended kalman filter.

III. Methodology

Fig. 2 shows the overall works on this research while Fig. 3 shows the methodology of the research. The performance of ATV will be tested through the experiment will be conducted for this research. The physical measurement will be conducted to measure the parameters including mass, centre of mass and moments of inertia are presented in the results as shown in Fig. 2. Besides, the derivation of mathematical modelling of the ATV also covered in this paper as shown in next section.

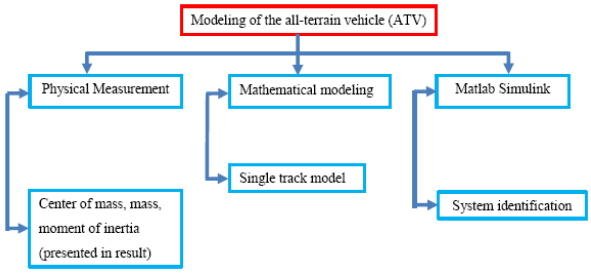

Fig. 2. Overall works on this research

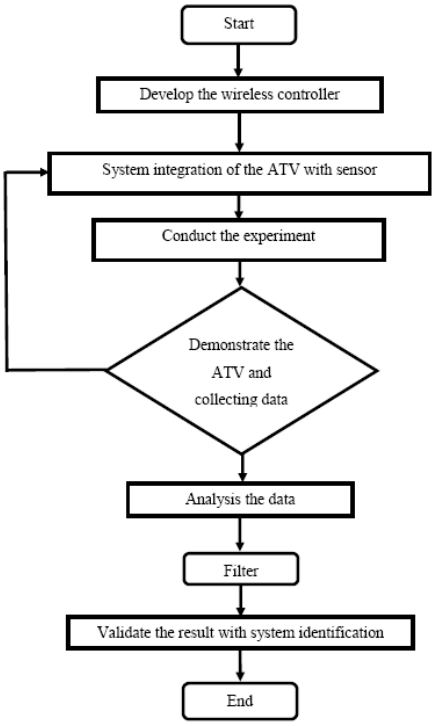

Fig. 3. Methodology of the research

The experiments and the procedures for the path-following planning track also will be elaborate in the paper.

IV. Mathematical Modeling of ATV

The single track model is a simple vehicle model which always is used to model 4Ws as shown in Fig. 4.

This model represents the left and right tire's characteristics have an equal tire characteristic of a two-wheel in plane vehicle with 2-degrees of freedom; yaw motion and lateral displacement [17]-[19]. Below are the assumptions applied on the bicycle model as shown in Fig. 5:

1. Heading velocity is constant, u (≈V).
2. No slope and body roll.
3. Steering input is constant.
4. Lateral accelerations (4 m/s^2).
5. Sideslip angle (β) is assumed small.

So, the equation of motion of the bicycle model is derive as below. Reference from Y-axis:

$$m(\dot{v} + ur) = F_{F_y} + F_{R_y} \tag{1}$$

$$I\dot{r} = aF_{F_y} - bF_{R_y} \tag{2}$$

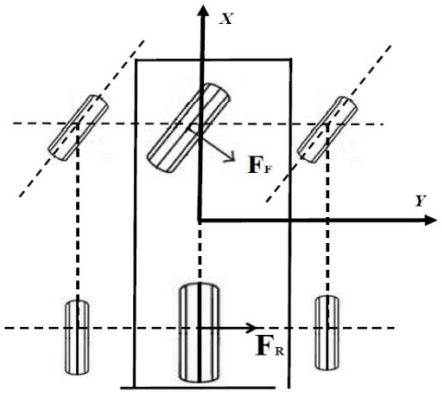

Fig. 4. Top view: Single track part will take at middle vertical X-axis as reference modelling

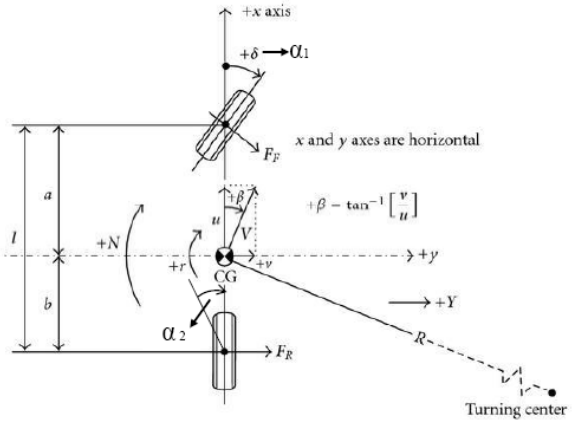

Fig. 5. The reference modelling is analyse by add some parameter and is known as "Bicycle Model"

The force acting on tire:

$$F_{F_y} = C_f \alpha_1 \tag{3}$$

$$F_{R_y} = C_r \alpha_2 \tag{4}$$

where:

$$\begin{aligned} \alpha_1 &= +\delta - \frac{1}{u}(v + ar) \\ \alpha_2 &= -\frac{1}{u}(v + br) \\ C_f &= \frac{a}{l}, \quad C_r = \frac{b}{l} \end{aligned} \tag{5}$$

To derived the steering angle, δ:
Substitute of $F_{F_y}$and F_{R_y} in Eqs. (1) and (2):

$$\begin{aligned} m(\dot{v} + ur) = &-\frac{v}{u}(C_f + C_r) + \\ &+ \frac{r}{u}(bC_r - aC_f) + \delta C_f \end{aligned} \tag{6}$$

$$\begin{aligned} I\dot{r} = &-\frac{r}{u}(a^2 C_f + b^2 C_r) + \\ &- \frac{v}{u}(aC_f - bC_r) + a\delta C_f \end{aligned} \tag{7}$$

Combined of (6) and (7) to eliminate v:

$$\begin{aligned} muI\dot{r} + &\left[I(C_f + C_r) + m(a^2 C_f + b^2 C_r)\right]\dot{r} + \\ &+ \frac{1}{u}\left[C_f C_r l^2 - mu^2(aC_f - bC_r)\right]r = \\ &= muaC_f\dot{\delta} + C_f C_r l\delta \end{aligned} \tag{8}$$

The circle test conditions:

$$\ddot{r} = 0 \quad \dot{r} = 0 \quad \dot{\delta} = 0 \tag{9}$$

then:

$$\frac{r}{u}\left[C_f C_r l^2 - mu^2(aC_f - bC_r)\right] = C_f C_r l\delta \tag{10}$$

and from (10), the δ is derived:

$$+\delta = \frac{L}{R} - \frac{mv^2}{Rl}\left(\frac{a}{C_r} - \frac{b}{C_f}\right) \tag{11}$$

$$a_y = \frac{v^2}{R} \tag{12}$$

By replacing a_y in (12):

$$\delta = \frac{L}{R} - \frac{ma_y}{l}\left(\frac{a}{C_r} - \frac{b}{C_f}\right) \tag{13}$$

The equation of β is derived from the front slip angle:

$$+\beta = -\frac{v}{u} \tag{14}$$

$$\alpha_2 = -\frac{1}{u}(v - br) = +\beta + \frac{br}{u} \tag{15}$$

$$+\beta = -\frac{b}{r} + \alpha^2 \tag{16}$$

and from the Eq. (3):

$$\beta = -\frac{b}{r} + \frac{\alpha m a_y}{C_r L} \tag{17}$$

Equations (13) and (17) show $+\beta$ and $+\delta$ linearly dependent on lateral acceleration a_y.

To describe the dynamic behaviour of the ATV model, a state space model is used. The state space model can be written:

$$\dot{x} = Ax + Bu \tag{18}$$

$$y = Cx + Du \tag{19}$$

where:

$$x = \begin{vmatrix} v \\ r \end{vmatrix}, \qquad y = \begin{vmatrix} a_y \\ r \end{vmatrix}, \qquad u = \delta$$

and:

$$A = -\begin{vmatrix} \frac{C_f + C_r}{mu} & u + \frac{aC_f - bC_r}{mu} \\ \frac{aC_f - bC_r}{I_z u} & \frac{a^2 C_f + b^2 C_r}{u I_z} \end{vmatrix}$$

$$B = \begin{vmatrix} \frac{C_f}{m} \\ \frac{aC_f}{I_z} \end{vmatrix} \tag{20}$$

$$C = -\begin{vmatrix} \frac{C_f + C_r}{mu} & \frac{aC_f - bC_r}{mu} \\ 0 & -1 \end{vmatrix}; \; D = \begin{vmatrix} \frac{C_f}{m} \\ 0 \end{vmatrix}$$

ATV configurations

In the process to design a wireless controller, there were 3 different parts have dissimilar functions and they contribute to the control differently. The wireless controller includes steering system (handle bar), switching system and brake system as shown in Fig. 6.

System Integration with sensor

The measured data for every test is based on the suitable selection of the sensor. The system integration of ATV with the sensor will be carried out by some experiment. However, the proposal for sensor's selection that shall be used in this project are accelerometer and gyro sensor.

Thus, in order to integrate the sensor at the same time while conduct the experiment, the 3-DOF of inertial measurement unit (IMU) is selected as shown in Fig. 7.

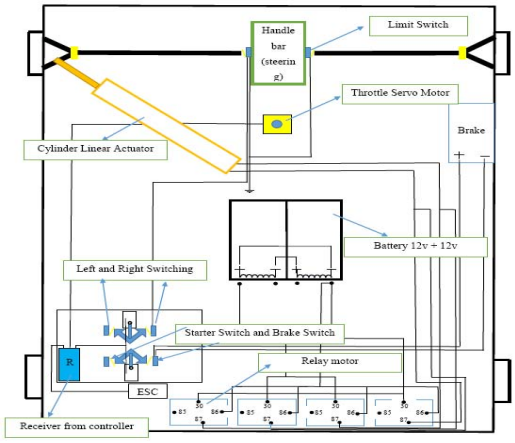

Fig. 6. Configuration of ATV modification

Fig. 7. 3-DOF IMU sensors

The function of IMU is by detecting the rate of acceleration, as well as the changes on rotational attributes such as pitch, roll and yaw [20].

Then, the data is fed into a computer to calculate the current speed and position given a known initial speed and position [21]. For the 3- DOF IMU, the sensors configurations is one gyroscope that measures yaw with two accelerometer. Since, the project is focus on linear single track model, the pitch and roll of the vehicle is ignored.

Complementary Filter

When integration with IMU sensor, the measured data is produce noise and disturbance. Thus, the complementary filter is used as shown in Fig. 8.

To design this filter, firstly, choose the time constant that is used as to calculate filter coefficients. By selecting the time constant, it can adjust the response. Besides, the time constant is the sample period which is simply the reciprocal of the sampling frequency and decided by ourselves. Set up the Complementary Filter as follows [22]–[23]:

$$y = a \times y + (1 - a) \times x \tag{21}$$

whereby:

a = time constant / (time constant + sample period).

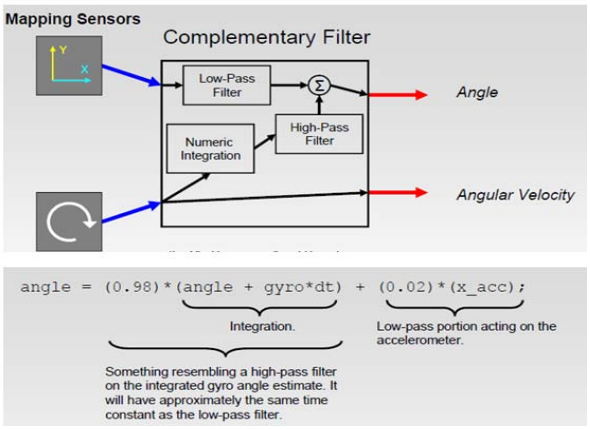

Fig. 8. Example of set-up complementary filter

The Validity and Reliability of Experimental Set Up

In this experimental set up, three procedures are introduced as to analysis the ATV whether it follows the path-following planning and then validate the result using system identification method. Besides that in order to get the valid and reliability of the data several method are selected. Table I shows the parameter for ATV based on measurement setting as shown in Fig. 9.

The data will be collected using IMU sensor via Arduino Uno microcontroller as shown in Fig. 10.

TABLE I
THE FIRST PARAMETER OF ATV

First Parameter	Measured data			
	Reading 1	Reading 2	Reading 3	Mean
Mass of ATV (kg)	90.1	90.3	90.2	**90.2**
Track length (m)	0.750	0.751	0.762	**0.754**
Wheelbase length (m)	0.880	0.889	0.882	**0.884**
Height of ATV (m)	0.700	0.720	0.720	**0.713**

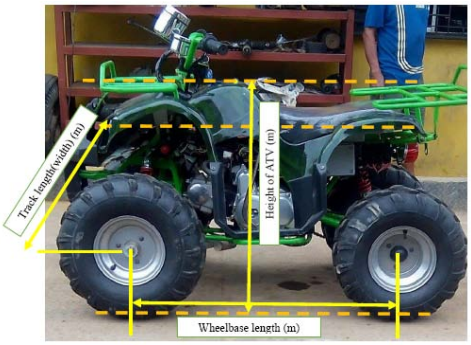

Fig. 9. Measurement of ATV

Fig. 10. Connection of IMU sensor SD card of Arduino Uno

Fig. 11. ATV testing for climb the obstacle

Fig. 12. ATV testing for lane change course track

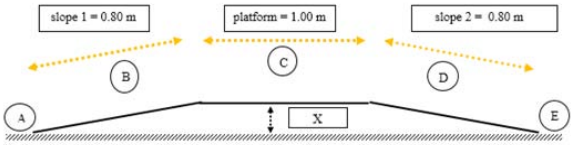

Fig. 13. The set up for the track

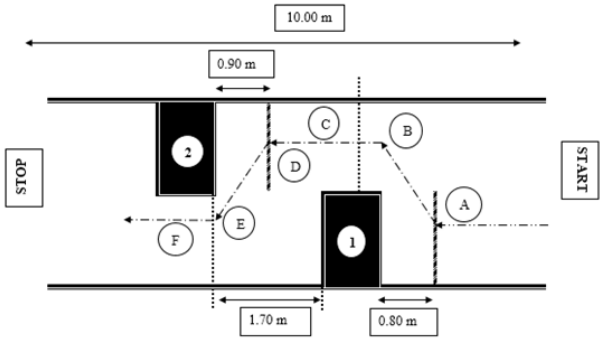

Fig. 14. Set up the lane change course track

Fig. 11 and Fig. 12 above show the experiment set up for climb the obstacle and the lane change course track, while Fig. 13 and Fig. 14 show the measurement for experiments set up.

From the mean value of first parameter based on Table I, the cornering stiffness and moment of inertia at x, y and z- axis with center of gravity can be calculated and determined as follows.

Stiffness Formula:

$$C = (mass,kg) \times \frac{60}{100} \times (0.50) \times \frac{16}{100} \times \frac{180}{\pi} \quad (22)$$

Moment inertia Formulae:

$$I = \frac{1}{12} \times [\text{mass, kg}] \times (\text{lengt, m}^2 + \text{lengt, m}^2) \quad (23)$$

1. Stiffness for front wheel:

$$90.2 \times \frac{60}{100} \times 0.50 \times \frac{16}{100} \times \frac{180}{\pi} = 248.07 \text{ (N /rad)}$$

2. Stiffness for rear wheel:

$$90.2 \times \frac{40}{100} \times 0.50 \times \frac{16}{100} \times \frac{180}{\pi} = 165.38 \text{ (N /rad)}$$

3. Moment inertia at x-axis:

$$I_x = \frac{1}{12}[90.2](0.754^2 + 0.713^2) = \underline{8.09 \text{ (kg m}^4\text{)}}$$

4. Moment inertia at y-axis:

$$I_y = \frac{1}{12}[90.2](0.884^2 + 0.713^2) = 9.695 \text{ (kg m}^4\text{)}$$

5. Moment inertia at z-axis:

$$I_z = \frac{1}{12}[90.2](0.884^2 + 0.754^2) = 10.15 \text{ (kg m}^4\text{)}$$

6. Centre of gravity from:

$$0.738(S_1) = 1.155(S_2) \quad (24)$$

$$S_1 + S_2 = 0.884 \quad (25)$$

From (4.1) S_1 is as subject matter;

$$S_2 = 1.565(S_2) \quad (26)$$

Insert (4. 3) into (4.2):

$$S_1 = 0.3446 \text{ m}$$

V. Result

MATLAB State-Space Model

Fig. 15 is the MATLAB/Simulink block diagram for open loop testing for yaw angle based on model as in Eq. (20) will obtained using system identification toolbox [24]-[26].

The data collected used for system identification based on data collected from IMU sensor on Arduino Uno microcontroller.

The Fig. 15 shows that the simulation of open loop system for the mathematical modelling of the ATV based on the single track model. By using Eq. (20) and result for the model state-space for the yawas shown in (27):

$$A = -\begin{bmatrix} 8.99 & 1.246 \\ 50.97 & 16.96 \end{bmatrix} \quad B = \begin{vmatrix} 3.32 \\ 44.5 \end{vmatrix}$$
$$C = -\begin{bmatrix} 8.99 & 0.6676 \\ 0 & -1 \end{bmatrix} \quad D = \begin{vmatrix} 3.316 \\ 0 \end{vmatrix} \quad (27)$$

After obtained the parameter and the state space model of ATV in Eq. (27), the simulation from the Fig. 15 is carried out. The result for the simulated state space model are shown in Figs. 16-18. Fig. 16, Fig. 17 and Fig. 18 show the result of open-loop system for the state-space model of yawing.

The output graph shows positive and negative of sine wave which are represented the yawing right and yawing left. However, there is no slip on rear tire because the ATV only steered at front wheel only.

This simulated result of yawing is show as the normal steering control at an angle approximately 45° whereas it considered reach point the stabilization when the ATV are driven to the regular turning surface.

The Fig. 19 shows that the simulation of open loop system for the mathematical modelling of the ATV based on the single track model.

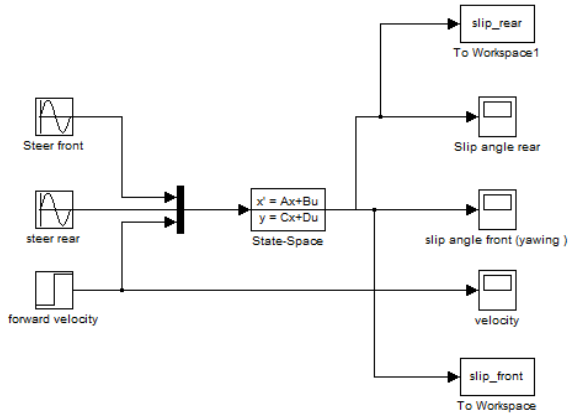

Fig. 15. MATLAB/Simulink block diagram for yaw

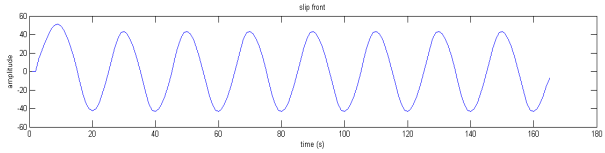

Fig. 16. Slip front tire

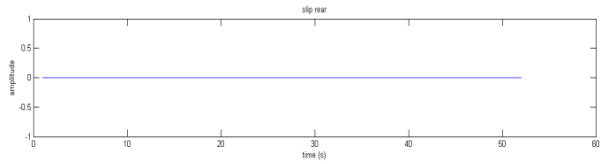

Fig. 17. Slip rear tire

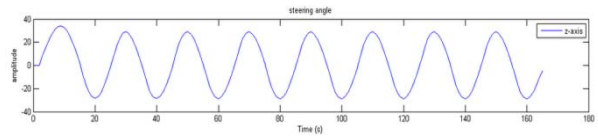

Fig. 18. Steering angle (yawing) at z-axis

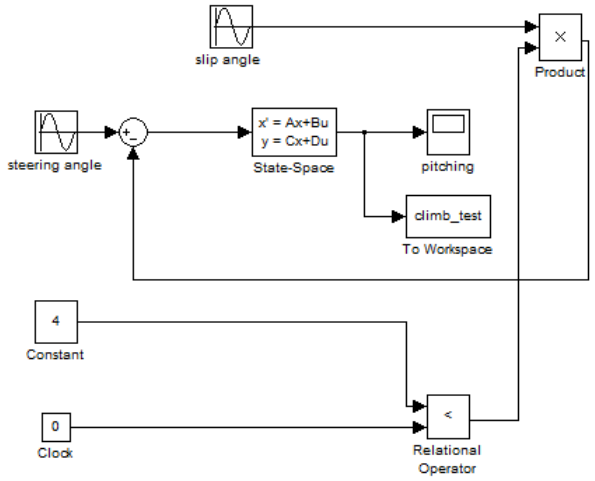

Fig. 19. Block diagram for pitch

By using Eq. (20) and the result forthe ATV model in state-space for the pitch as shown in (28):

$$A = -\begin{bmatrix} 8.99 & 1.246 \\ 86.41 & 28.75 \end{bmatrix}$$

$$B = \begin{vmatrix} 3.32 \\ 75.44 \end{vmatrix}$$

$$C = -\begin{bmatrix} 8.99 & 0.6676 \\ 0 & -1 \end{bmatrix} \quad (28)$$

$$D = \begin{vmatrix} 3.316 \\ 0 \end{vmatrix}$$

After obtained the parameter and the state space ATV model, the simulation from the Fig. 19 is carried out.

The result for the simulated state space model are shown in Fig. 20. From the Fig. 20 it shows the result of open-loop system for the state-space model of pitching. It indicates that the ATV is driven to the track which are approximately at 0.40 m height with 45° angle of slopes.

The graph output shows positive and negative of sine wave which are represent the pitching up and pitching down moment. This simulated result of pitch angles is shows as the normal moment effect whereas it considered as reach point the stabilization when the ATV are driven to the regular slope surface.

Fig. 21 shows the result of yaw stability using excel software while Fig. 22 shows the results of pitching stability. Fig. 23 shows the results of acceleration of ATV for yaw and pitch movement.

Fig. 24 shows the input and output signal using system identification toolbox based on data plotted to excel software and Fig. 25 is the best fit in system identification toolbox where 69.76 % best fit.

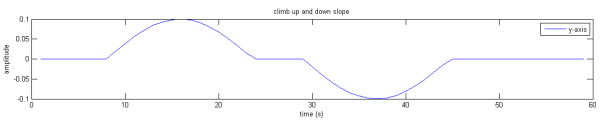

Fig. 20. The climb slope (pitching) at y-axis

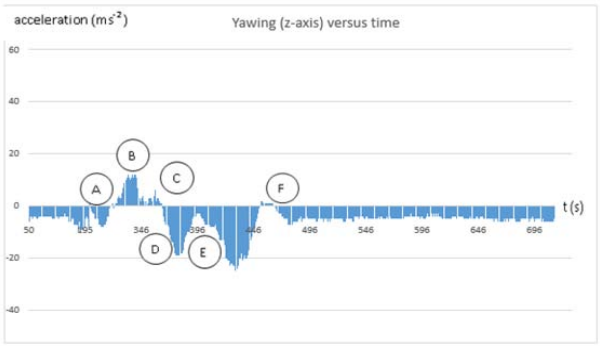

Fig. 21. Yaw stability

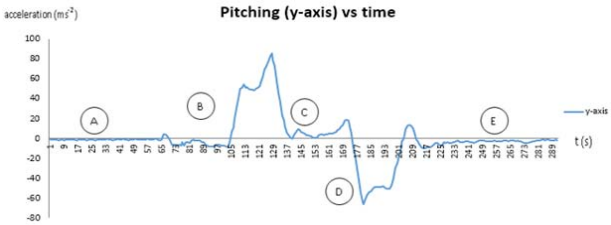

Fig. 22. Pitch stability

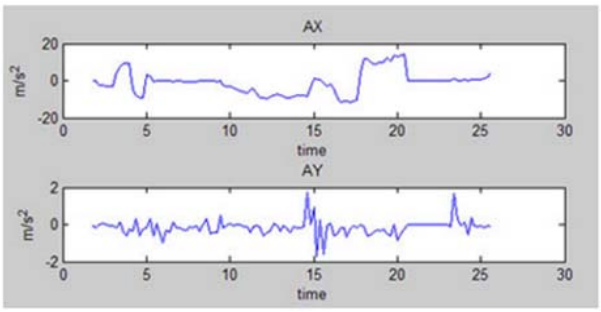

Fig. 23. Acceleration for yaw and pitch movement

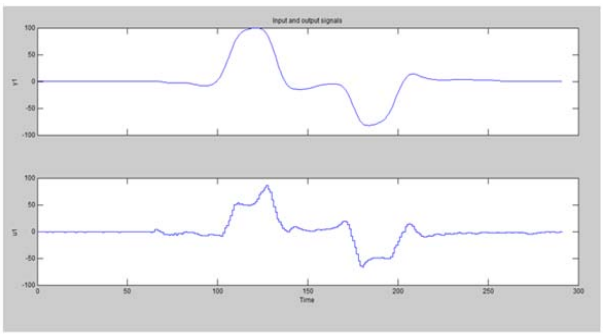

Fig. 24. Input and Output signals

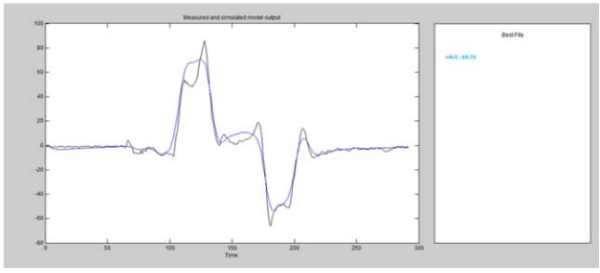

Fig. 25. The best fit in system identification toolbox

VI. Conclusion

The mathematical modelling of the ATV based on the single track system or also known as "bicycle model" has been described. The derivation of the mathematical modelling is in the form of state space from measuring parameter of the ATV.

Then, applied to MATLAB/Simulink to simulate the system based on open loop system. The step response of graph, it shows that the controller is needed to be design in order to improve the rise time and steady state error.

The stability of ATV based on the path -following planning are analyzed based on the yawing and pitching motion. In this experiment, the IMU sensor is used to collect the data and the SD card is used for data logger for this measured data. As a result, from this collected data, the analysis will be done by plotting the graph using Microsoft excel software.

Then, the result measured input and output data of track test analysis will be validated by using system identification method of time response. This is to estimate the value of the vehicle dynamic model of ATV based on the track test and get the best fits of the data.

From this data, the result will give more accurately the result about the motion of ATV. The single track model that has been proposed just make a linear part of the vehicle'sperformance only. It means that the stability of ATV is only cover when it been tested on the flat surface. Thus, the body roll of ATV is not considered. In order to test the stability irregular surface, the modelling of dynamic model of ATV cannot be implemented or predict the movement of a complex non-linear system.

Thus, to model the non-linear system, the new modelling approach is needed.

For the design of wireless controller also has the limitation. Firstly, the design of brake system cannot be done because of lack of force when use the mechanism of the brake that we made, the force that support the system is not enough, therefore, we need to add some equipment which is high torque and give high pressure to brake the cylinder wall, and to afford that also need a high of cost.

Second, the backward move with wireless stick movement design cannot be done, this is because, if we want to design for backward move, we need to add some motors with high-power torque, and with good reverse biased motor engine. For now, the solutions we used is only at throttle high and low puller to control the start and stop of the ATV movement, with lower the timing of ATV engine which is can low the speed of engine.

In next research, the project will be continue on how to integrate the IMU sensor with the hardware (ATV) by using X-Bee communication as to get the real time implementation of stability of ATV which can become as navigation system of ATV.

Secondly, the research of brake system need to be continue, whether make the design of the disc braking system, brake system wireless to improve the brake system that already existing.

Acknowledgements

We wish to express our gratitude to honorable University, UniversitiTeknikal Malaysia Melaka (UTeM) especially for Underwater Technology Research Group (UTeRG), Centre of Research and Innovation Management (CRIM) and to both Faculty of Electrical Engineering from UTeM to give the financial as well as moral support for complete this project successfully.

References

[1] Khaled Sailan, Klaus D. Kuhnert, and Hradik Karelia, Modeling, Design and Implement of Steering Fuzzy PID Control System for DORIS Robot, *International Journal of Computer and Communication Engineering* vol. 3, no. 1, pp. 57-62, 2014.

[2] Farshid A. Forouhar, "All-Terrain Vehicle Frequency Domain Analysis and Rider Behaviour. *Proceeding of the 1997 IEEE International Conference on Control Applications Hartford*," CT. 1997.

[3] P.Barec, M.Maly, R.Vozenilek. Control System of Vehicle Model with Four Wheels Steering (4WS). *International Scientific Meeting Motor Vehicles & Engines* Kragujeva, 2004.

[4] Donald D. Randolph, Keafur Grimes., "Mobility Analysis of Selected Lightweight Armoured Wheeled Concept Vehicles", TR GL-82-10, September 1982

[5] Christian Lundquist and Thomas Schon. "Recursive Identification of Cornering Stiffness Parameters for an Enhanced Single Track Model. *Proceedings of the 15th IFAC Symposium on System Identification*", Vol. 15, Part 1, 2009.

[6] Paul D. Ronney., Hydrocarbon-fueled internal combustion engines: "the worst form of vehicle propulsion except for all the other forms", Los Angeles, CA 90089-1453.

[7] Port Richey http://www.tpub.com.,Chapter12:Internal Combustion Engine 9438 US Hwy 19 N. #311, FL 34668,1998.

[8] Chetan Wadile, Rohan Dubal, Roshan Kolhe, Versha Rangaswamy, Aqleem Siddiqui & Nitin Gurav Selection, Modification and Analysis of Power Transmission and Braking System of an ATV, 2013 *International Journal on Mechanical Engineering and Robotics (IJMER)*.

[9] Amrit Om Nayak, G. Ramkumar, T. Manoj, M. A. Kannan, D. Manikandan and SibiChakravarthy, Holistic design and software aided finite element analysis (FEA) of an All-Terrain Vehicle Madurai, India. A11 May, 2001

[10] Changsui.W, Ming.Y,Yuanming.G,YuBin.Q. Analysis of vehicle handling and stability in frequency domain based on system identification method. *WASE International conference on Information Engineering*, 2010

[11] ChetanDhuri, Aditya Masur, AniketWarang& Aditya sudhir:Selection, Modification And Analysis of Steering Mechanism For An All-Terrain Vehicle, 2013 *International Journal on Theoretical and Applied Research in Mechanical Engineering*.

[12] H. B. Pacejka. Tire and vehicle dynamics. *Society of Automotive Engineers*, 2002.

[13] Smith N. D., "Understanding Parameters Influencing Tire Modeling", Colorado State, 2004.

[14] Ricardo Hinojosa "*Bearcats Baja Front Suspension System*", Baccalaureate thesis, April, 2013

[15] William Bombardier,AhmadFadel, XiangdongDing, Ian Fun ken hauser,Brian Zuccato,Mike Bowie,YeTao,Bo Huang "Baja Project - Suspension". August 3rd 2007.

[16] Melior Inc., "Steering and Suspension Systems Study Guide" 2004

[17] http://www.explainthatstuff.com/remote control. html,Disember 13/12/2014

[18] http://cytron.com.my/c-9-wireless-devices/c-282-rf-module,Disember 13/12/2014

[19] D.Eduoard, *Parameter Identification of a Linear Single Track Model*, traineeship report, Eindhoven University of Technology, Eindhoven, 2011.

[20] F.A.Azis, M.S.M. Aras, M.Z.A. Rashid, KS Khamis, OAA Ghani, MN Othman, Modelling and Analysis of All Terrain Vehicle (ATV) using System Identification for Yaw Stability.
[21] MSM Aras, SS Abdullah, AA Rahman, MAA Aziz, Thruster Modelling for Underwater Vehicle Using System Identification Method, *Int J Adv Robotic Sy* 10 (252), 2013.
[22] Emanuel Blanchard. "Parameter Estimation Method using an Extended Kalman Filter. *Proceedings of the Joint North America, Asia-Pacific ISTVS Conference and Annual Meeting of Japanese Society for Terra mechanics*" June 23-26, 2007
[24] M.S.M. Aras, M.N. Kamarudin, A.S. M Nor, H.I Jaafar,H.N.M Shah, A.M Kassim, M.Z.A Rashid Development and Modelling of Unmanned Underwater Glider using the System Identification Method. *Journal of Engineering and Technology*, 4 (2). pp. 1-22. ISSN 2180-3811. (2013).
[25] M.S.M. Aras, Abdullah, S.S, Rashid, M.Z.A, Rahman, A. A, Aziz, M.A.A., Development and Modeling of Unmanned Underwater Remotely Operated Vehicle Using System Identification for Depth Control. *Journal of Theoretical and Applied Information Technology*, Vol 56 (1). pp. 136-145. ISSN 1992-8645. (2013).
[25] M.S.M.Aras, M.F. Basar, N. Hasim, M.N. Kamaruddin, H.I. Jaafar, Development and Modeling of Water Tank System using System Identification Method. *International Journal of Engineering and Advanced Technology (IJEAT).* pp. 278-283. ISSN 2249 – 8958. (2013).
[26] M.S.M.Aras, S.S. Abdullah, S.S. Shafei, M. Z.A. Rashid, A.Jamali, Investigation and evaluation of low cost depth sensor system using pressure sensor for unmanned underwater vehicle, *Majlesi Journal of Electrical Engineering*, Vol. 6 (2). 2012.
[27] Liu, J., Cai, B., Wang, Y., Status and prospects of autonomous vehicle positioning method for cooperative vehicle infrastructure system, (2013) *International Review on Computers and Software (IRECOS)*, 8 (1), pp. 327-340.
[28] Jebelli, A., Yagoub, M.C.E., Abdul Rahim, R.H.J., Kazemi, H., Design and construction of an underwater robot based fuzzy logic controller, (2013) *International Review of Mechanical Engineering (IREME)*, 7 (1), pp. 147-153.

Authors' information

Mohd Shahrieel b Mohd Aras is a lecturer at Faculty of Electrical Engineering, Universiti Teknikal Malaysia Melaka UTeM. He currently pursues his PhD in Control and Automation, Faculty of Electrical Engineering, Universiti Teknology Malaysia. His current research is focusing on control system design of underwater technology. His primary interests related to underwater robotics and Artificial Intelligence.

Mohd Khairi Bin Mohd Zambri is a lecturer at Faculty of Electrical Engineering, Universiti Teknikal Malaysia Melaka (UTeM), He currently in the field of Industrial Power department. His current research is focusing on renewable energy, energy efficiency, and power system. His primary interests related to power system.

Mohd Zamzuri Ab Rashid received the B. Eng. (2006) and M. Eng (2012) in Mechatronic from International Islamic University of Malaysia. Currently he is a lecturer at the University Technical Malaysia Melaka, Ayer Keroh Melaka. His primary interests related to nonlinear control system, robotics and unmanned system.

Fadilah Binti Abdul Azis is a lecturer of Mechatronics Department in Universiti Teknikal Malaysia Melaka (UTeM). She has a Bachelor of Mechatronics Engineering (Hons) from International Islamic University Malaysia (IIUM) and an MSc in Mechatronics Engineering from University of Siegen, Germany. Her research interest includes in the Emerging Technology focus areas such as Underwater Technology and Smart Material Structures. She is currently working on the development of underwater vehicle for underwater industry.

Alias Khamis was born 22 March 1979 at Melaka, Malaysia. Works as Lecturer at Faculty of Electrical Engineering, UniversitiTeknikal Malaysia Melaka.He research interest Research area in Electrical Power System, Renewable Energy, and Designing Electrical Motor.

Praise Worthy Prize

International Review of Automatic Control (I.RE.A.CO.), Vol. 8, N. 2
ISSN 1974-6059 *March 2015*

Model Identification of an Underwater Remotely Operated Vehicle Using System Identification Approach Based on NNPC

Mohd Shahrieel Mohd Aras, Shahrum Shah Abdullah, Kyairul Azmi Baharin, Arfah Syahida Mohd Nor, Mohd Khairi Mohd Zambri

Abstract – *This paper described the development of modeling of an unmanned underwater vehicle (UUV) using system identification toolbox based on neural network model. The set of data based on neural network model generated by open-loop model of UUV and the input-output data produced using neural network predictive control technique. The model of UUV is an underwater Remotely Operated Vehicle (ROV) will be used in this study. Open-loop model of ROV created using system identification technique with implemented in real time experiment for open-loop system. Two data will be used such as the input and output neural network data for validation and training for infer a model of the ROV using system identification toolbox. The data re-generated using graph digitizer software. The accuracy of this software almost 90%. Then, the model obtained in this system will be controlled using conventional PID controller in MATLAB Simulink. The comparison between two models from different techniques of the ROV will be described. When the number of samples used in this project reduced, the best fit will be increased. A model obtained based on neural network model is acceptable to use in simulation and will be improved the best fit when reduced number of samples.* ***Copyright © 2015 Praise Worthy Prize S.r.l. - All rights reserved.***

Keywords: *Neural Network Predictive Control, Neural Network Model, Graph Digitizer, System Identification*

I. Introduction

Neural Network Predictive Control (NNPC) is one of intelligent controller that used to control the movement of underwater Remotely Operated Vehicle (ROV) [1]-[14]. In NNPC, the input-output plant data will be generated based on Neural Network Model (NNM).

The produced input-output data using open loop ROV model that was developed by Underwater Technology Research Group (UTeRG) [1], [2]. The NNPC reported used in [3] to control the Deep Submergence Rescue Vehicle (DSRV). Based on [3], the NNPC gives the best system response compared other controller (e.g PID controller, PD controller, and FLC controller).

But the time execution will be longer than others. Also stated to implement this controller to real time system more complicated programming also needed higher microprocessor. In [4], [5] used the DSRV model to design an intelligent controller that called single input fuzzy logic controller. This paper will be introduced one new techniques to generate a model of ROV based on NNM (training data) in NNPC toolbox. This technique is a novel and no reported to any published paper, and it is needed to use another techniques/software to re-generated data from graph obtained in NNPC.

The Graph Digitizer software will be used to re-generate data and then will be used to infer a model using system identification toolbox in MATLAB.

Other method can be used such as symbiosis in MATALB and origin software to re-generated data. The advantages of this digitizer software is easy and simple to use. Moreover, the accuracy of this software is better.

Then, the data obtained used to infer a model using system identification will be controlled using simple conventional controller using MATLAB software.

The conventional PID controller will be used to control this UUV system. The focused on this project is set to depth control. As stated in [6], [7], the depth control for ROV is needed to avoid any damage to both to the ROV and the environment such as operated in cluttered environment. For depth control the overshoot of the system response will be priority of the system.

In this paper a model obtained from [8] will be used to make a comparison between a models generated by NNM. The comparison between model generated by real time experiment and neural network forecasting data will be described in this paper.

At first trial, the both PID controller will be used same parameter to control both models. Then, the both PID controller will be tune to better performances of system response. The model of ROV was developed by UTeRG that called UTeRG ROV 1. Based on [8] the model of ROV developed using system identification technique.

UTeRG ROV 1 is the earlier model of ROV that has been built to in order to infer a model using system

identification technique as shown in Fig. 1. This ROV can be classified as observation class ROV.

This model is consists of 4 thrusters that allow this ROV to move in 4 DOF (degree of freedom).

The dimension for this model is 0.3m of length, 0.6m of width and 0.45m of height. The overall weight for this model is 18 kg and designed as open-frame model. It body are made of aluminum for its frame and using PVC for its pressure hull.

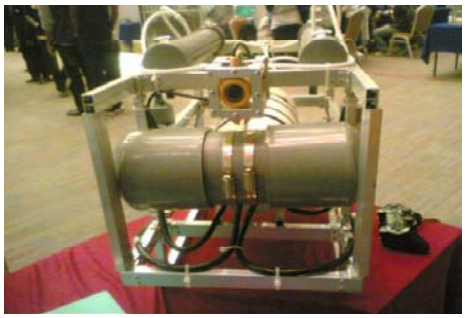

Fig. 1. UTeRG ROV 1[9]

II. Neural Network Model (NNM)

The design procedure utilizes MATLAB® Neural Network Predictive Control toolbox and was implemented using SIMULINK®. A neural network was designed to be used as the predictive model [9].

The objective of the controller is to maintain the depth of ROV by control the thrusters system.

Fig. 2(a) shows the window for designing the NNPC while Fig. 2(b) shows the plant identification for training data and Fig. 2(c) shows the training parameters. Based on training data, numbers of samples can be adjust and the training samples (input-output plant) shown in Fig. 3.

From this Fig. 3, it is difficult and take time to re-generated using digitizer software. Using Train Network in training parameter as shown in Fig. 2(c), the input graph and NN graph for training and validation respectively as shown in Figs. 4, 5. The two number of samples will be selected that is 5000 and 1000 samples.

Based in Fig. 6, the graph will be convert to data using Digitizer software. This software will useful to re-generate data from graph. The numbers of data up to user. It can make a detail plot of graph. Then the data can be re-plotted using excel or MATLAB as shown in Fig. 7. Figures 8 show the comparison between data using excel and neural network model. The dark blue is the data from excel while the blur blue is the neural network model. Based on this Figure shows that the error between both model 10%.

The accuracy of this comparison is about 90%. So, digitizer software valid to used to obtained data from fixed graph.

Once, data obtained the system identification toolbox in MATLAB will be used to infer a model. The best fits obtained for this system is 40.93 and 86.06 for 5000 and 1000 samples respectively and yields the transfer function as in Eqs. (1) and (2).

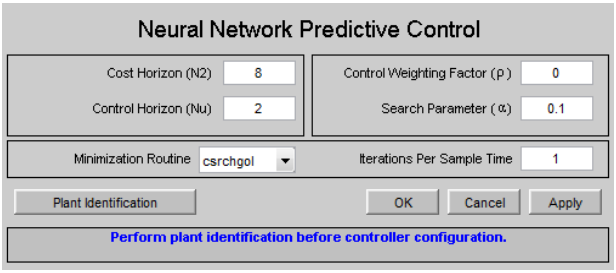

(a) Neural Network Predictive control

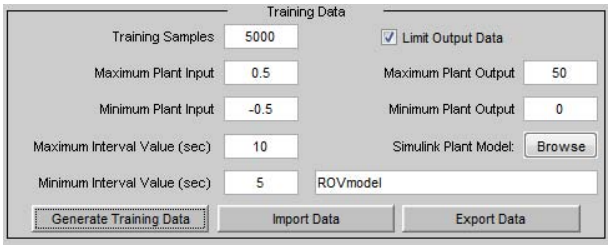

(b) Training Data

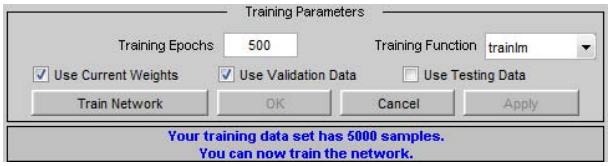

(c) Training Parameter

Figs. 2. Neural Network Predictive Window

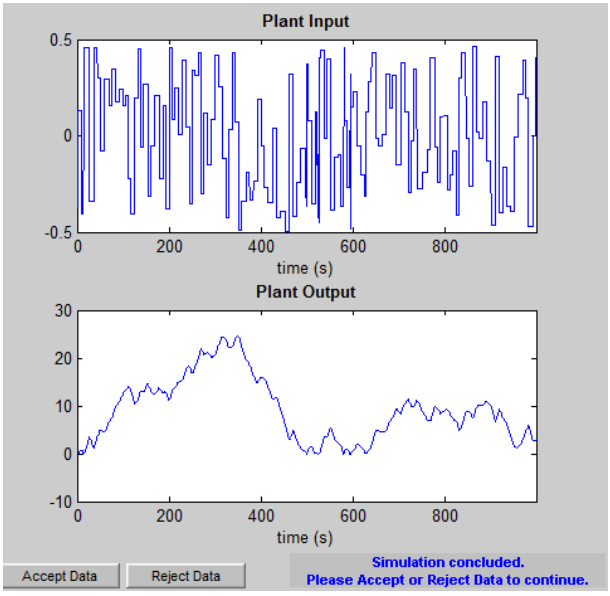

Fig. 3. Input-Output plant

The Simulink plant model based on open-loop model ROV generated by system identification technique as shown in Fig. 10. Transfer function state space technique yields:

$$\frac{4.736s + 3.749}{s^3 + 2.28s^2 + 2.07s + 0.07178} \quad (1)$$

$$\frac{1.32s + 0.89}{s^3 + 3.495s^2 + 3.51s - 0.013} \quad (2)$$

Based on Eq. (1) convert to state space matrix:

$$A = \begin{bmatrix} -2.28 & -2.07 & -0.07178 \\ 1 & 0 & 0 \\ 0 & 1 & 0 \end{bmatrix}$$

$$B = \begin{bmatrix} 1 \\ 0 \\ 0 \end{bmatrix}; C = \begin{bmatrix} 0 & 4.736 & 3.749 \end{bmatrix}; D = 0$$

Based on Eq. (1) convert to state space matrix:

$$A = \begin{bmatrix} -3.495 & -3.51 & 0.013 \\ 1 & 0 & 0 \\ 0 & 1 & 0 \end{bmatrix}$$

$$B = \begin{bmatrix} 1 \\ 0 \\ 0 \end{bmatrix}; C = \begin{bmatrix} 0 & 1.32 & 0.89 \end{bmatrix}; D = 0$$

The both model are control obtained from system identification technique will be analyse in terms of controllability and observability and also asymptotically stable. Based on state space matrices, the system is both controllable and observable because the system has a rank of 3. This system is asymptotically stable when all eigenvalues of A have negative real parts. Fig. 10 shows the Simulink of the ROV based on different model using PID controller.

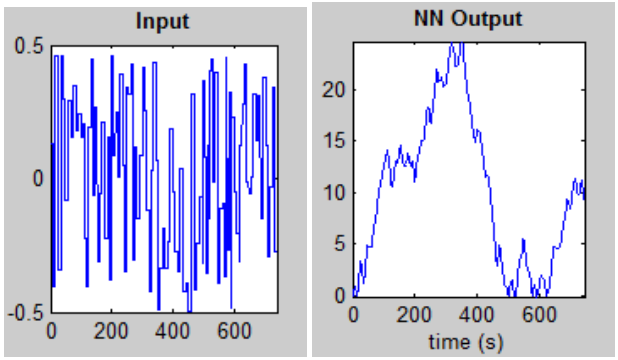

(a) Training data

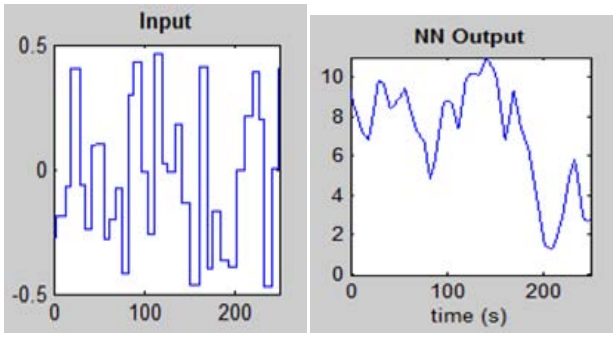

(b) Validation data

Figs. 4. Validation data and Training Data for NN Predictive Control using 5000 samples

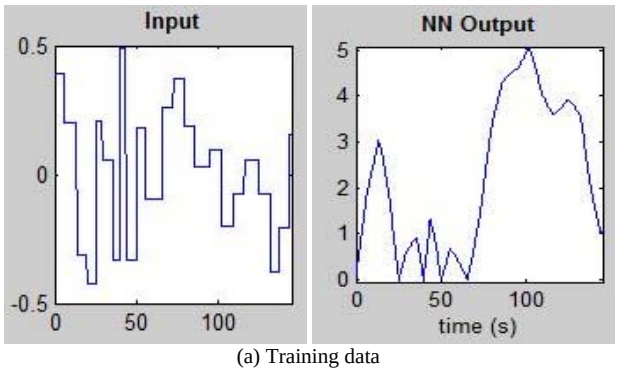

(a) Training data

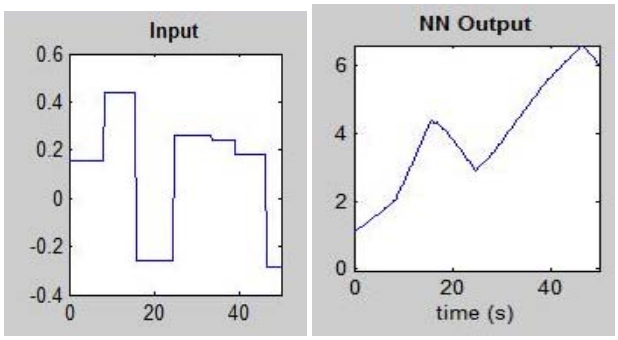

(b) Validation data

Figs. 5. Validation data and Training Data for NN Predictive Control using 1000 samples

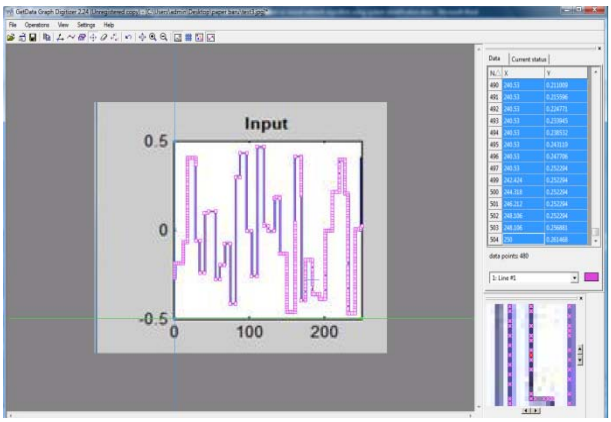

Fig. 6. GetData Graph Digitizer Software

Fig. 11(a) shows the system response of depth control between two models of the ROV.

Fig. 11(b) shows the system response with different set point. Model 1 is based on neural network forecasting technique while model 2 is based on system identification technique.

From this Figure shows the model 2 based on system identification technique better than Model 1 based on neural network forecasting technique. But the both model can be used to study a controller design for the future.

Fig. 11(c) the system response of depth control for 1000 samples model.

The response for 1000 samples is not smooth and higher the steady state error. The next recommendation is to design an intelligent controller such as using Fuzzy Logic Controller.

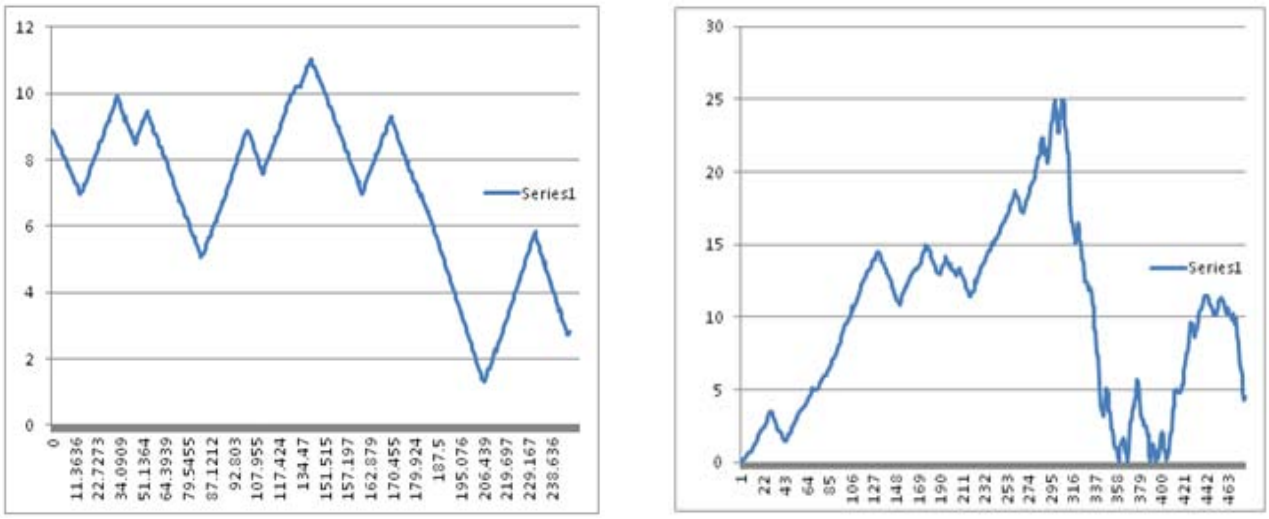

(a) (b)

Figs. 7. Plot output data using Excel based
on Digitizer software

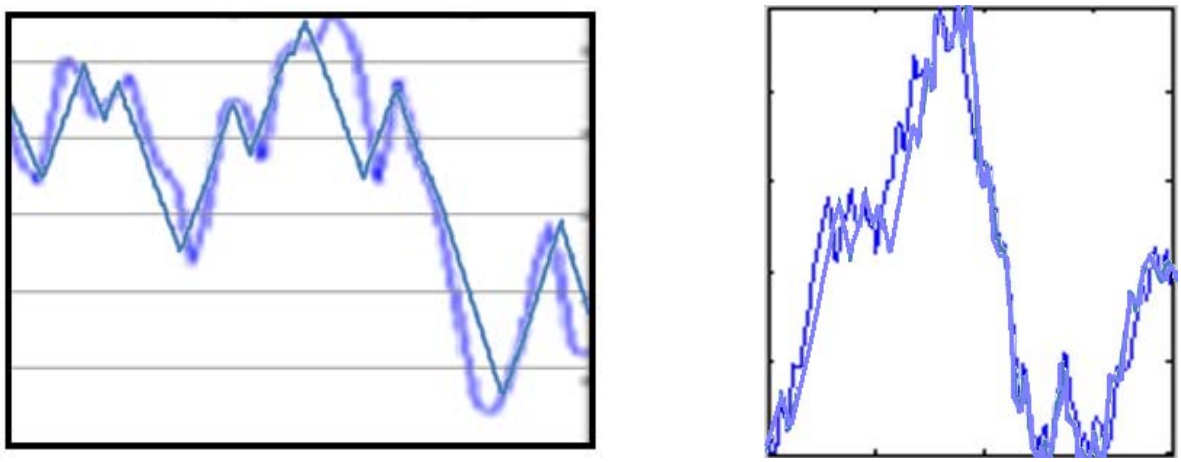

(a) (b)

Figs. 8. Comparison between Data using Excel
and Neural Network

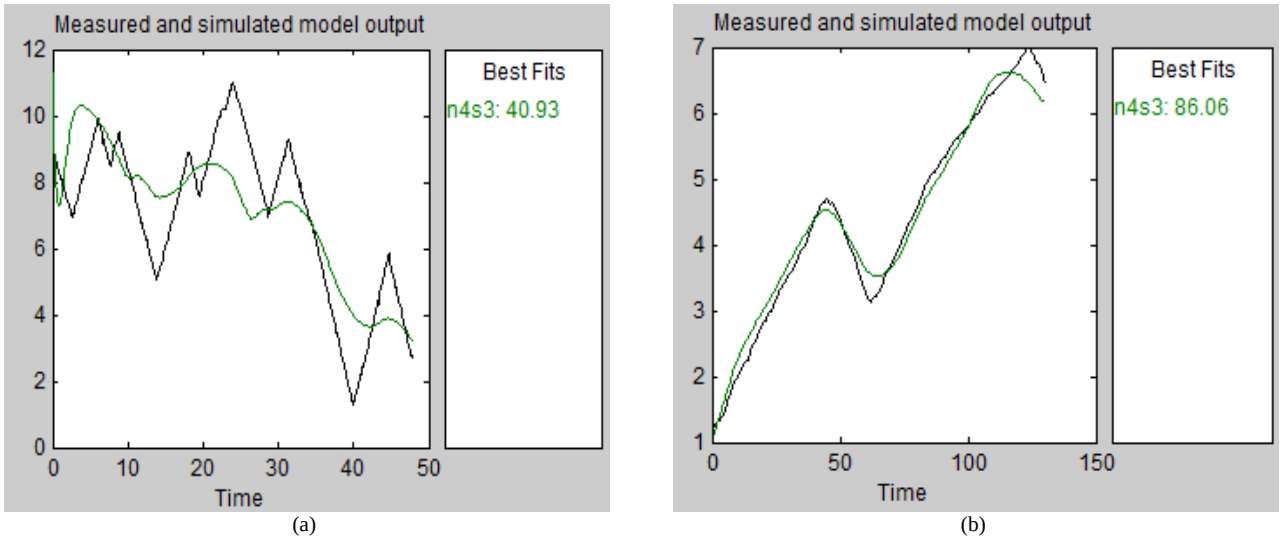

(a) (b)

Figs. 9. The best fits

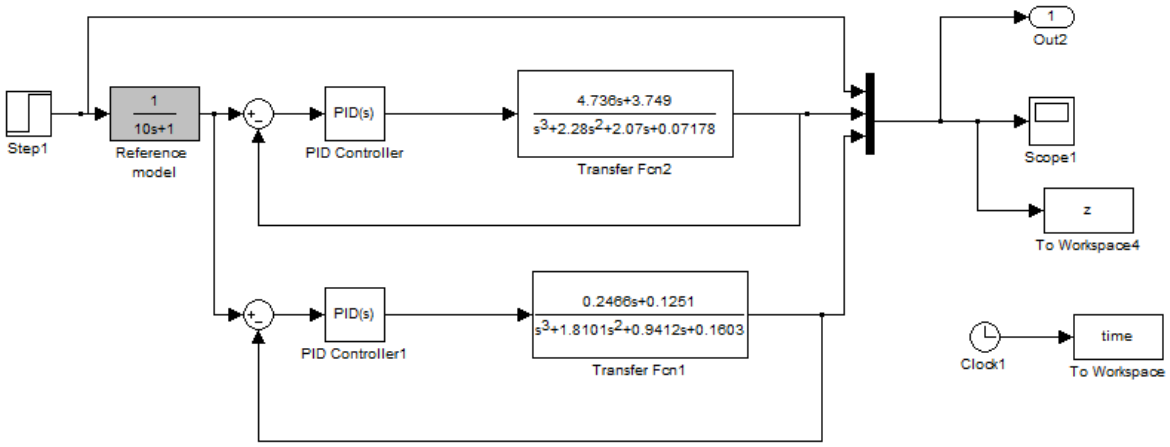

Fig. 10. Simulation for ROV depth control between two models

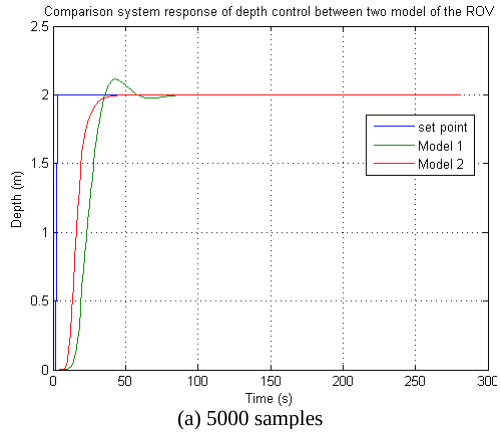

(a) 5000 samples

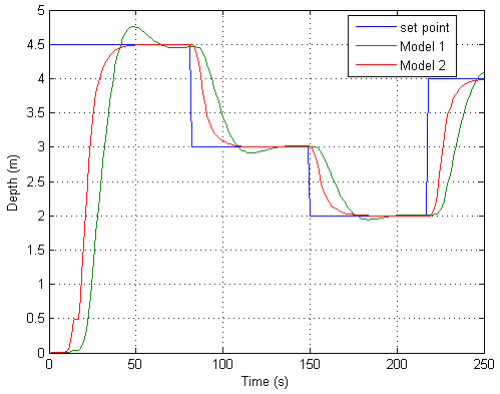

(b) 5000 Samples with different set point

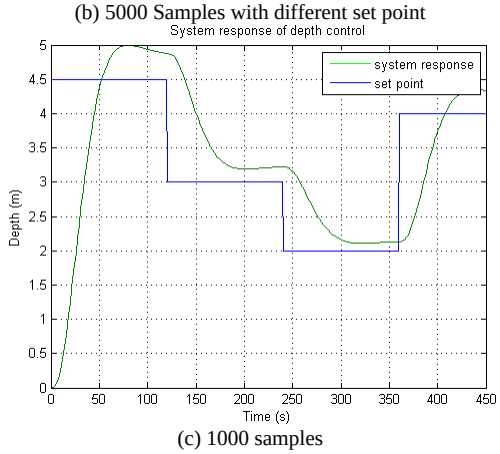

(c) 1000 samples

Figs. 11. System response for depth control of the ROV

III. Conclusion

The modeling of an underwater remotely operated vehicle using system identification toolbox based on neural network forecasting data is successfully. The set of data forecast based on open loop model of ROV and the input-output data are generated using neural network predictive control technique using Digitizer software.

The data then been used inside the MATLAB via system identification toolbox to come out the system modeling for the ROV. The modeling is done when the system identification infer a transfer function model and the controller for the system is designed based on a model obtained by using simple conventional PID controller. The PID controller can be used to control this system with good performances.

Acknowledgements

We wish to express our gratitude to honorable University, Universiti Teknikal Malaysia Melaka (UTeM) and UniversitiTeknologi Malaysia UTM) especially for Underwater Technology Research Group (UTeRG), Centre of Research and Innovation Management (CRIM) and to both Faculty of Electrical Engineering from UTeM and UTM to give the financial as well as moral support for complete this project successfully.

References

[1] F.A.Azis, M.S.M. Aras, S.S. Abdullah, Rashid, M.Z.A, M.N. Othman. Problem Identification for Underwater Remotely Operated Vehicle (ROV): A Case Study. *Procedia Engineering*. 2012; 41: 554-560.

[2] M. S. M. Aras, F.A.Azis, M.N.Othman, S.S.Abdullah. A Low Cost 4 DOF Remotely Operated Underwater Vehicle Integrated With IMU and Pressure Sensor. In: *4th International Conference on Underwater System Technology: Theory and Applications 2012 (USYS'12)*, pp 18-23, 2012.

[3] A.S.MohdNor, S.S.Abdullah, M.S.M.Aras, M.Z.A Rashid, Neural Network Predictive Control (NNPC) of a Deep Submergence Rescue Vehicle (DSRV), *4th International Conference on Underwater System Technology: Theory and Applications 2012 (USYS'12)*, 5th & 6th December, pp 24-29, 2012.

[4] Ali, F.A., Azis, F.A., Aras, M.S.M., Othman, M.N., Abdullah, S.S., Design of a magnetic contactless thruster of Unmanned Underwater Vehicle, (2013) *International Review of Mechanical Engineering (IREME)*, 7 (7), pp. 1413-1420.

[5] Aras, M.S.M, S.S. Abdullah, Rashid, M.Z.A, Rahman, A. Ab,Aziz, M.A.A, Development and Modeling of underwater Remotely Operated Vehicle using System Identification for depth control, *Journal of Theoretical and Applied Information Technology*, Vol. 56 No 1, pp 136-145, 2013.

[6] MohdShahrieelMohd Aras, Shahrum Shah Abdullah, Azhan Ab Rahman, Muhammad AzharAbd Aziz, Thruster Modelling for Underwater Vehicle Using System Identification Method, *International Journal of Advanced Robotic Systems*, Vol. 10, No 252, pp 1 – 12, 2013.

[7] Mohd Aras, MohdShahrieel and Abdullah, Shahrum Shah and Shafei, SitiSaodah, Investigation and Evaluation of Low cost Depth Sensor System Using Pressure Sensor for Unmanned Underwater Vehicle. *Majlesi Journal of Electrical Engineering*, Vol. 6, (No. 2), 2012.

[8] Mohd Aras, M.S., Abdullah, S.S., Abd Aziz, M.A., Rahman, A.F.N.A., Analysis of an improved Single Input Fuzzy Logic Controller designed for depth control using Microbox 2000/2000c interfacing, (2013) *International Review of Automatic Control (IREACO)*, 6 (6), pp. 728-733.

[9] Aras, M.S.M, S.S. Abdullah, Rashid, M.Z.A, Rahman, A. Ab, Aziz, M.A.A, Robust Control of Adaptive Single Input Fuzzy Logic Controller for Unmanned Underwater Vehicle, *Journal of Theoretical and Applied Information Technology*, Vol. 57, 2013.

[10] Mohd Aras, MohdShahrieel and MohdFarriz , MdBasar and Abdul Azis, Fadilah and FaraAshikin , Ali,Analysis Movement of Unmanned Underwater Vehicle using the Inertial Measurement Unit. *International Journal of Emerging Science and Engineering (IJESE)*, 1 (10). pp. 47-53. ISSN 2319–6378, 2013.

[11] Mohd Aras, MohdShahrieel and MdBasar, MohdFarriz and AbdAzis, Fadilah and Ali, FaraAshikin, Obstacle Avoidance System for Unmanned Underwater Vehicle using Fin System. *International Journal of Science and Modern Engineering (IJISME)*, 1 (9). pp. 24-30. ISSN 2319-6386, 2013.

[12] Jebelli, A., Yagoub, M.C.E., Abdul Rahim, R.H.J., Kazemi, H., Design and construction of an underwater robot based fuzzy logic controller, (2013) *International Review of Mechanical Engineering (IREME)*, 7 (1), pp. 147-153.

[13] Mashhad, A.M., Karsaz, A., Mashhadi, S.K.M., High maneuvering multiple-underwater robot tracking with optimal two-stage kalman filter and competitive hopfield neural network based data fusion, (2013) *International Journal on Communications Antenna and Propagation (IRECAP)*, 3 (4), pp. 191-198.

[14] Aras, M.S.M., Abdullah, S.S., Jaafar, H.I., Razilah, A.R., Arfah Ahmad, A., A comparison study between two algorithms particle swarm optimization for depth control of underwater remotely operated vehicle, (2013) *International Review on Modelling and Simulations (IREMOS)*, 6 (5), pp. 1687-1694.

Authors' information

Mohd Shahrieel b Mohd Aras is a lecturer at Faculty of Electrical Engineering, Universiti Teknikal Malaysia Melaka UTeM. He currently pursues his PhD in Control and Automation, Faculty of Electrical Engineering, Universiti Teknology Malaysia. His current research is focusing on control system design of underwater technology. His primary interests related to underwater robotics and Artificial Intelligence.

Dr. **Shahrum Shah b Abdullah** is a senior lecturer at Faculty of Electrical Engineering, UniversitiTeknologi Malaysia.14 Years of experience in this university .He got Ph.D in Artificial Neural Networks, Department of Electrical and Electronic Engineering, Faculty of Engineering, Imperial College of Science, Technology and Medicine, University of London. Thesis: Experiment Design for Deterministic Model Reduction and Neural Network Training. Currently he is Deputy Dean, Malaysia – Japan International Institute of Technology (MJIIT).
Website: http://ac.utm.my/web /shahrum

Kyairul Azmi bin Baharin is a lecturer at Faculty of Electrical Engineering, UniversitiTeknikal Malaysia Melaka. He is currently pursuing his PhD in electrical engineering. His research interests are performance evaluation and energy forecast of solar photovoltaics using artificial intelligence and machine learning models.

Arfah Syahida Binti Mohd Nor is a lecturer at Faculty of Electrical Engineering, Universiti Teknikal Malaysia Melaka UTeM. Her current research is focusing on control system design and artificial intelligent technology. Her primary interests related to underwater vehicle technology.

Mohd Khairi Bin Mohd Zambri is a lecturer at Faculty of Electrical Engineering, Universiti Teknikal Malaysia Melaka (UTeM), He currently in the field of Industrial Power department. His current research is focusing on renewable energy, energy efficiency, and power system. His primary interests related to power system.

Praise Worthy Prize

International Review of Automatic Control (I.RE.A.CO.), Vol. 8, N. 2
ISSN 1974-6059 *March 2015*

Robust Controller Design for T1DM Individualized Model: Gain-Scheduling Approach

A. Ilka, I. Ottinger, T. Ludwig, M. Tárník, V. Veselý, E. Miklovičová, J. Murgaš

Abstract – *This paper deals with the robust gain-scheduled controller design for individualized type 1 diabetes mellitus (T1DM) subject model. The controller is designed using LPV model created from T1DM minimal model with two additional subsystems - absorption of digested carbohydrates and subcutaneous insulin absorption. Data collected from continuous glucose monitoring with the help of pharmacodynamics and pharmacokinetics characteristics were used for model identification. The closed-loop stability and cost for all scheduled parameters is guaranteed by the controller design approach. The benefits of the presented approach are shown in the simulation results.*

Keywords: *LPV System, Robust Controller, Gain-Scheduling, Output Feedback, Quadratic Stability, Type 1 Diabetes Mellitus Model*

Nomenclature

G	Glucose concentration
I	Plasma insulin concentration
V_I	Distribution volume of plasma insulin
V_G	Glucose distribution volume per kilogram
S_G	Glucose rate constant
S_I	Insulin sensitivity index
T_I	Time constant
k_I	Decay rate of insulin in plasma
R_a	Rate of appearance of glucose in plasma
D	Amount of ingested carbohydrates
A_G	Carbohydrate bioavailability
δ	Dirac impulse approximation
v	Subcutaneous insulin infusion rate
x	State variable
y	System output
u	Controller output
w	Reference value
e	Control error
θ	Scheduling parameter
B_e	Bellman-Lyapunov function
V	Lyapunov function
J	Cost function
K	Gain matrix

I. Introduction

Computer modeling of type 1 diabetes mellitus (T1DM) has attracted considerable attention in the past decade. Patients with T1DM suffer from high levels of glucose concentration due to defective insulin secretion.

The lack of insulin is preventing glucose uptake and utilisation by cells.

Long-term high glucose concentration results in several health complications.

The most common intensified insulin therapy nowadays is based on manual exogenous insulin dosing to either keep the level of basal insulin or to suppress glycemic excursions after a meal. The patient needs to take several fingerstick blood glucose measurements a day and make decisions on insulin doses. A closed-loop blood glucose control would dramatically improve the life of T1DM subjects.

Despite the fast development of insulin pumps and continuous glucose measurement systems, a fully autonomous control of glycemia has not been introduced in a commercially available device yet.

The robust control theory is well established for linear systems but almost all real processes are more or less nonlinear. If the plant operating region is small, one can use the robust control approaches to design a linear robust controller where the nonlinearities are treated as model uncertainties. However, for real nonlinear processes, where the operating region is large, the above mentioned controller synthesis is inapplicable. For this reason the controller design for nonlinear systems is nowadays a very determinative and important field of research.

Gain-scheduling is one of the most common used controller design approaches for nonlinear systems and has a wide range of use in industrial applications. Many of the early articles were associated with flight control [1] and aerospace [2]. Then, gradually, this approach has been used almost everywhere in control engineering, which was greatly helped with the introduction of LPV systems. Linear parameter-varying (LPV) systems are time-varying plants whose state space matrices are fixed functions of some vector of varying parameters $\theta(t)$.

They were introduced first by Jeff S. Shamma in 1988 to model gain-scheduling. Today the LPV paradigm has become a standard formalism in systems and controls

with lot of researches and articles devoted to analysis, controller design and system identification of these models [3].

The main motivation of our paper were our previous results in gain-scheduling [4] - [8] and the results from T1DM research [9], [10] and [11]. In this paper a novel robust discrete gain-scheduling controller design for Bergman's minimal model of glucose-insulin dynamics coupled with insulin and carbohydrates absorption subsystems is proposed.

Our notations are standard, $D \in \mathbb{R}^{m\times n}$ denotes the set of real $m \times n$ matrices. I_m is an $m \times m$ identity matrix and Z_m denotes a zero matrix. If the size can be determined from the context, we will omit the subscript. $P > 0$ $(P \geq 0)$ is a real symmetric, positive definite (semidefinite) matrix.

Organisation of the paper is following. Section 2 includes problem formulation and some preliminaries are given. In Section 3 sufficient stability conditions in the form of BMI and/or LMI are given for the design of a robust discrete gain-scheduled controller. In Section 4 the obtained results are illustrated on the T1DM model.

II. Problem Formulation and Preliminaries

In this section we briefly describe the mathematical model of a T1DM subject, which was based on Bergman's minimal model of insulin-glucose interaction [12]. Later in this work the model will be used as a base for controller design and as a patient simulator for verification of the controller.

Our aim was to adjust the parameters of the proposed model so that the output of the model fits the continuous glucose monitoring (CGM) data of a particular T1DM subject. For identification of specific model parameters we used pharmacokinetics (PK) and pharmacodynamics (PD) measurements (as published in [13], [14]) of the particular insulin prescribed to the patient.

The information about ingested carbohydrates was also recorded during data acquisition.

II.1. T1DM Model

Bergman's minimal model consists of two differential equations in the form:

$$\dot{X}(t) = -p_2 X(t) + p_2 S_I \left(I(t) - I_b\right) \tag{1a}$$

$$\dot{G}(t) = -\left(S_G + X(t)\right)G(t) + S_G G_b + \left(\frac{1}{V_G}\right)R_a(t) \tag{1b}$$

where S_G [1/min] is the rate constant which gives the rate of change of glucose caused by deviation from the basal glucose concentration G_b [mg/dl], parameter S_I [ml/μU/min] is known as the insulin sensitivity index and p_2 [1/min] is a rate constant.

Parameter V_G [dl/kg] represents the glucose distribution volume per kilogram of body weight BW [kg]. $G(t)$ [mg/dl] is the blood glucose concentration and signal $X(t)$ [1/min] represents the insulin in remote compartment. Values I_b [μU/ml] and G_b [mg/dl] are the basal insulin concentration and the basal glucose concentration respectively. In a basal steady state we have $X(0) = 0$ and $G(0) = G_b$. Inputs of the model (1) are plasma insulin concentration $I(t)$ [μU/ml] and glucose rate of appearance $R_a(t)$ [mg/kg/min].

Signal $R_a(t)$ can have in general two sources – the absorption of glucose from gastro-intestinal tract (modeled as a subsystem) and direct intravenous glucose administration. Insulin absorption is modeled as a separate subsystem where the output is insulin concentration $I(t)$ [15], [16]. The subsystem has the form:

$$\dot{S}_1(t) = -\left(\frac{1}{T_I}\right)S_1(t) + v(t) \tag{2a}$$

$$\dot{S}_2(t) = -\left(\frac{1}{T_I}\right)S_2(t) + \left(\frac{1}{T_I}\right)S_1(t) \tag{2b}$$

$$\dot{I}(t) = -k_I I(t) + \left(\frac{1}{T_I}\right)\left(\frac{1}{V_I}\right)S_2(t) \tag{2c}$$

where parameter T_I [min] is a time constant of the subsystem, k_I [1/min] is a decay rate of insulin in plasma and parameter V_I [dl/kg] represents an insulin distribution volume per kilogram of body weight. Input $v(t)$ [μU/kg/min] is insulin subcutaneous infusion rate, $S_1(t)$ and $S_2(t)$ [μU/kg] represent the amount of insulin in compartments of the subsystem. Third subsystem describes the glucose absorption from gastrointestinal tract, i.e. output of the subsystem is the signal $R_a(t)$ [mg/kg/min]. The subsystem is described as follows:

$$\dot{D}(t) = -\left(\frac{1}{T_D}\right)D(t) + \left(\frac{1}{T_D}\right)A_G d(t) \tag{3a}$$

$$\dot{R}_a(t) = -\left(\frac{1}{T_D}\right)Ra(t) + \left(\frac{1}{T_D}\right)D(t) \tag{3b}$$

where parameter T_D [min] is a time constant and A_G [dimensionless] is a friction of ingested carbohydrates which are effectively absorbed.

Input $d(t)$ [mg/kg/min] is the rate of carbohydrate ingestion at meal time, i.e. signal $d(t)$ is an impulse with a width of one sampling period while the impulse area corresponds to the amount of ingested carbohydrates.

II.2. Identification of Model Parameters

For identification of model parameters we used data collected from a male T1DM subject aged 14, with

$BW = 64.6$ [kg] and using fast-acting insulin NovoRapid (insulin Aspart) from an insulin pump.

Insulin absorption subsystem

The first step in model identification was identifying of insulin absorption subsystem based on pharmacokinetics data of the used insulin.

PK data from [14] were used. An average basal insulin infusion rate v_b [μU/kg/min] of the subject during the day is known since data from insulin pump are available.

Signal $v(t)$ is a sum of bolus part $v_B(t)$ and basal part v_b. The aim is to identify the vector of unknown parameters $\Theta_1 = [T_I \quad k_I \quad V_I]$ so that the error between simulated insulin concentration $I(t)$ and PK data is minimized. In basal (steady) state for a given v_b we get the basal insulin concentration I_b as the output and $I(t)$ response after a bolus administration. We used the nonlinear least-squares optimization to identify the vector Θ_1.

Insulin sensitivity index and insulin action time

In the next step we identified the parameter related to insulin sensitivity S_I and insulin action time p_2.

These parameters determine dynamics of remote insulin signal $X(t)$. The measuring principle of pharmacodynamics is to maintain glycemia at basal concentration after bolus administration by intravenous glucose infusion. This glucose infusion corresponds to the signal $R_a(t)$ in the equation (1b).

If the Eq. (1b) is written in the form:

$$\dot{G}(t) = -S_G\left(G(t) - G_b\right) + \frac{1}{V_G}\left(Ra(t) - V_G X(t) G(t)\right) \quad (4)$$

and we measure the PK, i.e. $\dot{G}(t) = 0$, then $G(t) \approx G_b \; \forall \, t$. It is obvious that parameter S_G has minor influence in order to achieve $\dot{G}(t) = 0$, so we assume $S_G = 0$ during this step of parameter identification.

The aim is to identify vector of unknown parameters $\Theta_2 = [S_I \quad p_2]$ so that the error between $G(t)$ and G_b is minimized. Signal $R_a(t)$ is given by PD data.

Finalizing the model

At last, remaining parameters S_G and T_D are identified based on CGM data. The data containing both basal and bolus insulin dosing together with the amount of ingested carbohydrates were used as inputs to the model.

Now we are identifying a vector of unknown parameters $\Theta_3 = [S_G \quad T_D]$ so that the error between measured CGM data and the simulator output is minimized. Again, nonlinear least-square optimization was used. All identified parameters are reported in Table I. For the extended description of the identification process, please refer to our preliminary work [11].

TABLE I
T1DM IDENTIFIED MODEL PARAMTERS

T_I	k_I	V_I	S_I	p_2	S_G	T_D
44.55	0.1645	138.8	0.00159	0.0106	33.474	0.032

TABLE II
OTHER FIXED PARAMETERS OF THE MODEL

V_G	G_b	A_G
1.467	8.5	0.95

III. LPV-based Robust Gain-Scheduled Controller Design

In this section a new LPV model is presented on the base of the nonlinear Bergman's minimal model, which is then used to design a robust discrete LPV-based gain-scheduled controller for T1DM.

III.1. LPV Model of T1DM

The Bergman's model (1) with the insulin absorbation model (2) can be transformed to the following LPV model with substitutions $x_1(t) = G(t)$, $x_2(t) = X(t)$, $x_3(t) = S_1(t)$, $x_4(t) = S_2(t)$, $x_5(t) = I(t)$ and $u(t) = v(t)$:

$$\begin{aligned} \dot{x}(t) &= A(\theta)x(t) + Bu(t) + W(\theta) \\ y(t) &= Cx(t) \end{aligned} \quad (5)$$

where $\theta(t) \in \Omega$ is a vector of scheduled parameters and:

$$W(\theta) = \begin{bmatrix} p_1(\theta)G_b \\ -p_3(\theta)I_b \\ I \\ 0 \\ 0 \end{bmatrix}, B = \begin{bmatrix} 0 \\ 0 \\ 1 \\ 0 \\ 0 \end{bmatrix}, x = \begin{bmatrix} x_1 \\ x_2 \\ x_3 \\ x_4 \\ x_5 \end{bmatrix}$$

$$A(\theta) = \begin{bmatrix} -p_1(\theta) + b(\theta) & -a(\theta) & 0 & 0 & 0 \\ 0 & -p_2 & 0 & 0 & p_3(\theta) \\ 0 & 0 & -\frac{1}{T_i} & 0 & 0 \\ 0 & 0 & \frac{1}{T_i} & -\frac{1}{T_i} & 0 \\ 0 & 0 & 0 & \frac{1}{T_i V_i} & -k_i \end{bmatrix}$$

$$C = \begin{bmatrix} 1 & 0 & 0 & 0 & 0 \end{bmatrix}$$

furthermore:

$$p_1(\theta) = p_{10} + \sum_{i=1}^{p} p_{1i}\theta_i, \; p_3(\theta) = p_{30} + \sum_{i=1}^{p} p_{3i}\theta_i$$

$$a(\theta) = a_0 + \sum_{i=1}^{p} a_i\theta_i, \; b(\theta) = b_0 + \sum_{i=1}^{p} b_i\theta_i$$

The coefficient $a(\theta)$ is used to cover the nonlinear part of (1b) $X(t)G(t) \rightarrow x_1x_2$ in the following way:

$$a(\theta) = G(t) \Rightarrow a_0 + a_1\theta_1 = x_1 \Rightarrow a(\theta)x_2 = x_1x_2 \quad (6)$$

where $\theta_1(t) = \frac{y-a_0}{a_1}$. The coefficients a_0 and a_1 were calculated so as to maintain the scheduling parameter θ_1 in the range $\langle -1,1\rangle$:

$$a_0 = \frac{min(y) + max(y)}{2}, a_1 = \frac{min(y) - max(y)}{2} \quad (7)$$

Note, the coefficients $a_i, i = 2,3,4,5$ are equal to zero. Similarly, the coefficient $b(\theta)$ is calculated in the following way:

$$b(\theta)y = R_a(t) \Rightarrow b(\theta) = b_0 + b_2\theta_2 + b_3\theta_3 \quad (8)$$

where coefficients b_0 and b_2 are calculated so as to maintain the scheduling parameter θ_2 in the range $\langle -1,1\rangle$:

$$b_0 = \frac{min(R_a / y) + max(R_a / y)}{2}$$

$$b_2 = \frac{min(R_a / y) - max(R_a / y)}{2}, \ \theta_2 = \frac{\frac{R_a}{y} - b_0}{b_1}$$

Furthermore $b_3 = 5$ % of avarage $R_a(t)$ (uncertainty) and $b_i = 0, \ i = 1,4,5$ as well as $\theta_3(t) \in \langle -1,1\rangle$ is unknown but constant parameter describing uncertainty.

For parameters p_1 and p_3 we also considered an uncertainty ($\pm 5\%$):

$$p_1(\theta) = p_{10} + p_{14}\theta_4, \quad p_3(\theta) = p_{30} + p_{35}\theta_5 \quad (9)$$

where:
$p_{1_0} = p_1, p_{1_4} = 5$ % of $p_1, p_{3_0} = p_3, p_{3_5} = 5$ % of $p_3, p_{1_i} = 0, i = 1,2,3,5, p_{3_i} = 0, i = 1,2,3,4$ and $\theta_4, \theta_5 \in \langle -1,1\rangle$ are unknown but constant parameters.

For the robust discrete LPV-based gain-scheduling controller design the model (5) is transformed to discrete time-space and $W(\theta)$ is neglected, because has no effect on stability.

III.2. Robust Gain-Scheduled Controller Design

The output feedback gain-scheduled control law is considered for discrete-time PID (often denoted as PSD) controller in the form:

$$u(k) = K_P(\theta \mid k)e(k) + K_I(\theta \mid k)\sum_{i=0}^{k} e(i) + \\ + K_D(\theta \mid k)\big(e(k) - e(k-1)\big) \quad (10)$$

where $e(k) = y(k) - w(k)$ is control error, $w(k)$ is reference value and gain matrices $K_P(\cdot)$, $K_I(\cdot)$, $K_D(\cdot)$ are controller parameter matrices[1] (indexes P, I, D means proportional, sum (integral) and first difference (derivative), respectively) in the form:

$$K_P(\theta \mid k) = K_{P0} + \sum_{i=1}^{p} K_{Pi}\theta_i(k)$$

$$K_I(\theta \mid k) = K_{I0} + \sum_{i=1}^{p} K_{Ii}\theta_i(k)$$

$$K_D(\theta \mid k) = K_{D0} + \sum_{i=1}^{p} K_{Di}\theta_i(k)$$

Note that the number of controller gain matrices is only 2 (for θ_1 and θ_2), the rest 3 (uncertainty) is equal to zero. Because the reference signal $w(k)$ does not influence the closed-loop stability, we assume that it is equal to zero. For $w(k) = 0$, the control law (10) can be rewritten as:

$$u(k) = K_P(\theta \mid k)y(k) + K_I(\theta \mid k)\sum_{i=0}^{k} y(i) + \\ + K_D(\theta \mid k)\big(y(k) - y(k-1)\big) \quad (11)$$

State space description of PID controllers can be derived in the following way [17]. We can extend the system with two state variables $z(k) = [z_1^T(k), z_2^T(k)]^T$ where $z_1(k) = \sum_{i=0}^{k-2} y(i)$ and $z_2(k) = \sum_{i=0}^{k-1} y(i)$, then $y(k-1) = z_2(k) - z_1(k)$. Substituting to (11) one obtains:

$$u(k) = \big(K_P(\theta \mid k) + K_I(\theta \mid k) + K_D(\theta \mid k)\big)y(k) + \\ + K_I(\theta \mid k)z_2(k) - K_D(\theta \mid k)\big(z_2(k) - z_1(k)\big) \quad (12)$$

Control law (12) can be transformed to matrix form:

$$u(t) = F(\theta \mid k)\tilde{y}(k) \quad (13a)$$

where $\tilde{y} = \big[y(k), z_{1(k)}, z_{2(k)}\big]^T$ is the extended measurement output vector and:

$$F(\theta \mid k)^T = \begin{bmatrix} K_P(\theta \mid k) + K_I(\theta \mid k) + K_D(\theta \mid k) \\ K_D(\theta \mid k) \\ K_I(\theta \mid k) - K_D(\theta \mid k) \end{bmatrix} \quad (13b)$$

Substituting the control law (13a) to the discrete uncertain LPV system the closed-loop system is obtained in the form:

$$\tilde{x}(k+1) = A_c(\theta \mid k)\tilde{x}(k) \quad (14)$$

[1]For SISO systems they are scalars.

where:

$$\tilde{x}(k) = [x(k), z_1(k), z_2(k)]^T$$
$$A_c(\theta|k) = A_r(\theta|k) + B_r(\theta|k)F(\theta|k)\, C_r(\theta|k)$$

and:

$$A_r(\theta|k) = \begin{bmatrix} A(\theta|k) & 0 & 0 \\ 0 & 0 & I \\ C & 0 & I \end{bmatrix},\ B_r(\theta|k) = \begin{bmatrix} B(\theta|k) \\ 0 \\ 0 \end{bmatrix}$$
$$C_r(\theta|k) = \begin{bmatrix} C & 0 & 0 \\ 0 & I & 0 \\ 0 & 0 & I \end{bmatrix}$$

Remark 1. The controller's filter of the derivative (differential) part can be included in the system model.

To access the performance quality a quadratic cost function [18] known from LQ theory is used in this paper, where weighting matrices depends on scheduling parameters [19]. Using this approach we can affect performance quality in each operating point separately.

The quadratic cost function is then in the form:

$$J_{df}(\theta) = \sum_{k=0}^{\infty} \tilde{x}(k)^T Q(\theta|k)\tilde{x}(k) + u(k)^T Ru(k) = \sum_{k=0}^{\infty} J_d(\theta|k) \quad (15)$$

where $Q(\theta|k) = Q_0 + \sum_{i=1}^{p} Q_i\theta_i$, $Q_i = Q_i^T \geq 0$, $Q_0, Q_i \in \mathbb{R}^{n\times n}$, $R \in \mathbb{R}^{m\times m}$ are symmetric positive definite (semidefinite) and definite matrices, respectively. The concept of guaranteed cost control is used in a standard way.

Definition 1. Consider the system (5) with control algorithm (10). If there exists a control law u^* and a positive scalar J^* such that the closed-loop system (14) is stable and the value of closed-loop cost function (15) satisfies $J \leq J^*$ then J^* is said to be a guaranteed cost and u^* guaranteed cost control law for system (5).

Substituting the control law (12) to the quadratic cost function (15) we can obtain:

$$J_d(\theta|k) = \tilde{x}^T\left(Q(\theta|k) + C^T F(\theta|k)^T RF(\theta|k)C\right) \quad (16)$$

Definition 2. [20] The linear closed-loop system (14) for $\theta \in \Omega$ is quadratically stable if and only if there exist a symmetric positive definite matrix $P > 0$ and for the first difference of Lyapunov function $V(k) = x^T Px$ along the trajectory of closed-loop system (14) holds:

$$\Delta V(\theta|k) = A_c(\theta|k)^T PA_c(\theta|k) + P < 0 \quad (17)$$

From LQ theory we introduce the well known results.

Lemma 1. [21] Consider the closed-loop system (14). Closed-loop system (14) is quadratically stable with guaranteed cost if and only if the following inequality holds:

$$B_e = min_u\left\{\Delta V(\theta|k) + J_d(\theta|k)\right\} \leq 0 \quad (18)$$

for all $\theta(k) \in \Omega$. The main result of this section, the robust discrete gain-scheduled controller design procedure, relies on the concept of multi-convexity, that is, convexity along each direction θ_i of the parameter space. The implications of multiconvexity for scalar quadratic functions are given in the next lemma [22].

Lemma 2. Consider a scalar quadratic function of $\theta \in \mathbb{R}^p$:

$$f(\theta_1,\ldots,\theta_p) = a_0 + \sum_{i=1}^{p} a_i\theta_i + \sum_{i=1}^{p}\sum_{j>i}^{p} b_{ij}\theta_i\theta_j + \sum_{i=1}^{p} c_i\theta_i^2$$

and assume that $f(\theta_1, \ldots, \theta_p)$ is multi-convex, that is $\frac{\partial^2 f(\theta)}{\partial\theta_i^2} = 2\,c_i \geq 0$ for $i = 1,2,\ldots,p$. Then $f(\theta)$ is negative for all $\theta \in \Omega$ if and only if it takes negative values at the corners of θ. Using *Lemma 1* and *2* the following theorem is obtained.

Theorem 1. Closed-loop system (14) is quadratically stable with guaranteed cost if a positive defined $P > 0$ for all $\theta(k) \in \Omega$ exists, matrices $Q_i, R, i = 1,2,\ldots p$ and gain-scheduled controller matrices $F(\theta(k))$ satisfy:

$$M(\theta(k)) < 0;\quad \theta(k) \in \Omega \quad (19)$$

$$M_{ii} \geq 0;\quad i = 1,2,\ldots p \quad (20)$$

where:

$$M(\theta) = M_0 + \sum_{i=1}^{p} M_i\theta_i + \sum_{i=1}^{p}\sum_{j>i}^{p} M_{ij}\theta_i\theta_j + \sum_{i=1}^{p} M_{ii}\theta_i^2 \quad (21)$$

furthermore:

$$M_0 = \begin{bmatrix} -P + Q_0 & C^T F_0^T & Ac_0^T \\ F_0 C & -R^{-1} & 0 \\ Ac_0 & 0 & -P^{-1} \end{bmatrix}$$
$$M_i = \begin{bmatrix} Q_i & C^T F_i^T & Ac_i^T \\ F_i C & 0 & 0 \\ Ac_i & 0 & 0 \end{bmatrix}$$
$$M_{ij} = \begin{bmatrix} 0 & 0 & Ac_{ij}^T \\ 0 & 0 & 0 \\ Ac_{ij} & 0 & 0 \end{bmatrix}, M_{ii} = \begin{bmatrix} 0 & 0 & Ac_{ii}^T \\ 0 & 0 & 0 \\ Ac_{ii} & 0 & 0 \end{bmatrix}$$

$$
\begin{aligned}
Ac_0 &= A_{r0} + B_{r0}F_0C_r \\
Ac_i &= A_{ri} + B_{ri}F_0C_r + B_{r0}F_iC_r \\
Ac_{ij} &= B_{ri}F_jC_r + B_{rj}FiC_r \\
Ac_{ij} &= B_{ri}F_jC_r + B_{rj}FiC_r \\
Ac_{ii} &= B_{ri}F_iC_r
\end{aligned}
$$

Proof. Proof is based on *Lemma 1* and *2*. From (18) we can obtain:

$$
\begin{aligned}
M\left(\theta(k)\right) = A_c\left(\theta(k)\right)^T PA_c\left(\theta(k)\right) + P + \\
+ Q + C^T F\left(\theta(k)\right)^T RF\left(\theta(k)\right)C < 0
\end{aligned} \tag{22}
$$

Using Schur complement we obtain:

$$
M\left(\theta(k)\right) = \begin{bmatrix} W_{11} & W_{21}^T & W_{31}^T \\ W_{21} & W_{22} & W_{32}^T \\ W_{31} & W_{32} & W_{33} \end{bmatrix} < 0 \tag{23}
$$

where:

$$
\begin{aligned}
W_{11} &= -P + Q\left(\theta(k)\right) & W_{22} &= -R^{-1} \\
W_{21} &= F\left(\theta(k)\right)C & W_{32} &= 0 \\
W_{31} &= Ac\left(\theta(k)\right) & W_{33} &= -P^{-1}
\end{aligned}
$$

After we extend (23) to affine form we obtain (19) and (20) which proofs the *Theorem 1*. Note that *Theorem 1* in its presented form is in the form of BMI. One can use a free and open source BMI solver *PENLAB* or we can linearize the nonlinear part of (19) to use LMI solver (*LMILAB* or *SEDUMI*):

$$
lin\left(-P^{-1}\right) \le X^{-1}\left(P - X\right)X^{-1} - X^{-1} \tag{24}
$$

where in each iteration pores $X = P$. Using this linearization, the element obtaining the nonlinear part (M_0) become as follows:

$$
M_0 = \begin{bmatrix} -P + Q_0 & C^T F_0^T & Ac_0^T \\ F_0C & -R^{-1} & 0 \\ Ac_0 & 0 & X^{-1}(P - X)X^{-1} - X^{-1} \end{bmatrix}
$$

IV. Simulation Experiments

In this section the proposed robust discrete gain-scheduled controller is verified using the individualized T1DM Bergman's model served as a patient.

For controller synthesis the LPV model described in section 3.1 with parameters presented in section 2.2, transformed to discrete time-space with sample time T_s = 5 [min] was used. The response of Bergman's model with the discrete LPV model to an insulin bolus is shown in Fig. 1.

The disturbance has been considered in the form of mixed meal ingestion. The main objective was to keep the blood glucose concentration levels within normal glycemic range (3.8 - 10 [mmol/l]).

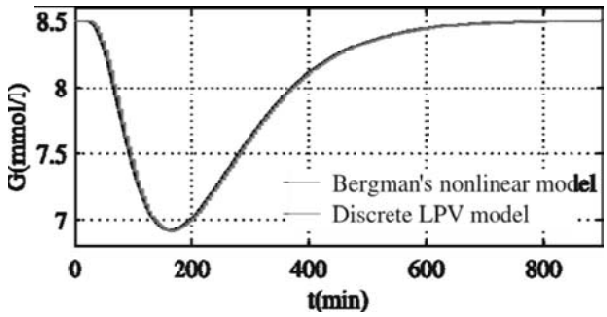

Fig. 1. Bergman's model with the discrete LPV model

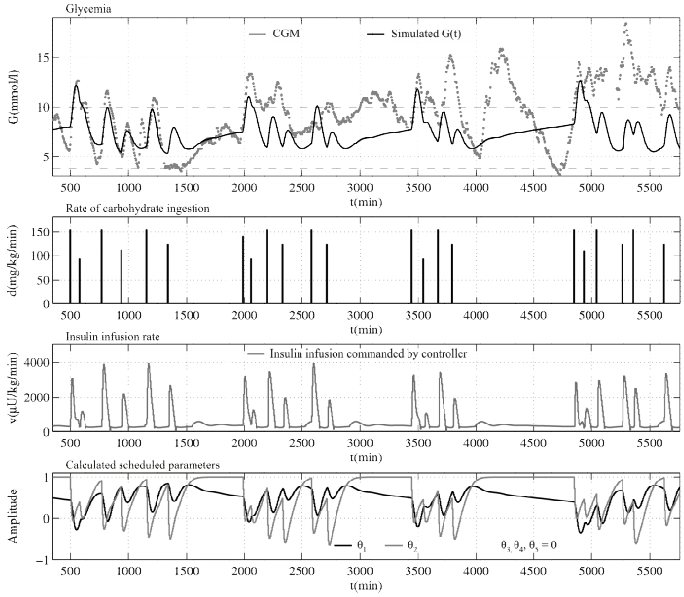

Fig. 2. Simulation results for time period of 4 days

The obtained model was extended for robust discrete gain-scheduled PID controller design (14).

Then using *Theorem 1* with weighting matrices $Q = q_i\, I$, $q_0 = 1 \times 10^{-5}$, $q_1 = 1 \times 10^{-1}$, $q_2 = 1 \times 10^{-2}$, $q_3 = q_4 = q_5 = 0$, $R = r\, I$, $r = 1$ and $\xi_U \leq P(\theta) \leq \xi_L$, $\xi_U = 1 \times 10^{8}$, $\xi_L = 1 \times 10^{-5}$, $T_s = 5$ [min] with *LMILAB* one can obtain robust discrete gain-scheduled controller in the form (10) where:

$$\begin{aligned} K_p(\theta) &= -101.1243 - 250.7895\theta_1 + 239.9897\theta_2 \\ K_i(\theta) &= -5.1342\times10^{-8} - 1.2379\times10^{-7}\theta_1 \\ &\quad -1.0598\times10^{-5}\theta_2 \\ K_d(\theta) &= -1012.1475 - 5998.7879\theta_1 + 0.1235\theta_2 \end{aligned}$$

For the illustration propose simulation experiment results are shown in Fig. 2.

During manual administration of insulin by the T1DM subject, the measured glycemia has been higher than 10 [mmol/l] during 45 % of the monitored time. In the case of automatic dosing controlled by the proposed gain-scheduled algorithm, the time when glycemia reached the level of 10 [mmol/l] or more was reduced to 9.9 % of the simulation time.

V. Conclusion

The robust discrete gain-scheduled controller design for Bergman's minimal model of glucose-insulin dynamics coupled with insulin absorption subsystem and carbohydrates absorption subsystem was proposed in this paper. In contrast to publications in literature we presented a completely new LPV description of Bergman's minimal model and a new approach to controller design. The obtained design procedure can be used in systems where we need to save the operation energy (e.g. low-cost micro-controllers).

The presented theory opens new possibilities for further research and study in this area.

Acknowledgements

The work has been supported by the Slovak Scientific Grant Agency VEGA, Grant No. 1/1241/12 and Grant No. 1/2256/12. The paper is one of the outcomes of the research work for the project entitled "Research center for severe diseases and related complications", "ITMS: 26240120038". "This project is being co-financed by the European Union. We support research activities in Slovakia".

References

[1] R.J. Adams, A. G. Sparks, S.S. Banda, A gain scheduled multivariable design for a manual light control system. *IEEE Conference on Control Applications, Vol. 1, pp. 584-589, 1992.*

[2] R.A. Hyde, K. Glover, The application of scheduled h_1 controllers to a VSTOL aircraft, *IEEE Transactions on Automatic Control, Vol. 38(*Issue 7*):1021-1039, 1993.*

[3] J. S. Shamma, Control of Linear Parameter Varying Systems with Applications, chapter An Overview of LPV Systems (Springer, 2012, pp. 3-26).

[4] V. Veselý, A. Ilka, Gain-scheduled PID controller design, *Journal of Process Control, Vol. 23(*Issue 8*)*:1141-1148, *September 2013.*

[5] A. Ilka, V, Veselý, Discrete Gain-Scheduled Controller Design: Variable Weighting Approach, *International Carpathian Control Conference (ICCC), Vol. 15, pp. 186-191, May 2014.*

[6] V. Veselý, A. Ilka, PID robust gain-scheduled controller design, *European Control Conference (ECC), pp. 2756-2761, June 2014.*

[7] J. Osuský, V. Veselý, Robust Gain Scheduling Control Design in Frequency Domain, *International Review of Automatic Control (IREACO), Vol. 7(*Issue 5*): 476-484, 2014.*

[8] D. Vozák, V. Veselý, Stable Predictive Control with Input Constraints Based on Variable Gain Approach, *International Review of Automatic Control (IREACO), Vol. 7(*Issue 2*): 131-139, 2014.*

[9] M. Tárník, J. Murgaš, E. Miklovičová, Ľ. Farkas, Adaptive control of time-delayed systems with application for control of glucose concentration in type 1 diabetic patients, *IFAC International Workshop on Adaptation and Learning in Control and Signal Processing, Vol. 11, Caen, France, July 3-5, 2013.*

[10] M. Tárník, E. Miklovičová, J. Murgaš, I. Ottinger, T. Ludwig, Model reference adaptive control of glucose in type 1 diabetics: A simulation study. *IFAC World Congress, Vol. 19, Cape Town International Convention Centre, Cape Town, South Africa, 2014.*

[11] I. Ottinger, T. Ludwig, E. Miklovičová, V. Bátora, J. Murgaš, M. Tárník, Individualized T1DM simulator for verification of adaptive controller. Accepted on *International Conference on Process Control, Vol. 20, June 9-12, 2015.*

[12] R.N. Bergman, Y.Z. Ider, C.R. Bowden, C. Cobelli, Quantitative estimation of insulin sensitivity, *Am. J. Physiol. Endocrinol. Metab. Vol. 236(*Issue 6*):E667-E677, 1979.*

[13] Novo-Nordisk, NovoRapid (insulin aspart) - Product Monograph, *Watermeadow Medical, Two Rivers House, Station Lane, Witney, Oxfordshire OX28 4BH, UK on behalf of Novo Nordisk A/S, 2002.*

[14] S.R. Mudaliar, F. A. Lindberg, M. Joyce, P. Beerdsen, P. Strange, A. Lin, R. R. Henry, Insulin aspart (b28 asp-insulin): A fast-acting analog of human insulin. *Diabetes Care, Vol. 22(*Issue 9*):1501-1506, September 1999.*

[15] P. Herrero, P. Georgiou, N. Oliver, M. Reddy, D. Johnston, Ch. Toumazou, A composite model of glucagon-glucose dynamics for in silico testing of bihormonal glucose controllers. *Journal of Diabetes Science and Technology, Vol. 7(*Issue 4*):941-951, July 2013.*

[16] R. Hovorka, V. Canonico, L. J. Chassin, U. Haueter, M. Massi-Benedetti, M. O. Federici, T. R. Pieber, H. C. Schaller, L. Schaupp, T. Vering, M. E. Wilinska, Nonlinear model predictive control of glucose concentration in subjects with type 1 diabetes. *Physiological Measurement, Vol. 25(*Issue 4*):905-913, 2004.*

[17] V. Veselý, D. Rosinová, Robust PID-PSD Controller Design: BMI Approach, *Asian Journal of Control, Vol. 15(*Issue 2*):469-478, 2013.*

[18] J. Engwerda, A. Weeren, A result on output feedback linear quadratic control, *Automatica, Vol. 44(*Issue 1*):265-271, 2008.*

[19] A. Ilka, V. Veselý, Gain-Scheduled Controller Design: Variable Weighting Approach, *Journal of Electrical Engineering, Vol. 65(*Issue 2*):116-120, March-April 2014.*

[20] P. Apkarian, P. Gahinet, G. Becker, Self-Scheduled H_1 Control of Linear Parameter-Varying Systems: A Design Example. *Automatica, Vol. 31(*Issue 9*):1251-1261, 1995.*

[21] V.M. Kuncevič, M.M. Lyčak, *Control system design using Lyapunov function approach* (Nauka, Moskva, 1977, in Russian).

[22] P. Gahinet, P. Apkarian, M. Chilali, Affine parameter-dependent Lyapunov functions and real parametric uncertainty, *IEEE Transactions on Automatic Control, Vol. 41(*Issue 3*):436-442, March, 1996.*

Authors' information

Institute of Robotics and Cybernetics, Faculty of Electrical Engineering and Information Technology, Slovak University of Technology in

Bratislava, Ilkovičova 3, 812 19 Bratislava, Slovak Republic.
E-mail: adrian.ilka@stuba.sk

Adrian Ilka (MSc.) was born in Dunajská Streda, Slovakia in 1987. He received BSc degree from the Faculty of Electrical Engineering and Information Technology, Slovak University of Technology in Bratislava in 2010 and MSc degree in technical cybernetics in 2012. Since 2012 until now he has pursued further studies to get his PhD. He is interested in optimal control, power system control, robust control, Lyapunov theory of stability, linear matrix inequalities and gain-scheduled control.

Ivan Ottinger (MSc.), born in 1987, graduated in robotics and cybernetics in 2012 form the Faculty of Electrical Engineering, Slovak University of Technology in Bratislava. He is currently a postgraduate student focused on bio cybernetics with the specialization in adaptive control.

Tomáš Ludwig (MSc.), born in 1988, graduated in robotics and cybernetics in 2012 form the Faculty of Electrical Engineering, Slovak University of Technology in Bratislava. He is currently a postgraduate student focused on bio cybernetics with the specialization in modeling diabetes.

Marián Tárník (MSc. PhD.) was born in Levice, Slovakia in 1986. He received Bachelor of Science degree from the Faculty of Electrical Engineering and Information Technology, Slovak University of Technology in Bratislava in 2008, Master of Science degree in technical cybernetics in 2010 and PhD. degree in 2013 at the same place where he is from 2013 until now doing further research as a researcher. He is interested in Adaptive Control, Lyapunov design approach and modeling and control of type one diabetes mellitus.

Vojtech Veselý (Prof. MSc. DSc.) was born in Veľké Kapušany, Slovakia in 1940. He received MSc degree in Electrical Engineering from the Leningrad Electrical Engineering Institute, St. Petersburg, Russia, in 1964, PhD and DSc degrees from the Slovak University of Technology, Bratislava, Slovak Republic, in 1971 and 1985, respectively. Since 1964 he has been with the Department of Automatic Control Systems, STU FEI in Bratislava. Since 1986 he has been a full professor. His research interests include the areas of power system control, decentralized control of large-scale systems, robust control, predictive control and optimization. He is author or coauthor of more than 300 scientific papers.

Eva Miklovičová (Assoc Prof. MSc. PhD.) obtained the MSc. in 1990 and the PhD. in Automation in 1997, both from the Slovak University of Technology in Bratislava. Currently she is with the Institute of Robotics and Cybernetics at the Faculty of Electrical Engineering and Information Technology, STU in Bratislava. Her research interests include predictive control, adaptive control, system modeling and identification.

Ján Murgaš (Prof. MSc. PhD.), born in 1951, graduated in control engineering in 1975 and received the PhD degree in 1980 form the Faculty of Electrical Engineering, Slovak University of Technology in Bratislava. Since 1996 he has been Full Professor for control engineering. His research interests include adaptive and non-linear control, large-scale systems. He is a member of the IEEE, of the American Mathematical Society and of the Slovak Society for Cybernetics and Informatics.

Praise Worthy Prize

International Review of Automatic Control (I.RE.A.CO.), Vol. 8, N. 2
ISSN 1974-6059 *March 2015*

Challenges in Model Predictive Control Application for Transient Stability Improvement Using TCSC

S. Kulkarni, S. Wagh, N. Singh

Abstract – *Performance of a system is always dominated by constraints rather than dynamics. Conventional controllers determine off-line, a feedback policy that provides optimal control action based on minimization of one or more cost functions with or without constraints using linear or nonlinear model of the system. Increased system complexity and demanding performance requirements have rendered classical control laws inadequate in spite of their simplicity as in case of PID loop or robustness in case of H_2 or H_∞ control designs.*
The only generic control that can meet these challenges is Model Predictive Control (MPC). The most challenging MPC application would be maintaining stability after large disturbances in highly nonlinear, complex and hybrid system such as power system. The practical difficulties are due to large system having strong interactions in various parameters with hard constraints. The paper discusses various issues in tuning and maintaining constraints on states and control variables for a Single Machine Infinite Bus (SMIB) system using Thyristor Controlled Series Compensator (TCSC) as a controller.

Keywords: *Constrained Model Predictive Control, DAE Model, SMIB, TCSC, Transient Stability*

Nomenclature

A, B, C	System, input, output matrices respectively
k	Current time instant
$\hat{x}(k+1)$	Vector of predicted state variables at the next sampling instant
$\hat{u}(k)$	Vector of predicted control variables at the current sampling instant
N_P	Length of prediction horizon
N_C	Length of control horizon
J_K	Objective function
Y	Vector of output variables
Q, R	Weighting matrices for state and control respectively (Tuning parameters)
E, F, G	Constraint matrices corresponding to change in control input, magnitude of control input and output parameter to be controlled respectively
y_{ref}	Reference trajectory of output variables
δ	Rotor angle
x_{tcsc}	TCSC reactance

I. Introduction

Appreciating constraints handling strengths of MPC which is not just cutting off inputs at boundaries but also a control law generation using online optimization, performed over a finite horizon, has resulted in tremendous popularity of MPC applications, ranging from slow process industries to fast aerospace dynamics replacing a traditional fixed control.

Since 1970 various versions of MPC have evolved such as, Model Predictive Heuristic Control (MPHC) [1], Model Algorithmic Control (MAC) or Dynamic Matrix Control (DMC) [2], Quadratic Dynamic Matrix Control (QDMC) [3] etc.

Initially, MPC was targeted to applications such as petroleum refineries, chemical industries where the data could be made available easily from the plant located at one place. In addition, the processes being slow, the required control update rates were low which could easily afford long computation time required for on-line calculation of control. However, with the fast development in digital processors, computation time reduced tremendously, as a result of which MPC is now found everywhere including applications in communication.

Around 1990 linear MPC reached sufficient maturity with respect to modeling, identification and issues like stability and robustness. For the systems that are inherently nonlinear, linear models were not found to describe system dynamics adequately which led to the need of nonlinear models. This motivated control engineers towards Nonlinear MPC (NMPC). In fact, the most challenging MPC application would be maintaining stability after large disturbances in highly nonlinear, complex and hybrid system such as power system.

In literature, power system related applications of MPC include mainly voltage stability issues [4], formulation of a minimization problem with boundary values for obtaining critical conditions such as Critical Clearing Time (CCT), for transient stability [5], HVDC

power flow modulation to improve transient stability [6], a flatness based TCSC for transient stability enhancement [7], [14], MPC using trajectory sensitivity for voltage recovery [8], [9], trajectory sensitivity analysis for effective choice of TCSC location, along with effect of variation of firing angle for transient stability assessment [10], to name a few.

However, in most of the applications either a classical model is used to represent the power system which fails to replicate the real power system, or a simplified version of MPC is implemented to limit the computational burden by restricting number of control moves while formulating the optimization problem. In [11] MPC was implemented to control the reactance of TCSC which in turn controlled the rotor angle delta, where a power system model was represented by taking into account a fifth order generator dynamics, exciter with saturation and governor dynamics.

Although, MPC strategy was implemented for a tenth order power system model, major strength of MPC of handling constraints was not appreciated in the paper.

In view of this, present paper describes systematic development of MPC with constraints on state and input variables for improving transient stability of power system using detailed DAE model, focusing on constraint handling issues involved.

The paper is organized as follows: Section II explains detailed procedure of general MPC formulation and applies it to SMIB while third Section elaborates objective function formulation. Fourth Section describes difficulties involved in defining reference trajectories.

Fifth Section describes constraint handling, followed by analysis supported by case-study simulations performed on representative SMIB using MATLAB in Section VI.

Last section concludes with contribution and outcome of the paper.

II. Constrained MPC Formulation for SMIB

To explain the MPC problem formulation in detail for power system application, a simple SMIB as shown in Fig. 1 is considered. As given in [11] a nonlinear detailed Differential Algebraic Equations (DAE) model of the power system is obtained considering the rotor swing, rotor flux, and exciter with saturation, prime mover and governor dynamics.

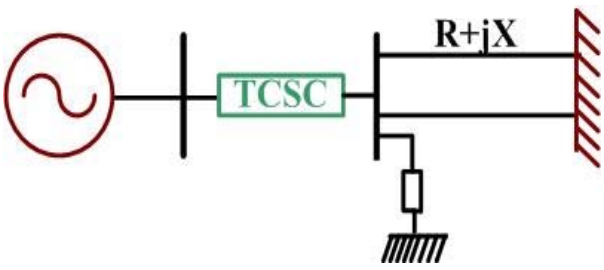

Fig. 1. Single Machine Infinite Bus System

For a discrete time setting requirement of MPC the nonlinear model is linearized, a general form of which is given as [13]:

$$x(k+1) = Ax(k) + Bu(k) \tag{1}$$

If all the states of the system are assumed to be measurable, then predicted values of the states at the next sampling instant are shown as $\hat{x}(k+1)$ instead of $x(k+1)$. When the future trajectory is predicted at the present sampling instant$k$, the present control input is still unknown, represented a s$\hat{u}(k)$. This modifies (1)to:

$$\hat{x}(k+1) = Ax(k) + B\hat{u}(k) \tag{2}$$

Using the outputs in the past, i.e. $y(k-1), y(k-2), \ldots$,control function in the past, i.e.$u(k-1), u(k-2), \ldots$, and using the explicit proper model of the system, control input in the future including that at the present time instant is predicted. Input control trajectory is assumed to vary over a finite horizon called control horizonN_c, and remains constant thereafter. By iterating (2) over a finite prediction horizon N_p, (3) is obtained:

$$\begin{bmatrix} \hat{x}(k+1|k) \\ \vdots \\ \hat{x}(k+N_p|1) \end{bmatrix} = \underbrace{\underbrace{\begin{bmatrix} A \\ \vdots \\ A^{N_p} \end{bmatrix}}_{\Phi} x(k) + \underbrace{\begin{bmatrix} B \\ \vdots \\ \sum_{i=0}^{N_p-1} A^i B \end{bmatrix}}_{\Gamma} u(k-1)}_{past} + \underbrace{\underbrace{\begin{bmatrix} B & \ldots & 0 \\ B+AB & B & 0 \\ \sum_{i=0}^{N_p-1} A^i B & \ldots & \sum_{i=0}^{N_p-N_c} A^i B \end{bmatrix}}_{G_y} \begin{bmatrix} \Delta\hat{u}(k|k) \\ \vdots \\ \Delta\hat{u}(k+N_c-1|k) \end{bmatrix}}_{future} \tag{3}$$

where, Φ, Γ and G_y are suitable matrices.

III. Objective Function Formulation of SMIB

MPC problem is thus formulated as solving on-line, a finite horizon open loop optimal control problem, subject to quadratic cost function and constraints in the form of linear inequalities [12]. A cost function Jpenalizes deviations of the predicted controlled outputs $y(k+j|k)$ from a reference trajectory $y_{ref}(k+j|k)$. Defining the objective function as::

$$J_k(x(k), u) = \sum_{j=1}^{N_p} \| y(k+j|k) - y_{ref}(k+j|k) \|^2_{Q(j)} + \sum_{j=0}^{N_c-1} \| \Delta u(k+j|k) \|^2_{R(j)} \tag{4}$$

Subject to element wise constraints:

$$y_{min} \leq y(k+j|k) \leq y_{max} \text{ for } j = 1, \dots, N_p \quad (5)$$

$$u_{min} \leq u(k+j|k) \leq u_{max} \text{ for } j = 0,., N_c - 1 \quad (6)$$

$$\Delta u_{min} \leq \Delta u(k+j|k) \leq \Delta u_{max} \text{ for } j = 0,., N_c - 1 \quad (7)$$

It should be noted that cost function penalizes rates of input vector, Δu , and not its value,u. Simplified form of the cost function (4) is:

$$J_k = \| Y(k) - Y_{ref}(k) \|_Q^2 + |\Delta U(k)|_R^2 \quad (8)$$

It is assumed that $N_c < N_p$, and $\Delta u(k+j|k) = 0$ for $j > N_c$ so that $u(k+j|k) = u(k+N_c-1|k)$ for $j \geq N_c$which means that zero order hold is applied on the input for $j > N_c$. The weighting matrices Q and R are given by:

$$Q = \underbrace{\begin{bmatrix} Q(1) & 0 & \dots & 0 \\ 0 & Q(2) & \dots & 0 \\ \vdots & \vdots & \ddots & \vdots \\ 0 & 0 & \dots & Q(N_p) \end{bmatrix}}_{(n \times N_p) \times (n \times N_p)} \quad (9)$$

$$R = \underbrace{\begin{bmatrix} R(0) & 0 & \dots & 0 \\ 0 & R(1) & \dots & 0 \\ \vdots & \vdots & \ddots & \vdots \\ 0 & 0 & \dots & R(N_c-1) \end{bmatrix}}_{(r \times N_c) \times (r \times N_c)} \quad (10)$$

The form of cost function (8) indicates that the error vector $(Y(k+j|k) - Y_{ref}(k+j|k))$ is penalized at every point in the prediction horizon if $Q(j) > 0$, which is the most common situation in prediction control.

However, it is possible to penalize the error at only a few coincidence points, by setting $Q(j) \neq 0$ for those points [5]. It is also possible to have different coincidence points for different components of error vector by setting the appropriate elements of weighting matrices to zero ($Q(j) = 0$). Thus, instead of $Q(j) > 0$, a slightly weaker condition $Q(j) \geq 0$ may be allowed to ensure$J(k) \geq 0$. Moreover, $R(j) \geq 0$ is needed to get $j(K) > 0$. A more strict condition i. e. $R(j) > 0$ is not required because there are cases in which the changes in the control signal are not penalized. $R(j)$ are called as Move Suppression Factors (MSF), since increasing them penalizes changes in the input vector more heavily.

It is also observed that cost function penalizes the rates of inputs and not the mere values [13].

$N_p, N_c, Q(j), R(j)$, and the reference trajectory $y_{ref}(k+j)$ affect the behavior of closed loop system with predictive controller.

Weights may be dictated by economic objectives of the control system but usually they are tuning parameters adjusted to give satisfactory dynamic performance.

With the output trajectory:

$$y(k+i|k) = Cx(k+i|k) \quad (11)$$

the compact form (3) becomes:

$$Y(k) = \Phi X(k) + \Gamma\, u(k-1) + G_y \Delta U(k) \quad (12)$$

The error between $Y(k)$ and $Y_{ref}(k)$ is called as tracking error, which is the difference between future target trajectory and free responses of the system:

$$E(k) = Y_{ref}(k) - \Phi X(k) - \Gamma u(k-1) \quad (13)$$

Free responses are those that would occur over the prediction horizon if no input changes were made ($\Delta U(k) = 0$). If the error $E(k)$ is zero then it would be correct to set $\Delta U(k) = 0$. (No change in input is required because the error is zero):

$$\begin{gathered} Y(k) - Y_{ref}(k) = \Phi X(k) + \Gamma u(k-1) + \\ + G_y \Delta U(k) - \big(E(k) + \Phi X(k) + \Gamma u(k-1)\big) = \\ = G_y \Delta U(k) - E(k) \end{gathered} \quad (14)$$

Rewriting the objective function as:

$$J_k = \| G_y \Delta U(k) - E(k) \|_Q^2 + \| \Delta U(k) \|_R^2 \quad (15)$$

Expanding the norms:

$$\begin{gathered} J_k = \big[\Delta U^T(k) G_y^T - E^T(k)\big] Q \big[G_y \Delta U(k) - E(k)\big] \\ + \Delta U^T(k) R \Delta U(k) \end{gathered} \quad (16)$$

This is further expanded as:

$$\begin{gathered} J_k = \Delta U^T(k) G_y^T Q G_y \Delta U(k) - \Delta U^T(k) G_y^T Q E(k) + \\ - E^T(k) Q G_y \Delta U(k) + E^T(k) Q E(k) + \\ + \Delta U^T(k) R \Delta U(k) \Delta U^T(k) \big[G_y^T Q G_y + R\big] \Delta U(k) + \\ - 2E^T(k) Q G_y \Delta U(k) \end{gathered} \quad (17)$$

This has the quadratic form:

$$J_k = \frac{1}{2} \Delta U^T(k) H \Delta U(k) + f^T \Delta U(k) + constant \quad (18)$$

where:

$$H = 2(G_y^T Q G_y + R) \quad (19)$$

and:

$$f = -2 G_y^T Q E(k) \quad (20)$$

H and f are independent of $\Delta U(k)$.

IV. Formation of Reference Trajectory

In the formulation of (MPC) optimization problem, formation of reference trajectory plays an important role.

The reference trajectory depends upon measurements $y(k)$ available up to present sampling instant k.

If the future evolution of the reference is known apriori, the system can react before the change actually happens, thereby reducing the effects of delays.

Appropriate selection of reference trajectory allows a shorter prediction horizon [12], saving in computation burden and computation time which is a prime requirement of real time controllers. The formation of reference trajectory issue in power systems is altogether different from process industry applications where, reference may be simply a constant or a fixed trajectory.

For a power system, defining an appropriate reference trajectory is a challenge. For example, for power system dynamics represented by second order classical, the reference trajectory is formed with two variables such as rotor angle and rotor speed. However, for acceptable operation of power system from practical constraints point of view, it is impossible to force rotor angle and/or speed to one fixed value and any value in given tolerance band is acceptable.

The problem becomes more complicated if the power system scenario changes in post-disturbance from that of pre-disturbance conditions. Whenever a fault occurs on a transmission line or generator, every time it may not be possible to clear fault immediately and power system may have to face forced generator or transmission line outage. In such circumstances, with changed system topology, stable power system operation may be possible at a new operating point different from that at the pre-disturbance conditions. As the type of disturbance and its location is never known in advance, prediction of such post-disturbance topology and new reference trajectories is challenging. If the power system dynamics is represented by higher order model, then the number of reference trajectories will grow in proportion.

The problem of reference trajectory formation for (SMIB) could be simplified by assumption of system having same operating power system scenario as that of pre-disturbance. However, even with this assumption, the reference trajectory formation for (MMPS) is challenging because rotor angle stability concept is totally different in (MMPS). As compared to (SMIB), (MMPS) will have to satisfy the condition of maintaining synchronism in addition to maximum allowable rotor angle swing.

For a (MMPS), the reference trajectory for rotor angle of every generator needs to be formed for relative rotor angle deviation with respect to the reference generator.

For (MMPS), the problem size will grow with complexity and dimension of the power system and also with the lengths of prediction and control horizon.

Since the time and location of the fault is not known a priory, it is challenging to find reference trajectories in a (MMPS) for real time controller.

V. Handling Constraints

Having formed the objective function and reference trajectory, the next important step is constraint formulation.

The constraints in the form of linear inequalities could be on the rates of control signals and/or on the ranges of control signals and/or on the state variables as:

$$E\begin{bmatrix}\Delta\hat{u}(k|k)\\ \vdots \\ \Delta\hat{u}(k+N_c-1|k)\end{bmatrix}\leq\begin{bmatrix}0\\ \vdots\\ 0\end{bmatrix} \tag{21}$$

$$F\begin{bmatrix}\hat{u}(k|k)\\ \vdots \\ \hat{u}(k+N_c-1)\end{bmatrix}\leq\begin{bmatrix}0\\ \vdots\\ 0\end{bmatrix} \tag{22}$$

$$G\begin{bmatrix}\hat{z}(k+1|k)\\ \vdots \\ \hat{z}(k+N_p|k)\end{bmatrix}\leq\begin{bmatrix}0\\ \vdots\\ 0\end{bmatrix} \tag{23}$$

when optimization problem is solved, all these inequalities need to be translated into inequalities concerning $\Delta U(k+i|k)$. Although, it is possible to constrain all the state variables, only rotor angle delta is constrained in the present formulation, since only the first swing is required to be controlled. Allowable excursion of delta is between -150 to +150. For N_p=5, controlled parameter δin (23) becomes:

$$\underbrace{\begin{bmatrix}\underbrace{-1}_{(1,1)} & 0 & 0 & -\delta_{1max}^{-1}\\ \underbrace{+1}_{(2,1)} & 0 & 0 & -\delta_{1min}^{-1}\\ 0 & 0 & \underbrace{-1}_{(81,41))} & -\delta_{1max}^{-1}\\ 0 & \cdots & \underbrace{+1}_{(81,41)} & -\delta_{1min}^{-1}\end{bmatrix}}_{100\times51}\underbrace{\begin{bmatrix}\underbrace{\delta_1(k+1|K)}_{(1,1)}\\ \underbrace{\delta_1(k+2|k)}_{(2,1)}\\ \underbrace{\delta_1(k+5|k)}_{(41,1)}\\ 1\end{bmatrix}}_{51\times1}\leq[0] \tag{24}$$

$$\begin{bmatrix}\underbrace{G_d}_{100\times50} & \underbrace{g}_{100\times1}\end{bmatrix}\times \begin{bmatrix}\underbrace{\Phi}_{50\times10} & \underbrace{X(k)}_{10\times1}+\underbrace{\Gamma}_{50\times2}\underbrace{u(k-1)}_{2\times1}+\underbrace{G_y}_{50\times6}\underbrace{\Delta U(k)}_{6\times1}\\ 1\end{bmatrix}<[0] \tag{25}$$

Simplifying it further:

$$G_d\big(\Phi\,X(k)+\Gamma u(k-1)\big)+G_dG_y\Delta U(k)+g<[0] \tag{26}$$

Rearranging (26) as:

$$G_dG_y\Delta U(k)<-G_d(\Phi X(k)+\Gamma u(k-1)-g \tag{27}$$

In the present problem formulation, although there are two inputs, u_{pss} and x_{tcsc}, u_{pss} is kept inactive and constraints are imposed onx_{tcsc}:

$$-0.3<x_{tcsc}<0.4 \tag{28}$$

The predicted control input at the next sampling instant is:

$$\Delta\hat{u}(k+i|k)=\hat{u}(k+i|k)-\hat{u}(k+i-1|k) \tag{29}$$

which results into:

$$\begin{gathered}\hat{u}(k|k) = \Delta\hat{u}(k|k) + u(k-1)\\ \hat{u}(k+1|k) = \Delta\hat{u}(k+1|k) + \Delta\hat{u}(k|k) + u(k-1)\\ \vdots\\ \hat{u}(k+N_c-1|k) = \Delta\hat{u}(k+N_c-1|k) + \cdots +\\ +\Delta\hat{u}(k|k) + u(k-1)\end{gathered} \tag{30}$$

Input changes only at time instants $k, k+1$, ...which is acknowledged by replacing $\hat{u}(k+i|k)$ by $\Delta\hat{u}(k+i|k)$.

Adding all the terms on Left Hand Side (LHS) of (30) for $N_c = 3$ results into:

$$LHS = \hat{u}(k|k) + \hat{u}(k+1|k) + \hat{u}(k+2|k) \tag{31}$$

As discussed earlier, inequalities need to be translated into inequalities concerning Δu. Also, assuming zero order hold for time beyond N_c:

$$\hat{u}(k+1|k) = \hat{u}(k+N_c-1), \text{ for } N_c \le i \le N_p - 1 \tag{32}$$

Collecting proper terms Right Hand Side (RHS) of (30) is found to be:

$$\begin{gathered}RHS = \sum_{j=1}^{j=3} F_j\Delta\hat{u}(k|k) + \sum_{j=2}^{j=3} F_j\Delta\hat{u}(k+1|k) +\\ +F_3\Delta\hat{u}(k+2|k) + \sum_{j=1}^{j=3} F_j u(k-1)\end{gathered} \tag{33}$$

In general:

$$\begin{gathered}\sum_{j=1}^{j=N_c} F_j\Delta\hat{u}(k|k) + \sum_{j=2}^{j=N_c} F_j\Delta\hat{u}(k+1|k) +\\ +F_{N_c}\Delta\hat{u}(k+N_c-1|k) + \sum_{j=1}^{j=N_c} F_j u(k-1) \le 0\end{gathered} \tag{34}$$

which means that:

$$F\Delta U(k) \le -F_j u(k-1) - f \tag{35}$$

For the problem at hand, with $N_c = 3$, (35) becomes:

$$\begin{gathered}\begin{bmatrix}0&0&0&0\\0&-1&0&0\\0&1&0&0\\0&0&0&0\\0&0&0&1\\0&0&0&-1\end{bmatrix}\begin{bmatrix}\Delta u_{pss}(k|k)\\ \Delta x_{tcsc}(k|k)\\ \Delta u_{pss}(k+1|k)\\ \Delta x_{tcsc}(k+1|k)\\ \Delta u_{pss}(k+2|k)\\ \Delta x_{tcsc}(k+2|k)\end{bmatrix} +\\ \begin{bmatrix}-u_{pss}(k-1) + u_{pssmin}\\ u_{pss}(k-1) - u_{pssmax})\\ -x_{tcsc}(k-1) + x_{tcscmin}\\ x_{tcsc}(k-1) - x_{tcscmax}\\ -u_{pss}(k-1) + u_{pssmin}\\ u_{pss}(k-1) - u_{pssmax}\end{bmatrix} \le [0]\end{gathered} \tag{36}$$

Collectively the inequalities (21), (22) and (23) are written as:

$$\begin{bmatrix}F\\ \Gamma G_y\\ W\end{bmatrix}\Delta U(k) \le \begin{bmatrix}-F_1 u(k-1) - f\\ -G_d\big(\Phi\, X(k) + \Gamma u(k-1)\big) - g\\ w\end{bmatrix} \tag{37}$$

To demonstrate the constraint handling issue, (SMIB) model is represented with its detailed dynamics having ten state variables and two control variables.

Main objective of the present work being control of first swing of rotor angle delta, (TCSC) reactance is the only control variable that needs to be constrained.

The additional advantage of having only one control variable is reduced computation burden.

The optimization problem at hand is:

$$\min_u J$$

subject to: (38)

$$\begin{gathered}-0.3 \le x_{tcsc} \le 0.4\\ -150 \le \delta \le 150\end{gathered}$$

where x_{tcsc} is the input control $u(k)$. The matrices F, G are of the order $(12 \times 7), (100 \times 51)$ respectively, for a tenth order (SMIB) model with $N_P = 5$ and $N_c = 3$.

VI. Simulation Result and Analysis

To prove the effectiveness of proposed constraint MPC, it is applied to an SMIB power system represented by a model of order ten.

The linearized system model is used to formulate quadratic optimization problem to find the required capacitive compensation from series connected TCSC in a given transmission line. MPC is used to bring the system back to pre-fault healthy conditions after the fault is cleared with fault clearing time greater than CCT.

Although the problem formulation is capable of handling constraints on all the state variables, rotor angle delta, being the key parameter is considered to form a reference trajectory. In the present paper constraints on rotor angle delta (state of a system) and that on TCSC reactance (input control variable) are formulated as linear inequalities and penalized in the objective function.

The 3 phase short circuit fault occurs on a power system at time t=1 sec and is cleared beyond CCT. The uncontrolled behavior of rotor angle delta is as shown in Fig. 2. If a controller is activated in the post fault region, then the system regains its stability. Nature of first swing is generalized by tuning MPC and/ or by varying the lengths of prediction horizon N_p and control horizon N_c.

Case 1: Equal lengths of prediction and control horizon:

Keeping lengths of prediction horizon N_p and control horizon N_c equal (=2) and tuning MPC by applying different weights on different state variables by varying $Q(i)$, similarly adjusting the MSF R so as to Power

System Stabilizer (PSS) inactive and applying weight on x_{tcsc}, steepness of first swing is observed.

The TCSC reactance is found to follow constraints imposed by MPC as shown in Figs. 3 and 4.

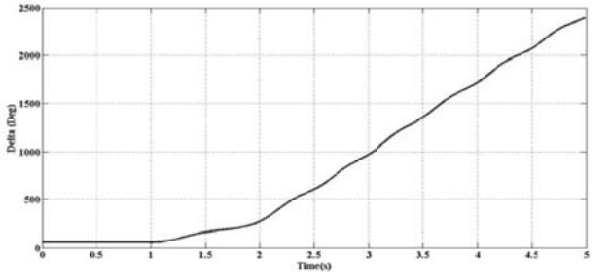

Fig. 2. Variation of delta without controller

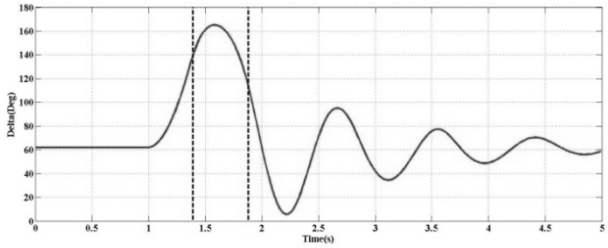

Fig. 3. Variation of delta for equal length of prediction and control horizon

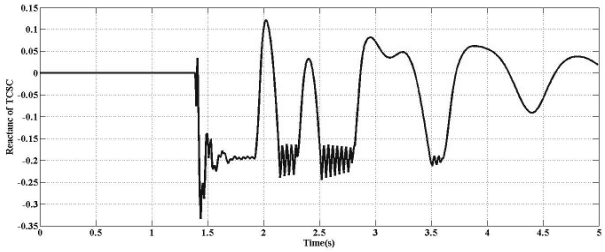

Fig. 4. Required TCSC reactance for equal lengths of prediction and control horizon

Case 2: Moderate lengths of prediction and control horizon.

A trade-off between computation burden and sharpness of first swing, smooth variation of TCSC reactance can be achieved by keeping $N_p = 5$ and $N_c = 3$ and tuning MPC appropriately. Fig. 5 shows variation of rotor angle delta and Fig. 6 corresponding TCSC reactance variation.

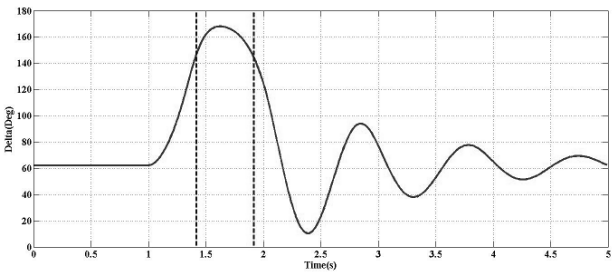

Fig. 5. Variation of delta for moderate length of prediction and control horizon

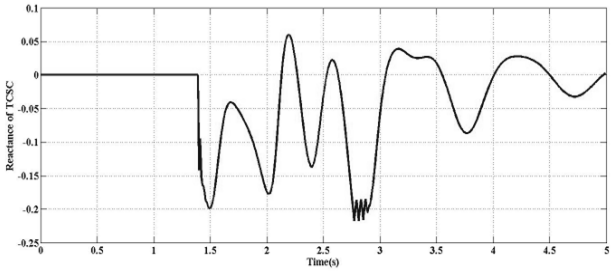

Fig. 6. Required TCSC reactance for moderate lengths of prediction and control horizon

VII. Conclusion

Present paper has described a systematic treatment of implementing MPC with inequality constraints on input control (reactance of TCSC) and state variable (rotor angle delta). It is observed that by properly tuning MPC, algorithm works equally well, irrespective of short or long prediction horizons.

As against conventional controllers, MPC can naturally handle constraints on-line, achieving better performance suitable for real time applications. It has been observed in several case study simulations that controlling key parameter, delta, is capable of keeping all other parameters within their specified limits.

The additional advantage achieved by this approach considerable reduction in computation burden. Since the power system model considered is nonlinear, the increased region of attraction allows the system to come back to the pre-fault operating point even if the fault is cleared beyond the critical clearing time.

After the insertion of TCSC the required performance (in terms of peak value of first swing and/ or rate of decay of oscillations) is achieved by adequately tuning MPC.

Acknowledgements

The authors would like to acknowledge the support of Center of Excellence in Complex and Nonlinear Dynamical Systems (CoE-CNDS), VJTI, Mumbai, India.

References

[1] J. Richalet, ARault, JL Testud, and J. Papo. Model predictive heuristic control: Application to industrial processes. *Automation*, 14(5):413-428. 1978.

[2] C.R.Cutler and BL Ramaker. Dynamic matric control – a computer control algorithm. In *proceedings of the joint automatic control conference*, volume 1, pages Wp5-B. American Automatic Control Council Piscataway. NJ, 1980.

[3] Carlos E. Garicia and A.M.Morshedi. Quadratic programming solution of dynamic matrix control (QDMC). *Chemical Engineering Communications.* 46(1-3); 73-87, 1986.

[4] M. Larsson, David J Hill, and Gustaf Olsson.Emergency voltage control using search and predictive control. *International journal of electrical power & energy systems*, 24(2):121-130, 2002.

[5] Mania Pavella, Damien Ernst, and Daniel Ruiz-Vega. Transient stability of power systems unified approach to assessment and control. Kluwer Academic Publishers, 2000.

[6] YannikPhulpin, JagabondhuHazra, and Damien Ernst. Model predictive control of HDVC power flow to improve transient stability in power systems. In *Smart Grid Communications (Smart Grid Comm), 2011 IEE International Conference on*, pages 593-598, IEE, 2011.

[7] ChVenkatesh, T Deepak, K Rajesh, K Krishna, and AK Kamath. Flatness based TCSC controller for transient stability enhancement of power systems. In *Modern Electric Power systems (MEPS), 2010 Proceedings of the International Symposium* pages 1-6, IEEE, 2010.

[8] Mark Zima and Goran Anderson. Model predictive control employing trajectory sensitivities for power systems applications. In *Decision and Control. 2005 and 2005 European Control conference.* CDC-ECC'05, 44th IEEE *Conference on*, pages 4452-4456, IEEE, 2005

[9] Giovanni Becuti, Tobias Geyer, and Manfred Morari. A Hysbrid system approach to power systems voltage control. In In *Decision and Control. 2005 and 2005 European Control conference.* CDC-ECC'05, 44th IEEE *Conference on*, pages 6774-6779, IEEE, 2005

[10] DheemanChatterji and ArindamGhosh. Application of trajectory sensitivity for the evaluation of the effect of TSCS placement on transient stability. *International Journal of Emerging Electric Power Systems*, 8(1), 2007.

[11] SushamaWagh, AK Kamath and NM Singh. "Non-linear model predictive control for improving transient stability of power system using TCSC controller". *In* 7thAsian Control Conference, 2009, pages 1627-1632. IEEE 2009.

[12] V. Rajkumar and RR Mohler. Non-linear predictive control for the damping of multi machine power system transients using facts devices. In *Decision and Control, 1994, Proceedings of the 33rd IEEE Conference on* Volume 4, pages 4074-4079. IEEE, 1994.

[13] Jan M Maciejowaskiand MihalHuzmezan.*Predictive Control*, Springs, 1997.

[14] Sepahvand, H., Joorabian, M., Saniei, M., Optimal Location and Setting of TCSC and TCPST to Reduce Transmission Congestion in Deregulated Electricity Market, (2013) *International Journal on Energy Conversion (IRECON)*, 1 (1), pp. 47-56.

Authors' information

S. Kulkarni, Received her BE (Electrical Engineering) from Govt. College of Engineering, Amravati, Nagpur University, 1984, ME(Control systems) from VJTI, Mumbai, 1999. She is a Research scholar in Electrical Engineering Department, VJTI, Mumbai and is Associate Professor in Electronics Department, K J Somaiya College of Engineering.Her research interests are: Nonlinear control, Digital system design,Signal processing.

S. Wagh, received her ME degree from Mumbai University, India, in 2003 and PhD degree from The University of Western Australia, Australia, in 2012, all in Electrical Engineering. Currently, she is working at V.J.T.I., Mumbai, India. Her research interests include electrical machines, power system stability and optimal control. Book Publication: Power System Transient Stability Enhancement.

N. M. Singh was born in Mumbai, India in 1959. He received his, B E degree from Mumbai University, Master and PhD degree, from Indian Institute of Technology (IIT) Bombay, India in 1981, 1983 and 1990 respectively. He is currently working asa professor at Veermata Jijabai Technological Institute (VJTI), Mumbai, India. His research interests are Geometric Mechanics Control, Control of Un-actuated Mechanical systems.

1974-6067(201503)8:2;1-T